

**UNIVERSITY OF CANTERBURY**

Department of Mechanical Engineering

Christchurch New Zealand



**Acoustic Absorber Design**

*by*

*Jerome P Parkinson*

**Master of Engineering**

**Thesis**

*March 1999*

# **Acoustic Absorber Design**

by

Jerome P Parkinson

A thesis submitted in  
fulfilment of the requirements for  
the Degree of Master of Engineering

in the

Department of Mechanical Engineering  
University of Canterbury  
Christchurch, New Zealand

March 1999

---

# Project Summary

---

The aim of the Acoustic Absorber Project was to investigate the performance of a range of materials as acoustic absorbers. A literature search on acoustic absorbers was carried out first and is presented with a summary of commercially available absorbers in the Absorber Survey. Modifications were made to the Reverberation Room in the Department of Mechanical Engineering, University of Canterbury. Tests showed that the Room modifications and diffuser installation improved its sound field diffusivity and uniformity, ensuring reliable absorption measurements. Apparatus was then built and used to measure the flow resistance of porous materials. This equipment was pivotal to the successful specification of materials used as acoustic absorbers. More than fifty different absorbers were tested in the refurbished Reverberation Room to determine their absorption coefficients. Subsequent analysis was carried out to compare the different materials, thicknesses and systems used as absorbers. Various models were used and developed to predict the measured results. The models produced similar trends to the measured data but with lower absorption coefficients. It was found that tuned absorbers could be produced from CMSG foam with impervious films, giving high absorption in selected frequencies. Wideband absorbers could be made at low cost from low density foam, polyester or fibreglass with fabric coverings, each optimised for flow resistance. Contoured foams were also found to be very effective wideband absorbers. Optimal acoustic absorbers can now be designed and produced to satisfy different absorption requirements.

## Acknowledgments

Firstly, I would like to thank Dr John Pearse for providing comprehensive project supervision, from administration through to technical support; for ensuring that the project was completed on schedule.

I wish to extend special thanks to Mr Mike Latimer of D.G.Latimer and Associates for the prompt supply, specifications and selection of materials for use as absorbers.

I would also like to thank Professor Cliff Stevenson for his thorough analysis and advice with regard to many aspects of the absorber project.

I would like to thank Professor Walter Eversman, Professor Jeremy Astley and Professor Stuart Bolton for timely advice and comments on the modelling of acoustical materials.

Finally, I wish to thank various people for technical support during the project; Mr Graeme Harris for help in building the flow resistance apparatus; Mr Otto Bolt and many postgraduate students, especially Kent Roache, for help when installing diffuser panels.

## Opening Quotation

If such optimality properties exist, and it seems they do, then still further questions arise: Can we show that the usable expressions do not raise problems of unfeasible computation, while unusable ones may do so - perhaps the source of their unusability? These are hard and interesting questions. We understand enough to formulate them intelligibly today, but not much more.

Noam Chomsky, *Powers and Prospects - Reflections on human nature and the social order*. Allen & Unwin Pty Ltd, Australia, 1996.

# Table of Contents

Conventions .....	iv
Project Objectives.....	v
Project Outline.....	v

## Chapter 1 Absorber Survey

Table of Contents .....	vi
List of Figures .....	vii
1. Requirements .....	1
2. Porous Absorbers.....	1
3. Membrane/panel absorbers .....	3
4. Helmholtz/cavity absorbers .....	5
5. Multi-layered Absorbers .....	5
6. Materials .....	8
7. Commercially Available Absorbers.....	9
References.....	10
Bibliography .....	12
Summary of Commercial Absorbers.....	13

## Chapter 2 Reverberation Room Calibration

Table of Contents .....	viii
List of Figures .....	ix
List of Tables .....	ix
1. Introduction.....	14
2. Aims.....	15
3. Theory.....	15
4. Equipment.....	16
5. Procedures.....	20
6. Results and Discussion .....	23
7. Conclusions.....	29
References.....	30

### Chapter 3 Absorber Materials

Table of Contents .....	x
List of Figures .....	xi
List of Tables.....	xi
1. Introduction.....	32
2. Aims.....	32
3. Theory.....	33
4. Equipment.....	33
5. Procedure .....	36
6. Results and Discussion.....	37
7. Conclusions.....	42
References .....	43
Bibliography.....	43

### Chapter 4 Absorption Testing

Table of Contents .....	xii
List of Figures .....	xiii
List of Tables.....	xiii
1. Introduction.....	44
2. Aims.....	45
3. Theory.....	45
4. Equipment.....	45
5. Procedure .....	46
6. Results.....	46
7. Conclusions.....	68
References .....	69
Bibliography.....	69

### Chapter 5 Modelling

Table of Contents .....	xiv
List of Figures .....	xv

List of Tables .....	xv
1. Introduction.....	70
2. Aims.....	70
3. Rigid Framed Fibrous Materials .....	70
4. Elastic Framed Porous Materials .....	71
5. Layered Porous Materials .....	76
6. A Matrix Representation of Layered Materials .....	78
7. Model Comparisons .....	84
8. Conclusion .....	93
References.....	94
Bibliography .....	95
<b>Chapter 6 Project Findings</b>	
Table of Contents.....	xvi
List of Tables .....	xvi
1. Introduction.....	97
2. Aims.....	97
3. Results.....	97
4. Conclusions.....	100
<b>Project Conclusion.....</b>	<b>101</b>
Further Work .....	101
<b>Appendices.....</b>	<b>103</b>
Appendix A.....	103
Appendix B.....	107
Appendix C.....	113
Appendix D .....	132

## Conventions

Porous absorbing materials, such as CMSG foam and polyester, are sometimes referred to in the text as bulk materials or substrate.

The measured results are in one third octave frequency bands and hence should be referred to as frequency bands. To avoid needless repetition much of the discussion refers to frequencies and frequency ranges instead of frequency bands and frequency band ranges.

The Reverberation Room is located in the Department of Mechanical Engineering, University of Canterbury. It is referred to in capitals, “Reverberation Room” or in some cases, “Room”.

The project is presented in chapters. A table of contents, list of figures and list of tables are included at the start of each chapter which relate to that chapter. Similarly, a list of references and bibliography are given at the end of each chapter.



## **Project Objectives**

The objective of the Absorber Project was to analyse the acoustic performance of a range of materials as acoustic absorbers. The significant parameters were to be identified and the application of these materials in tuned and wideband absorbers considered.

The outcome from the project was the acoustic performance of a range of absorbers using optimised materials to achieve a user specified performance.

## **Project Outline**

The Acoustic Absorber Design project is presented herein as six chapters – Absorber Survey, Reverberation Room Calibration, Absorber Materials, Absorption Testing, Modelling and Project Findings. The results of a literature search on acoustic absorbers and a summary of commercially available absorbers are given in the Absorber Survey. The second chapter describes the successful calibration of the Reverberation Room. Following on from this, the materials used as absorbers are described and specified in the Absorber Materials chapter. The measured results are presented and compared in the Absorption Testing chapter. Next, the Modelling chapter describes the theories used and gives a comparison of predicted and measured results. The concluding chapter, Project Findings, summarises and compares the tested absorbers.

---

# 1

# Absorber Survey

---

## Summary

The Absorber Survey is comprised of a literature search on absorbers and a summary of commercially available absorbers. This research was carried out to gather knowledge on absorber theory and to ascertain the performance of existing absorber technologies. The main types of absorbers in the literature were porous, membrane, helmholtz and multilayered absorbers. These were described in terms of the materials commonly used and their acoustic performance. A theoretical optimum flow resistance has been found for rigidly backed bulk porous materials and is equal to  $3\rho c$  (1235 mks rayls) where  $\rho$  is the density of air and  $c$  is the speed of sound in air. Similarly, an optimum flow resistance for fabric coverings has been found to be  $1\rho c$  (412 mks rayls). An extensive range of absorbers are currently available. Most of these use fibreglass or foam as the bulk absorbing layer and are sometimes combined with impervious films or perforated metal coverings. The highest NRC (arithmetic average of absorption coefficients in octave bands from 125 Hz to 2 kHz) at 25 mm thickness was 0.87 for a polyester infill covered with a porous acoustic textile. The acoustic characteristics of commercially available absorbers are given at the end of this chapter.

## Table of Contents

Table of Contents .....	vi
List of Figures .....	vii
1. Requirements.....	1
2. Porous Absorbers .....	1
2.1 Description.....	1
2.2 Theoretical performance.....	2
3. Membrane/panel absorbers .....	3
3.1 Description.....	3
3.2 Theoretical performance.....	4
4. Helmholtz/cavity absorbers.....	5
4.1 Description.....	5
4.2 Theoretical performance.....	5
5. Multi-layered Absorbers .....	5
5.1 Description.....	5
5.2 Theoretical performance.....	6
5.3 Practical performance .....	7
6. Materials.....	8
7. Commercially Available Absorbers .....	9
References .....	10
Bibliography.....	12
Summary of Commercial Absorbers .....	13

## List of Figures

<u>Figure No.</u>	<u>Page</u>
Figure 1.1 Typical absorption curve for a porous material. ....	2
Figure 2.1 Typical absorption curve for a membrane or panel absorber.....	4
Figure 3.1 Typical absorption curve for a cavity absorber.....	5

## 1. Requirements

Absorbers are required:

1. To control the reverberation time and reduce the reverberant sound levels within a room.
2. To reduce the undesirable effects of standing wave resonance.
3. To attenuate noise inside ductwork.
4. To have a low unit cost (preferably less than \$80/m<sup>2</sup>).
5. To be aesthetically pleasing.
6. To meet the relevant fire standards.

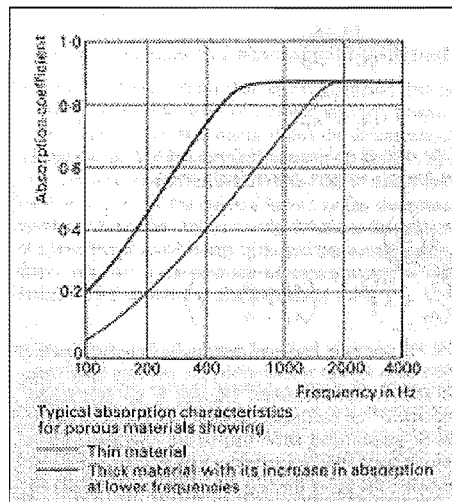
In a typical room, carpet and curtains absorb high frequency sound while walls absorb low frequency sound. Absorbers are usually required for the mid-frequency range, 100 to 5000 Hz. Within this range, absorption is often required at 300 Hz.

Acoustically sensitive rooms, such as TV studios, usually have specific absorption requirements. Wide band, highly absorbing wall treatments of limited depth are often necessary. The ability to tune the absorbers to particular frequencies is also desirable.

## 2. Porous Absorbers

### 2.1 Description

Porous absorbers typically consist of a network of interlocking pores that convert sound energy into heat. Granular or fibrous substances combined with adhesives are compacted into layers by pressing or weaving. Fibreboard, wools, fibreglass panels, foams and tiles are common examples of porous absorbers. These generally absorb more sound at higher frequencies as shown in Figure 2.1.



**Figure 2.1 Typical absorption curve for a porous material.**

## 2.2 Theoretical performance

Delany and Bazley (1969) measured the acoustic properties of many fibrous absorbent materials. They found that the characteristic impedance and propagation constant of these materials normalised as a function of frequency divided by flow resistance. Hence, power laws were used to model the measured results. The impedance and propagation constants were then used to predict normal incidence absorption coefficients for rigidly backed porous materials; see section 3 in Chapter 5 for more details.

New expressions to model sound propagation in fibrous materials were developed by Allard and Champoux (1991). These theoretical equations were based on the general frequency dependence of viscous forces in porous materials. The predictions were valid at low frequencies whereas Delany and Bazley's model was less accurate at low frequencies.

Bies and Hansen (1979) carried out an in-depth study of porous materials concentrating on the effect of flow resistance. They found that a material's flow resistance was sufficient to characterise its acoustical performance. An equation was presented to predict the flow resistance of fibreglass materials based on its fibre diameter and density. Delany and Bazley's power laws were used to predict the normal incidence absorption coefficients of porous materials. Statistically averaged absorption coefficients were calculated through established formulae to give closer agreement with reverberation room measurements. Absorption coefficients were then plotted versus normalised frequency for various flow resistances and air cavity depths. An optimum total flow resistance of  $3\rho c$  (1235 mks rays) was found for both zero and  $\frac{1}{4}$  wavelength cavity depths. The ratio of cavity depth to porous

material thickness was also investigated. A one to one ratio was found to be optimal for a total flow resistance of  $2.8\rho c$  to  $3.5\rho c$ .

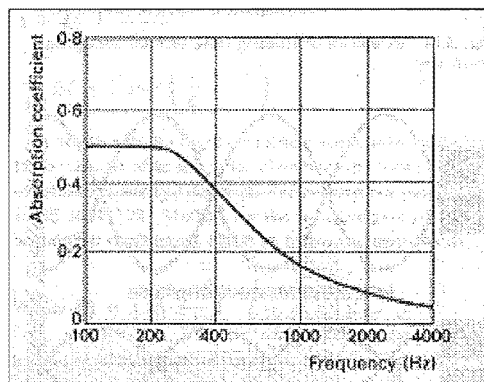
Ingard (1994) carried out an in-depth investigation into theoretical absorption. His study showed, similarly to Bies and Hansen, that the frequency dependence of absorption coefficient for a rigid porous layer backed by a wall was predominantly determined by its thickness and flow resistance. The material's porosity and structure factor had a small effect on absorption for a given flow resistance. Absorption of 80% was achieved with a layer flow resistance of  $4\rho c$  and a layer thickness larger than  $1/10$  of the wavelength of interest. At 300Hz the wavelength of sound in air is 1.1m. Hence, a 110 mm thick rigid porous absorber is required to attain at least 80% absorption at 300Hz. An absorber this size is generally too thick for typical application as it has high material costs and uses valuable room space. Ingard showed that multi-layered absorbers can reduce this thickness; see section 5.

Flexible porous absorbers such as foams were also considered by Ingard. An open cell absorber's flexibility tended to reduce its low frequency absorption but increased its mid-frequency absorption. Open cell foams with large flow resistances could be programmed to give large resonant type absorption at low frequencies. Closed cell foams typically gave narrow bandwidth absorption.

### **3. Membrane/panel absorbers**

#### **3.1 Description**

Membrane absorbers consist of a thin porous sheet positioned with an air space in front of a rigid wall. They are often fortuitously present in the form of suspended ceilings or double glazed windows. The semi-rigid sheet is forced into vibration by an incident sound field. The vibrations produce non-reversible, periodic bending deformation which transfers energy into the sheet. Wood, plastic, wire mesh and flexible fabrics are used as membrane panels. These give high absorption at low frequencies as shown in Figure 3.1.



**Figure 3.1** Typical absorption curve for a membrane absorber.

### **3.2 Theoretical performance**

The acoustic properties of permeable membranes were studied by Sakagami, Morimoto and Takahashi (1995). In particular, the density, thickness, tension and permeability of the membranes were investigated. The membranes were often used as coverings for building materials or porous absorbent materials due to their transmissibility and reflective properties. Membrane tension and density had a small effect on absorption. Again, it was found that flow resistance was critical to acoustic performance.

Ingard (1994) modelled the acoustical performance of thin porous sheets backed by an air cavity. He found that a  $\frac{1}{4}$  wavelength air cavity gave around 70-80% absorption over an octave around the resonant frequency. In a diffuse field the optimum flow resistance was  $2\rho c$  at the  $\frac{1}{4}$  wavelength. He found that a sheet absorber was inferior to a uniform porous layer as the sheet's absorption dropped to zero at certain frequencies. Similar to the rigid porous layer, absorption of 80% was possible if the air cavity was larger than  $\frac{1}{10}$  of the wavelength of interest with a sheet flow resistance of  $4\rho c$ . A 110 mm air cavity would be required to absorb 80% of the sound at 300Hz. Ingard suggested an optimum sheet flow resistance of 2 to  $4\rho c$  for all frequencies and larger resistances for low frequencies. This raises the idea of a thin porous sheet in combination with a rigid porous layer to give wideband absorption; see section 5.

Ingard also modelled parallel, porous sheet absorbers. These consisted of alternating sheet and air cavity layers. Using unequal separations between the sheets and gradually increasing the flow resistance per sheet gave more absorption than a uniform porous layer of the same total thickness.



## 4. Helmholtz/cavity absorbers

### 4.1 Description

These absorbers consist of an air volume enclosed by rigid boundaries and coupled to a surrounding space by an aperture. Containers with small open necks are generally used. Absorption takes place through air resonance within the cavity. In practice, cavity absorbers consist of a panel with many holes backed by an air space or fibrous absorbing material. Slotted or perforated boards are similarly used. These absorbers give narrow bandwidth absorption as shown in Figure 4.1.

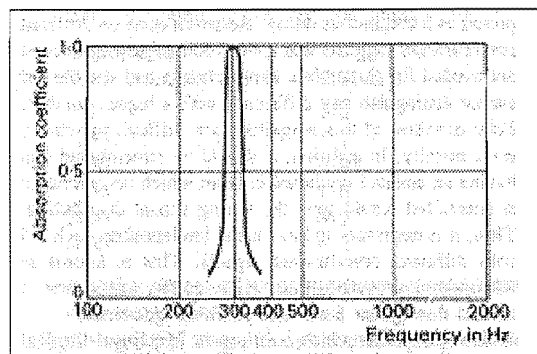


Figure 4.1 Typical absorption curve for a cavity absorber.

### 4.2 Theoretical performance

Maa (1987) investigated the acoustical performance of microperforated-panel wideband absorbers. The frequency band of predominant sound absorption depended on the perforation diameter. Large theoretical absorption was attained in one to two octaves with submillimetre holes. These resonators were programmed to give peak absorption at certain frequencies. Double resonators were found to extend the absorption to lower frequencies without affecting high frequencies. Microperforated-panel double resonators gave good absorption covering four octaves. In general, these panels gave good medium to low frequency absorption but performed poorly in frequencies greater than 1600Hz.

## 5. Multi-layered absorbers

### 5.1 Description

Multi-layered absorbers comprise two or more materials to increase or tune the absorption. Most of these systems use a porous absorbing material in combination with a screen, covering

or film. Air cavities behind the absorber can also be incorporated to improve the performance.

### **5.2 Theoretical performance**

Sakagami, Morimoto and Takahashi (1995) modelled the combination of permeable membranes with fibreglass and air layers. A membrane was combined with 50 mm of 32 kg/m<sup>3</sup> glass wool and a 300 mm air cavity. Membrane flow resistances of 240 and 680 mks rays coincided with the most absorption while those with infinite resistance (impermeable) gave the least absorption. This agrees with a Dunn and Davern (1986) hypothesis that multi-layered absorbers should have low frontal reflectance to allow easy entrance of the sound into the absorber while second or third layers provide the attenuation. The predictions were verified experimentally in a reverberation room. Agreement between the model and practice was very good except for deviations at frequencies less than 250Hz.

Dunn and Davern (1986) developed a method for calculating the acoustic impedance of multi-layered systems. A database of wave impedances and propagation constants was used to generate the absorption coefficients of different layer combinations. They recommended the selection of a low flow resistance material to minimise frontal reflections for solid backed single layers. Systems using air cavities were studied. In general, for the same amount of material it was better to have an air space than not to have one. For the same overall thickness (>100 mm) it was better to have solid material than incorporating an air cavity. Dunn and Davern also compared their model to experimental results and found good agreement.

Brouard, Allard, Bruneau, et al (1992) modelled the acoustical impedance and absorption characteristics of porous layers with slotted facings. They found that an absorber with good low frequency absorption and limited depth could be made by modifying slit width and separation. However these absorbers produced a typical narrow band resonant peak. Similarly, Ballagh (1997) presented a method for predicting random incidence absorption of porous materials with slotted, perforated or panel facings. In both cases good agreement was found between the theoretical and experimental results.

Ingard (1994) showed that multi-layered absorbers can be used to attain more absorption than a rigid backed single layer of the same thickness. Increasing the flow resistance from outer to inner layers produced more absorption than decreasing the flow resistance per layer. This

lends further credence to the Dunn and Davern (1986) hypothesis that multi-layered absorbers should have low frontal reflectance to allow sound into the absorber while deeper layers provide the attenuation. He also found that layers of different flow resistance gave more absorption than a material with uniform flow resistance for the same thickness.

A rigid porous layer in combination with a thin porous sheet was modelled by Ingard. He found that adding a thin porous cover screen gave a significant increase in low frequency absorption. The porous layer's high frequency absorption started to reduce when the screen's flow resistance reached 1pc (412 mks rayls).

Ingard also studied the effect of air layers on porous absorbers. Incorporating an air cavity into an absorber while retaining the same overall flow resistance always gave less absorption than a solid absorber.

Most multilayered absorbers have their layers aligned parallel to the backing surface. Takahashi (1989) studied the phenomenon of excess sound absorption of periodically arranged flat surfaces. He carried out a theoretical and experimental investigation into the effect of surface impedance discontinuity on absorption. An absorber made of alternating strips of wood and fibreglass was modelled. Excess sound absorption is present if more sound is absorbed from the combination of materials than just the average of each material's absorption. He found that excess sound absorption occurred in all cases of periodically arranged surfaces. The material's flow resistance affected excess absorption at mid to high frequencies. The thickness of the rigidly backed layer was related to absorption at low frequencies. Absorption at high frequencies was affected by the period of the two materials. The width of the materials affected the absorption in all frequencies. The results showed that a combined material width of 0.125 to 0.5 m and a width ratio of 0.25 gave the most absorption in all frequencies gave the best wideband absorption.

### **5.3 Practical performance**

Dodd, Ballagh and Camp (1991) investigated "tandem" absorbers - aiming for a multi-layered, low cost, wideband absorber of reduced depth. A variety of systems were trialed based on combinations of fibreglass, rigid board and air cavities. A combination of 25 mm fibreglass, 5 mm Kappa board and 25 mm fibreglass gave peak absorption from 125 to 250Hz and medium absorption at higher frequencies. Similar trends with a larger peak were obtained

with 25 mm fibreglass, 2 mm Kappa board and 25 mm fibreglass. In general, high absorption peaks were attainable but with a narrow bandwidth.

Dodd and Trimble continued the “tandem” absorber investigation. They aimed to combine the separate performance of panel absorbers with porous absorbers. This was achieved with 20 mm fibreglass and hardboard. This tandem system had a narrow peak at 200Hz and a typical porous layer absorption trend in the high frequencies. The effect of fibreglass position within the cavity was also studied. This system had a peak at 630Hz but poor absorption on either side. There was small variation in absorption with fibreglass position. As the fibreglass moved closer to the septum, the bandwidth of absorption increased, as did the effective flow resistance. With fibreglass in the middle of the cavity, doubling the septum mass moved the resonance frequency down by  $\sqrt{2}$  but narrowed the bandwidth by 2.

## 6. Materials

The use of foam additives to reduce sound transmission was investigated by Cushman (1995). Common polymers with additives demonstrated excellent bulk acoustic absorption. Attenuation is based on the mechanism of phase cancellation. High impedance particles produce in-phase acoustic reflections while lower impedance particles give out of phase reflections. Simultaneous in-phase and out of phase reflections increase the probability of phase cancellation. Hence, a combination of high and low impedance particles gives good attenuation. It was found that if the correct proportions of high and low impedance particles were mixed in a polymer matrix more attenuation was possible than the sum of the particle’s individual attenuations. He suggested using a mix of iron powder and glass microspheres, for high and low impedance particles respectively, in a polymer foam matrix.

Surface films are often combined with acoustic foams to increase the life of the absorber. Masiak (1974) studied the change in absorption with surface film, strip adhered or totally adhered to an open cell urethane foam. He used 0.5 and 1 mm thick polyester films. It was found that the films shifted the maximum absorption peak to lower frequencies while reducing the absorption at higher frequencies.

## 7. Commercially Available Absorbers

A large range of commercially available absorbers were discovered during the survey. Most of these products were designed as general wideband absorbers. Fibreglass and foam were predominantly used while mineral wool and polyester systems were used to a lesser extent. Impervious films, perforated films, perforated metal and fabric coverings were commonly used to protect or enhance the absorbers. A polyester infill covered with porous acoustic textile produced by INC had the largest NRC (0.87) at 25 mm thickness. Some of the absorbers had a NRC equal to 1.0 at 50 mm thickness. However, this was due to absorption coefficients exceeding unity in some high frequency bands. It was difficult to compare these results as it was hard to relate the absorption coefficients greater than 1.0.

## References

- Allard, J.F., Champoux, Y. (1991), "New empirical equations for sound propagation in rigid frame fibrous materials", *J. Acoust. Soc. Am.*, v91, 1992:3346-3353.
- Ballagh, K. (1997), "Predicting sound absorption of perforated and slotted absorbers", *NZ Acoustics*, v9, 1997:15-22.
- Bies, D.A., Hansen, C.H. (1979), "Flow resistance information for acoustical design", *Applied Acoustics*, 13, 1980:357-391.
- Brouard, B., Allard, J.F., Bruneau, H., Lauriks, W., Verhaegen, C. (1992), "Acoustical impedance and absorption coefficients of porous layers covered by a facing perforated by parallel slits", *Noise Control Engineering Journal*, v41, 1993:289-296.
- Cushman, W.B. (1995), "Using additives to reduce sound transmission", *Modern Plastics*, April, 1995:75-79.
- Delany, M., Bazley, E., (1969), "Acoustical properties of fibrous absorbent materials", *Applied Acoustics*, v3, 1970:105-116.
- Dodd, G., Ballagh, K., Camp, S. (1991), "The tandem absorber – a programmable wide-band absorptive treatment.", *Proceedings, Internoise 1991*:593.
- Dunn, I.P., Davern, W.A. (1986), "Calculation of acoustic impedance of multi-layer absorbers", *Applied Acoustics*, 19, 1986:321-334.
- Maa, D.Y. (1987), "Microperforated-panel wideband absorbers", *Noise Control Engineering Journal*, v29, 1987:77-84.
- Masiak., (1974), "The effect of surface films on acoustical foam performance", *Journal of Sound and Vibration*, 1974:24-29.

Morimoto, M., Sakagami, K., Takahashi, D., (1995), "Acoustic properties of permeable membranes", J. Acoust. Soc. Am., v99, 1996:3003-3009.

Takahashi, D., (1989), "Excess sound absorption due to periodically arranged absorptive materials", J. Acoust. Soc. Am., v86, 1990:2215-2222.

## Bibliography

- TA Allard, J.F., "Propagation of sound in porous media: modelling sound  
418.9 absorbing materials", Elsevier, New York, 1993.  
.P6  
.A419
- TD Beranek, L.L., "Noise and vibration control", McGraw Hill, 1988.  
892  
.n784
- QC Ingard, U., "Notes on sound absorption technology", Noise Control  
233 Foundation, 1994.  
.I44
- NA Kuttruff, H., "Room acoustics", Applied Science Publishers, London,  
2800 1979.  
.K97
- TA Smith, B.J., Peters, R.J., Owen, S., "Acoustics and noise control",  
365 Addison Wesley Longman, 1996.  
.S643a
- QC Zwicker, C., Kosten, C.W., "Sound absorbing materials", Elsevier, New  
233 York, 1949.  
.Z98



## Summary of Commercial Absorbers

TYPE	MANUFACTURER	DESCRIPTION	PERFORMANCE/TYPE	NRC
POROUS				
Wall panels	Acoustical Solutions	Semi-rigid glass wool 90kg/m <sup>3</sup> (24,48,80,130 kg/m <sup>3</sup> avail) at 25,50,75,100mm thickness. Optional aluminium foil backing available.	Typical high frequency	
		Perforated metal packed with high density polyester blanket, faced with fabric. Optional mount away from wall. 25,50mm thickness.	Typical high frequency	
Wall panel	Armstrong	Perforated mineral or fibreglass substrate. Fabric or vinyl finish		0.7
Decifill P	INC	Polyester infill laminated to textile	50mm cavity	0.71*
Corridor Panel	Euroacoustic	Rigid stonewool lined with fibreglass tissue. 25mm thick.	250-1000Hz $\alpha=0.8$ >1000Hz $\alpha=0.9$	
Wall panel	Euroacoustic	Rigid stonewool with fibreglass mat facings. 50,80mm.	300mm plenum, >250Hz $\alpha=0.9-1.0$	
Notice board	Acoustical Solutions	Semi-rigid glass wool 90kg/m <sup>3</sup> . Optional aluminium foil backing or 4mm perforated/plain MDF available.	Typical high frequency	
Baffles	Acoustical Solutions	Acoustic foam		
Tubular foam	Acoustical Solutions	Acoustic foam		

TYPE	MANUFACTURER	DESCRIPTION	PERFORMANCE/TYPE	NRC
Hygiene panel	Acoustical Solutions	48kg/m <sup>3</sup> polyester board 50mm thick or 32-34kg/m <sup>3</sup> glass wool board 50mm thick. 30micron facing film. Aluminium frame.	Typical high frequency with resonant peak at 500Hz.	
Ceiling panel	Euroacoustic	Stonewool panel lined with fibreglass tissue. 20mm thick	300mm plenum, >250Hz $\alpha=0.8-0.9$	
Foam	Acoustical Solutions	Rectangular 32-35kg/m <sup>3</sup> . 25,50mm thick. Optional 3,6mm perforated/plain MDF backing. Plain/convoluted facings. Optional nylon fibre finish	Resonance peak at 1000Hz**	
Decifoam ALR	INC	25mm foam faced with aluminium foil.	Resonance peaks at 315,1600Hz	0.61*
Decifoam F	INC	12,25,50mm foam faced with film	Typical high frequency. 12mm 25mm 50mm	0.51* 0.78* 1.0*
Decifoam Fl	INC	Foam with impermeable film. 12,25,50mm thick.	Peak at 400Hz	0.65*
Decifoam M	INC	Foam with metallised polyester film	M12 Peak at 600, 2000Hz M25 Peak at 315Hz M50 Peak at 125-250,1000,3000Hz	0.49* 0.59* 0.60*
Decifoam T	INC	Foam with textile facing.	T12 T25 T50	0.51* 0.73* 0.94*

TYPE	MANUFACTURER	DESCRIPTION	PERFORMANCE/TYPE	NRC
Decifoam V	INC	Foam with perforated vinyl facing	V12 Peak at 800Hz V25 Peak at 1000Hz V50 Peak at 500Hz	0.48* 0.74* 0.94*
Rigid foam	Novio Pty	Phenolic 50kg/m <sup>3</sup> rigid open cell foam	Resonance peak at 4-500Hz and typical high frequency.	
MEMBRANE				
Decitex P16 sheet	INC	Acoustic textile (porous) with air space.	Typical high frequency. 25mm cavity 100mm cavity	0.24* 0.65*
HELMHOLTZ				
Decitex P52	INC	Perforated metal 11-30% open area. 25,50,250,500mm cavities.	25,50mm cavities - Typ. high frequency 250mm cavity - peak at 250-500Hz 500mm cavity - peak at 200Hz	
MULTILAYER				
Wall panel	Euroacoustic	Stonewool with fibreglass tissue glued to perforated metal sheet. 40mm thick.	>500Hz $\alpha=1.0$	
Decipol	INC	As per Decitex P16 (INC) with polyester infill	Decifill P350 25mm cavity Decipol P25 25mm cavity	0.68* 0.87*
Ceiling panels	Acoustical Solutions	MDF with fibreglass or foam. 4.5kg. 12,15,50mm thick	130g/m <sup>3</sup> glass wool 25mm Typical high frequency	0.79

TYPE	MANUFACTURER	DESCRIPTION	PERFORMANCE/TYPE	NRC
Ceiling panel	Fjord Armstrong	Mineral wool faced with glass fibre fabric. 18,25mm thick.	Typical high frequency	
Ceiling panel	ACI Sonoacoustic	Fibreglass faced with pin perforated vinyl facing. 17,22mm thick	250 and 500 Hz peaks - 17mm 22mm	0.75* 0.80*
Duct liner	CSR Bradford	Fibreglass with various perforated metal facings. 32kg/m <sup>3</sup> . 13,25,50,75,100mm thick.	25mm perf. facing. Peak at 2000Hz 50mm perf. facing >500Hz $\alpha > 0.97$ 25mm glass tissue facing 50mm glass tissue facing, >500Hz $\alpha > 1.0$	0.75* 1.0* 0.65* 0.95*

\* Tested according to AS 1045-1971 or 1988, reverberation chamber.

\*\* Tested according to AS 1935-1976.

$\alpha$  = Absorption coefficient.

---

# 2

## Reverberation Room Calibration

---

### Summary

The Reverberation Room calibration was performed to ensure that reliable absorption measurements were made in the Room. A reverberation room's performance can be quantified by examining its sound diffusivity, reverberation and uniformity. Following initial tests in the Room it was decided to refurbish the Room to improve its acoustic characteristics. A ventilation duct and window were removed, the floor was levelled, all surfaces were repainted and six diffusing panels were added to improve its diffusivity. The refurbished Room's reverberation times increased dramatically above the original Room's times and were even doubled in some frequencies. The sound field uniformity and diffusivity in the refurbished Room were also improved. Materials that had previously been tested in a Telarc registered room were tested to benchmark the Room, equipment and procedures used. The Reverberation Room produced absorption coefficients that were 5 to 15% different than the registered room's absorption coefficients across the frequency range. Repeatable results indicate that the Room's performance has significantly improved and that it will produce reliable data.

## Table of Contents

Table of Contents.....	viii
List of Figures.....	ix
List of Tables.....	ix
<b>1. Introduction.....</b>	<b>14</b>
1.1 Reverberation.....	14
1.2 Reverberation rooms.....	14
1.3 Diffusivity.....	14
1.4 Measurements.....	14
<b>2. Aims.....</b>	<b>15</b>
<b>3. Theory.....</b>	<b>15</b>
3.1 Calculation of absorption.....	15
3.2 Calibration of reverberation rooms.....	15
<b>4. Equipment.....</b>	<b>16</b>
4.1 Reverberation Room.....	16
4.2 Diffusers.....	17
4.3 Modular precision sound analyser, Type 2260B.....	18
4.4 JBL EON Power 10.....	19
4.5 Sound intensity analyser, Type 4433.....	19
4.6 Materials for calibration.....	20
<b>5. Procedures.....</b>	<b>20</b>
5.1 Diffusivity.....	20
5.2 Reverberation.....	22
5.3 Uniformity.....	22
5.4 Benchmark.....	22
<b>6. Results and Discussion.....</b>	<b>23</b>
6.1 Diffusivity.....	23
6.2 Reverberation.....	26
6.3 Uniformity.....	27
6.4 Benchmark.....	28
<b>7. Conclusions.....</b>	<b>29</b>
<b>References.....</b>	<b>30</b>

## List of Figures

<u>Figure No.</u>	<u>Page</u>
Figure 4.1 Reverberation Room dimensions, modifications and diffuser locations.....	17
Figure 5.1 Test specimen - Bonded foil on foam (foam up) in (a) refurbished Room, (b) refurbished Room with diffusers. ....	23
Figure 6.1 Standard deviation of intensity in the Reverberation Room. ....	23
Figure 6.2 Diffuser installation - average absorption versus diffuser area. ....	24
Figure 6.3 Standard deviation of reverberation times in original Room. ....	25
Figure 6.4 Standard deviation of reverberation times in, (a) original Room; (b) refurbished Room. ....	25
Figure 6.5 Reverberation times in the original Room and the Refurbished Room.....	26
Figure 6.6 Normalised reverberation times in the original Room and refurbished Room. ....	27
Figure 6.7 Variation of pressure levels in the refurbished Reverberation Room. ....	27
Figure 6.8 Benchmark absorption test for Tedlar™ film on foam. ....	28
Figure 6.9 Benchmark absorption test for Bonded foil on foam (foam up). ....	28
Figure 6.10 Effect of curvature on test specimen. ....	29

## List of Tables

<u>Table No.</u>	<u>Page</u>
Table 4.1 Reverberation Room areas and volume.....	16
Table 4.2 Diffuser area percentages. ....	18
Table 4.3 Software settings .....	19
Table 4.4 Calibration materials. ....	20
Table 5.1 Intensity measurements - speaker and microphone locations.....	20
Table 5.2 Reverberation time speaker and microphone locations.....	21
Table 5.3 Benchmark speaker and microphone positions .....	22

## 1. Introduction

### 1.1 Reverberation

Sound does not die away the instant it is produced but continues to be heard for some time due to reflections from walls, floors, ceilings and other surfaces. It mixes with later direct sound and is called reverberant sound. Reverberant sound can convey atmosphere to an audience, from the haunted house with a long reverberation time to the padded cell. Reverberation time is the time it takes for a sound to decay by 60 dB. This is found by generating a noise of large amplitude and measuring its rate of decay. In practice, this is difficult to measure and so 20 dB and 30 dB decays are used and extrapolated to find the 60 dB decay.

### 1.2 Reverberation rooms

Reverberation rooms are typically large empty rooms with long reverberation times. These usually have volumes greater than 200m<sup>3</sup> and non-parallel wall and ceiling surfaces. A truly reverberant room is one where energy from a noise source is diffused throughout the room so that the sound pressure level is the same everywhere. Absorption coefficients of an item can be calculated by measuring reverberation times in a reverberation room, with and without the item present.

### 1.3 Diffusivity

In a diffuse field sound is reflected many times so that it travels in all directions with equal magnitude and probability. A perfectly diffuse room should have equal intensity in all directions. It is important that a reverberation room is diffuse to ensure accurate measurements.

### 1.4 Measurements

The variation of sound intensity and reverberation time within a room is inversely related to the degree of diffusivity in the room. The correct amount of diffusers can be obtained from the diffuser installation procedure outlined in ISO 354:1988<sup>1</sup>. An ideal amount of reverberation is specified by ISO 3743:1988<sup>2</sup>. The variation in sound pressure level within a room is inversely related to the sound field uniformity. A room's performance can also be

---

<sup>1</sup> Acoustics - Measurement of sound absorption in a reverberation room.

<sup>2</sup> Sound power levels of noise sources. Part 3: Engineering methods for determination of sound power levels for sources in special reverberation test rooms.



benchmarked by measuring the absorption of materials that have been previously tested in other laboratories.

## 2. Aims

The main aim of the Reverberation Room calibration was to improve the Room's acoustic characteristics so that accurate absorption measurements could be carried out. This was to be achieved by:

1. Improving the diffusivity. This was identified as critical to the validity and repeatability of absorption measurements.
2. Improving the reverberation times. The aim was to move the normalised times closer to the limits as specified in the international standard ISO 3743:1988 - especially in the frequency band of interest (300Hz).
3. Improving the sound field uniformity.
4. Benchmarking the Room against a Telarc registered room. This would be done by comparing the absorption of a test specimen in the registered room and in the Reverberation Room.

## 3. Theory

### 3.1 Calculation of absorption, ISO 354:1988

$$\alpha = 55.3 \frac{V}{cA} \left( \frac{1}{T_2} - \frac{1}{T_1} \right) \quad (3.1)$$

$\alpha$  = absorption coefficient.

$V$  = volume of empty Reverberation Room, m<sup>3</sup>.

$c$  = speed of sound in air (343m/s).

$A$  = area of test specimen, m<sup>2</sup>.

$T_1$  = reverberation time of empty Reverberation Room (s).

$T_2$  = reverberation time of Reverberation Room with test specimen present (s).

### 3.2 Calibration of reverberation rooms

An in-depth study was carried by Warnock (1983) on the practical aspects of absorption measurements in reverberation rooms. He carried out a series of computer controlled measurements of absorption coefficients in a single reverberation room of similar size and shape to the Reverberation Room. He discovered that it was not possible to meet ASTM

C423-81<sup>3</sup> diffusivity requirements in the room with only fixed diffusers. Several microphone positions were required for precise measurements. He found strong variations in reverberation time with position in the room, especially at low frequencies. It was concluded that ISO 354 met the requirements for precise reverberation time measurements by specifying multiple source, absorber and microphone positions.

## 4. Equipment

### 4.1 Reverberation Room

#### 4.1.1 Dimensions

See Figure 4.1 for the Room's size and shape. Table 4.1 shows the area and volume of the original and refurbished rooms.

**Table 4.1 Reverberation Room areas and volume.**

	<b>Original Room</b>	<b>Refurbished Room</b>
Floor area (m <sup>2</sup> )	59.7 +/- 0.1	60.1 +/- 0.1
Total surface area (m <sup>2</sup> )	266.9 +/- 0.7	270.5 +/- 0.6
Room volume (m <sup>3</sup> )	215.7 +/- 0.7	216.8 +/- 0.7

#### 4.1.2 Refurbishment

The Reverberation Room was refurbished to improve its acoustic performance. The floor was levelled with a self levelling compound. This was done so that the test specimen would lie flat on the Room's floor. An observation window was removed and bricked up as it was thought that sound was being transmitted through the window. An air conditioning duct was removed and all surfaces in the Room were repainted, Figure 4.1 and Figure 5.1 (b).

<sup>3</sup> Standard test method for sound absorption and sound absorption coefficients by reverberation room method.

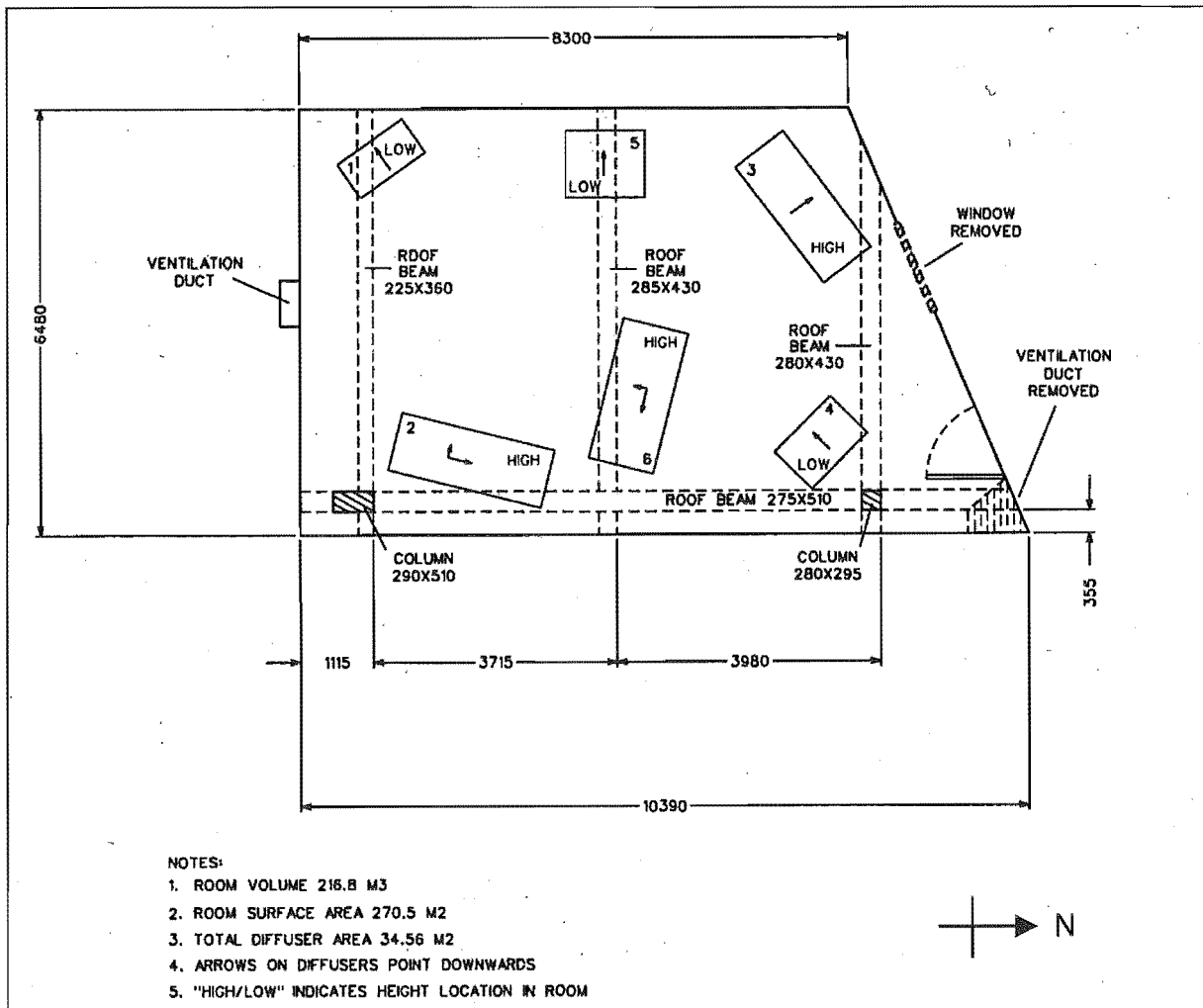


Figure 4.1 Reverberation Room dimensions, modifications and diffuser locations.

## 4.2 Diffusers

International standard, ISO 354-1985 recommends diffusers:

1. Using damped sheets with low absorption.
2. Having a mass/unit area of greater than 5kg/m<sup>2</sup>.
3. With a size range of 0.8-3 m<sup>2</sup> (on one side).
4. Having an area (both sides) 15-25% of the total surface area in rectangular rooms.

Six diffusers were made from 1200 by 2400 by 12 mm medium density fibreboard (MDF) laminated between two galvanised steel sheets (22 gauge); MDF edges were sealed with paint. The diffusers were attached to steel rope through three eyelets and wire clamps. The steel rope ran through hooked dynabolts in the ceiling and walls to fix the diffuser's height and angle in the Room, Figure 4.1. Each diffuser's area was 2.88 m<sup>2</sup> on one side (5.76m<sup>2</sup> on both sides).

**Table 4.2 Diffuser area percentages.**

	University of Canterbury	ISO 354 Recommendation	RMIT*	NRCC**
Total diffuser area / Total Room surface area	12.8 %	15-25%	12.8 %	8.2%

\* Royal Melbourne Institute of Technology.

\*\* National Research Council Canada, Warnock (1983).

The diffusers used ( $17.4 \text{ kg/m}^2$ ) were heavier than recommended by ISO 354:1988 ( $5 \text{ kg/m}^2$ ) to reduce the effect of panel resonances. This was important as the diffusers were supported at three points by flexible steel wire. Diffusers with a large area were used ( $2.88 \text{ m}^2$ ) to ensure that low frequency sound waves were interrupted. Six diffusers were added to the room – three located high and three located low. Each diffuser was placed at random angles in the Room but avoiding 30 and 45 degree standing wave reflections. Six diffusers were used as this represented a total diffuser area, 12.8% of the total Room surface area. ISO 354:1988 recommends 15-25% area ratio for rectangular rooms. The Reverberation Room has one angled wall and so a smaller area ratio was chosen. The area ratio used is also the same used at RMIT\* and more than the ratio used at NRCC\*\*, both of which were comparable in volume and surface area to the Reverberation Room.

### **4.3 Modular precision sound analyser, Type 2260B.**

This is a Bruel and Kjaer hand held, battery operated, two channel instrument comprising hardware and embedded operating system software. It meets IEC and ANSI type 1 sound level meter standards.

Enhanced Sound Analysis Software, type BZ 7202 was used for pressure level measurements. Building Acoustics Software, type BZ 7204 was used for reverberation time measurements, with the settings of Table 4.3.

A pre-polarised free field  $\frac{1}{2}$ '' microphone, type 4189 was used. Calibration was achieved by Internal "charge injection" along with external calibration via a Sound Level Calibrator, type 4231.

**Table 4.3 Software settings**

$\frac{1}{3}$ Octave	On
Autorange	On
Manual range	29.7-111.7 dB
Escape time	10s
Buildup time	10s
Autostore	On
No. of decays	2
Decay time	18s (empty Room) 12s (when testing absorbers).
Internal generator	Pink
SI corr	Random
Calibration level	94.0 dB re 20 $\mu$ Pa
Sensitivity	Nominally -25.9 re 1V/Pa

#### **4.4 JBL EON Power 10**

A 110W portable speaker and amplifier (tilted at 30 degrees).

#### **4.5 Sound intensity analyser, Type 4433**

The sound intensity analyser is a Bruel and Kjaer portable, battery operated instrument designed to measure sound pressure level, particle velocity level and sound intensity level in single octave bands. It fulfils IEC 651 type 1 requirements.

The intensity analyser was used with a sound intensity probe, type 3520, to measure sound intensity levels. Two pre-polarised, phase matched, free field  $\frac{1}{2}$ " microphones, type 4183 were connected to the intensity probe with a 12 mm spacer. External calibration was achieved with a piston-phone, type 4220.

#### 4.6 Materials for calibration

**Table 4.4 Calibration materials.**

Material	Mass	Thickness	Flow resistivity
Foam SPF	29 kg/m <sup>3</sup>	25 mm	13820 mks rayls/m
Tedlar™ film	56.4 g/m <sup>2</sup>	37.5 μm	Impervious
Aluminium foil	70 g/m <sup>2</sup>	120 μm	Impervious

SPF foam is an open cell flexible polyurethane foam of the polyether type. It typically has 35–40 cells per 25 mm and a density of 27–29 kg/m<sup>3</sup>.

## 5. Procedures

### 5.1 Diffusivity

#### 5.1.1 Intensity

Sound intensity measurements were made in the Reverberation Room with the Sound Intensity Analyser probe 1.5m from the floor in six microphone directions (north, south, east, west, up and down) in the positions shown in Table 5.1. The measurements were repeated for each microphone direction. Pink noise, generated by the 2260 sound analyser, was played through the JBL speaker which was tilted at approximately 30 degrees. Tests were carried out in the original Room and in the refurbished Room, with and without diffusers. The Intensity Analyser's autorange and autoscan functions were used along with a 2s averaging time.

**Table 5.1 Intensity measurements - speaker and microphone locations.**

Original Room		Refurbished Room	
Speaker	Mic.	Speaker	Mic.
Pt 14 Northwest	Pt 20	Pt 17 North	Pt 6
		Pt 38 South	Pt 30

See Figure A.1 in Appendix A for the point locations in the Room.

### 5.1.2 Diffuser installation

Diffusers were installed in the Reverberation Room according to the procedure outlined in Annex A of ISO 354-1985. Sound absorption measurements were carried out, as in section 5.4, on a foam test specimen:

- i. without diffusers in the Room;
- ii. with one stationary diffuser in the Room; and
- iii. with increasing quantities of diffusers (up to six diffusers).

The test specimen comprised 125 mm of polyurethane foam. See Figure A.2 in Appendix A for its absorption characteristics. Figure 4.1 shows the diffuser positions in the Room. Average absorption coefficients were calculated for the range, 500 to 4000Hz, for each diffuser installed. A plot of mean absorption versus diffuser area should approach a maximum and thereafter remain constant with increasing diffuser area (ISO 354:1988). The optimum number of diffusers is obtained at the point where the mean absorption reaches a constant value.

### 5.1.3 Variation of reverberation times

The 2260 sound analyser, building acoustics software and JBL speaker were used to measure reverberation times in the Reverberation Room. The 2260 analyser was calibrated externally and internally before each set of measurements. Measurements were made at a variety of speaker and microphone locations within the Room as shown in Table 5.2. See Figure A.1 in Appendix A for point locations in the Room. The noise level was nominally 85 dB(A). Reverberation times were measured with the microphone at 1m and 1.5m from the floor for each speaker and microphone combination.

**Table 5.2 Reverberation time speaker and microphone locations.**

Original Room		Original Room + four diffusers		Refurbished		Refurbished + six diffusers	
Speaker	Mic	Speaker	Mic	Speaker	Mic	Speaker	Mic
Pt 6 East	Pt 19	Pt 6 East	Pt 19	Pt 6 East	Pts 2, 17, 33	Pt 6 East	Pts 2, 17, 33
Pt 9 Northwest	Pt 14	Pt 9 Northwest	Pt 14	Pt 9 Northwest	Pts 35, 19, 4	Pt 9 Northwest	Pts 19, 4
Pt 19 North	Pt 14	Pt 19 North	Pt 14	Pt 29 South	Pts 6, 21, 37	Pt 29 South	Pts 6, 21, 37
Pt 38 South	Pt 12	Pt 38 South	Pt 12	Pt 11 North	Pts 39, 24	Pt 11 North	Pts 39, 24
		Pt 13 West	Pt 22				
		Pt 16 South	Pt 36				
		Pt 6 East	Pt 19				

See Figure A.1 in Appendix A for the point locations in the Room.

## 5.2 Reverberation

Average reverberation times were calculated, for the original and refurbished Room, from the positions in Table 5.2.. These were normalised according to ISO 3743:1988.

## 5.3 Uniformity

Sound pressure levels were measured in the refurbished Room with six diffusers installed. The 2260 analyser was used to generate pink noise and to measure 15s  $L_{eq}$  pressure levels. The JBL speaker and amplifier were used to produce a nominal sound pressure of 85 dB(A). Pressure levels were measured at 1m and 1.5m heights in seven positions throughout the Room.

## 5.4 Benchmark

The absorption coefficients of four different specimen were measured in a Telarc registered laboratory in Auckland. These specimen were then tested in the Reverberation Room.

The 2260 sound analyser, building acoustics software and JBL speaker were used to measure reverberation times in the Room, with and without the test specimen present. The 2260 analyser was calibrated externally and internally before each set of measurements. A variety of speaker and microphone positions were used within the Room as shown in Table 5.3. The JBL amplifier and speaker was set to produce approximately 85 dB(A). Reverberation times were measured with the 2260 analyser's microphone at 1m and 1.5m heights for each speaker and microphone combination. Two reverberation decays were measured at each microphone height. A total of 12 reverberation decays were measured for each test specimen.

**Table 5.3 Benchmark speaker and microphone positions**

Speaker	Microphone
Pt 4 South	Pt 23
Pt 17 East	Pt 6
Pt 38 Northwest	Pt 30

See Figure A.1 in Appendix A for the point locations in the Room.

Each test specimen was placed on the Room's floor and enclosed by a 20x25 mm medium density fibreboard (MDF) frame, Figure 5.1 (a, b). Absorption coefficients were calculated from the averaged reverberation times of the empty Room, averaged reverberation times with a test specimen present, specimen area and Room volume according to ISO 354:1988.



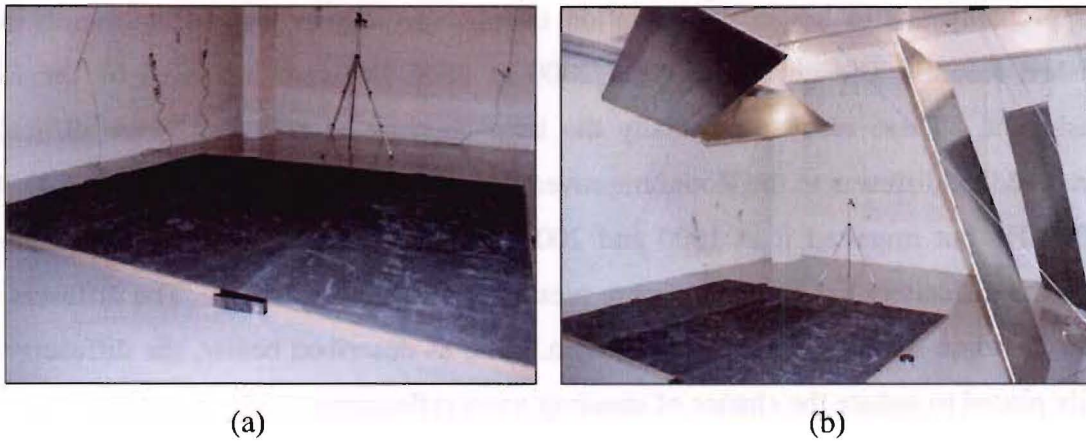


Figure 5.1 Test specimen - Bonded foil on foam (foam up) in (a) refurbished Room, (b) refurbished Room with diffusers.

## 6. Results and Discussion

### 6.1 Diffusivity

#### 6.1.1 Intensity

It was difficult to draw any general conclusions from the intensity results. Refurbishing the Room seems to have improved the diffusivity at 125, 500 and 1000 Hz; as seen by smaller deviations in intensity, Figure 6.1.

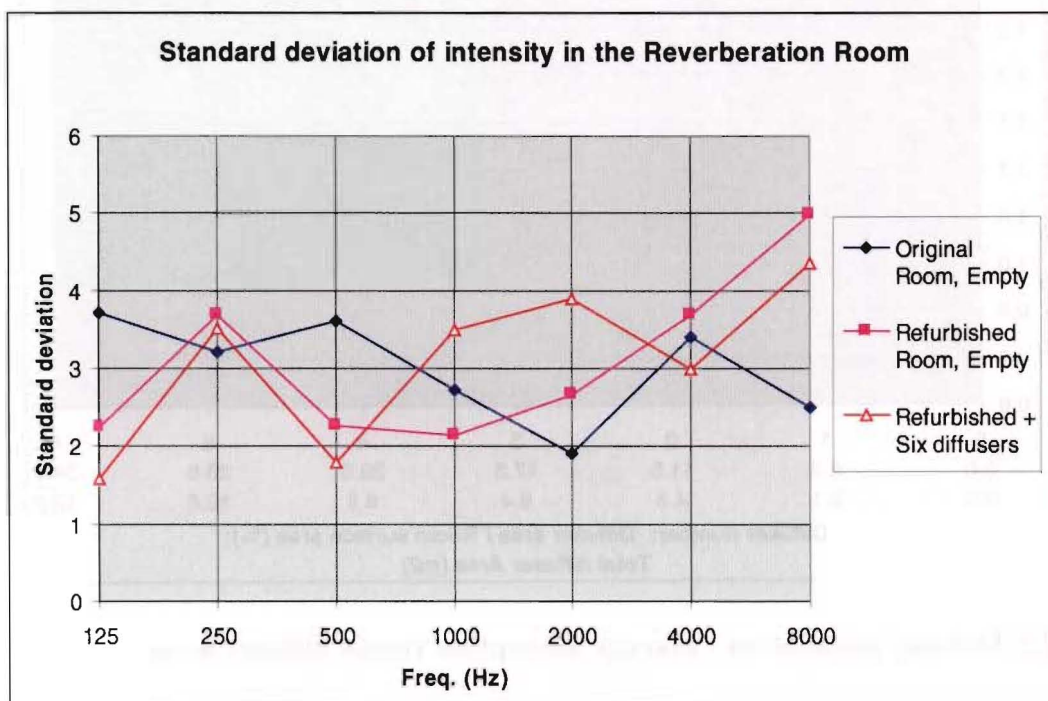
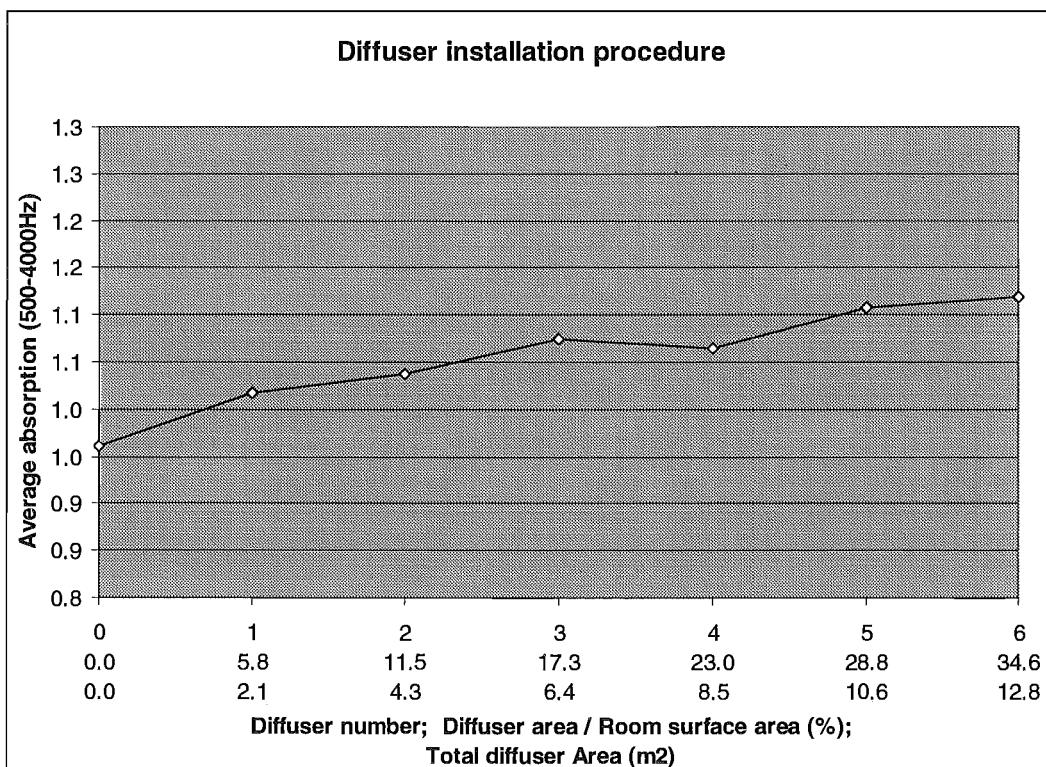


Figure 6.1 Standard deviation of intensity in the Reverberation Room.

This is probably due to longer reverberation times, especially at lower frequencies, in the refurbished Room. The deviations from 2000 to 8000 Hz were increased by the Room refurbishment. These results, especially the large increase at 8000 Hz, were difficult to explain. Adding diffusers to the Room improved the diffusivity further at 125, 250, 500, 4000 and 8000 Hz but impaired it at 1000 and 2000 Hz. The addition of diffusers seemed to improve the diffusivity but anomalies were present at 1000 and 2000 Hz. The diffusers may have set up some standing waves in the Room. But, as described below, the diffusers were carefully placed to reduce the chance of standing wave reflections.

### 6.1.2 Diffuser installation

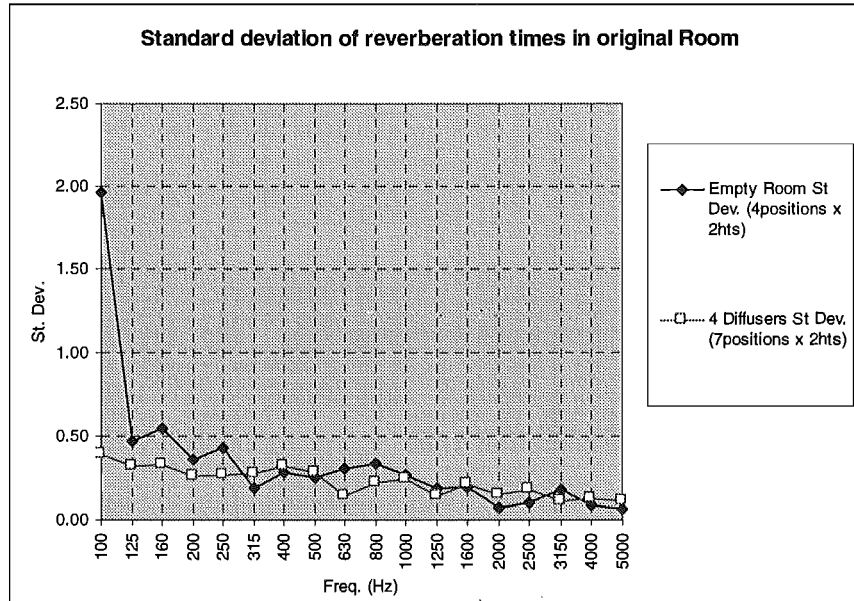
It would appear that the characteristic absorption peak occurred with three to four diffusers, Figure 6.2. However, it is clear that with the addition of diffusers five and six that the absorption increased further. The individual frequency versus diffuser area plots, Figure A.3 (a) to (c) in Appendix A, show that the secondary increase is due to absorption in the 630 to 1000 Hz and 2500 to 4000 Hz frequency bands. These results would indicate that one to two more diffusers are required to reach maximum absorption.



**Figure 6.2 Diffuser installation - average absorption versus diffuser area.**

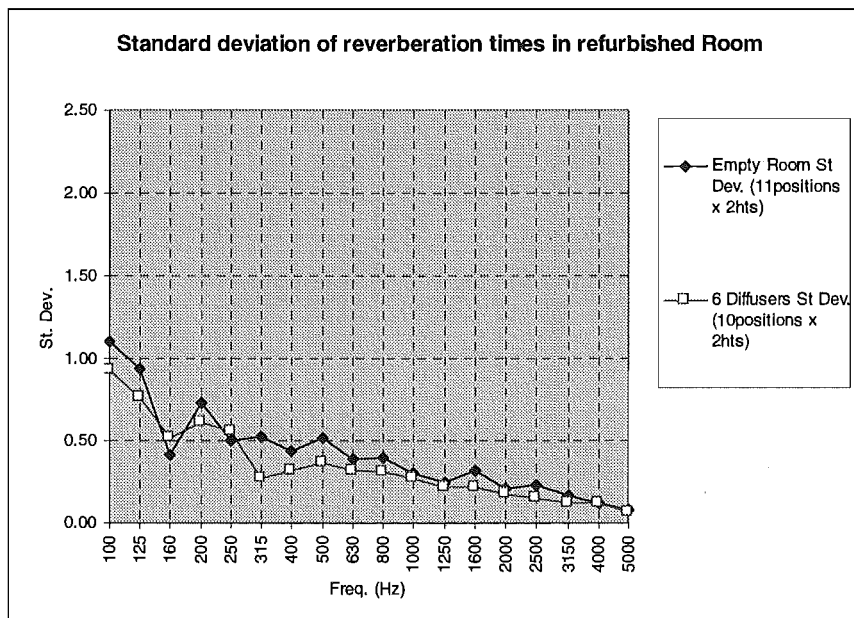
### 6.1.3 Reverberation time variation

Figure 6.3 shows that the addition of four diffusers to the original Room had the most effect at lower frequencies (100-250 Hz). The diffusers vastly improved the Room's performance at low frequencies. This was due to the large size of the diffusers used.



**Figure 6.3 Standard deviation of reverberation times in original Room.**

Addition of six diffusers to the refurbished Room decreased the variation in reverberation time in the 100 to 125 Hz and 315 to 5000 Hz frequency ranges, Figure 6.4. However, between 160 and 250 Hz the deviations were quite similar. The diffusers have improved the Room's performance across most of the frequency range.



**Figure 6.4 Standard deviation of reverberation times in, (a) original Room; (b) refurbished Room.**

The refurbished Room's variation in reverberation times were generally higher than in the original room. This is thought to be due to a larger number of measurements made in the refurbished Room (10 to 11 positions) than in the original Room (4 and 7 positions). The increase in variation towards lower frequencies may be due to the variation of a function of a random variable being greater at lower frequencies. A similar trend is apparent in the standard deviation of pressure levels in the refurbished Room, section 6.3. These results would indicate that the Reverberation Room is less diffuse at frequencies lower than 315 Hz.

## 6.2 Reverberation

Refurbishing the Room dramatically increased the amount of reverberation at low frequencies but had a lesser effect at high frequencies, Figure 6.5. The refurbishment significantly increased the normalised times below 1000 Hz and decreased those above 1000 Hz, Figure 6.6. The large increases in reverberation time at low frequencies were attributed to the removal of the observation window and ventilation duct. Painting the Room's surfaces would account for the increase in times at mid to high frequencies. It can be seen that with diffusers present, the 100 to 160 Hz and 1000 to 1250 Hz frequency bands meet ISO 354:1988 requirements. However, it is clear that the other frequency bands do not fit within the standard's limits. Meeting the standard's requirements does not appear to be critical for the Room's performance, as seen by the benchmark results, section 6.4.

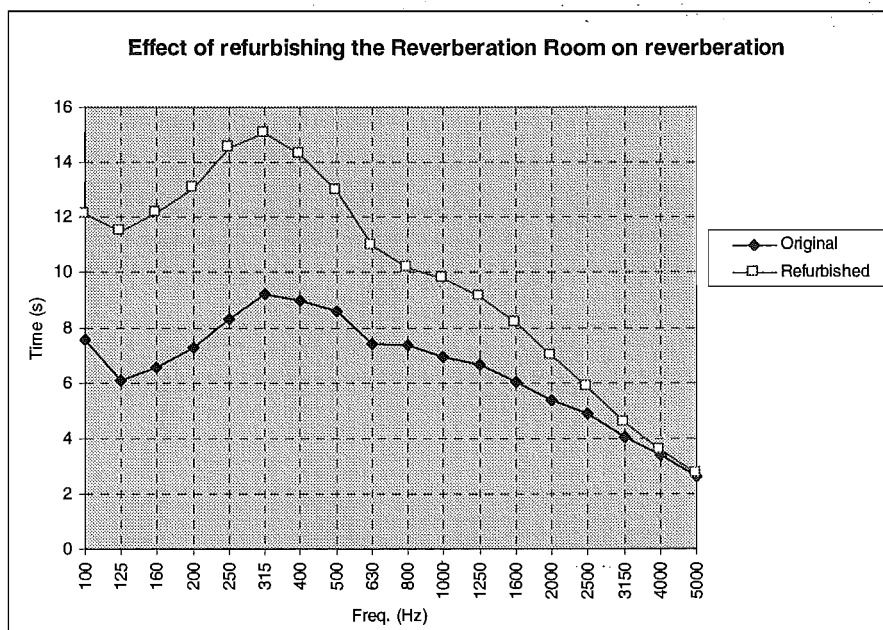


Figure 6.5 Reverberation times in the original Room and the Refurbished Room.

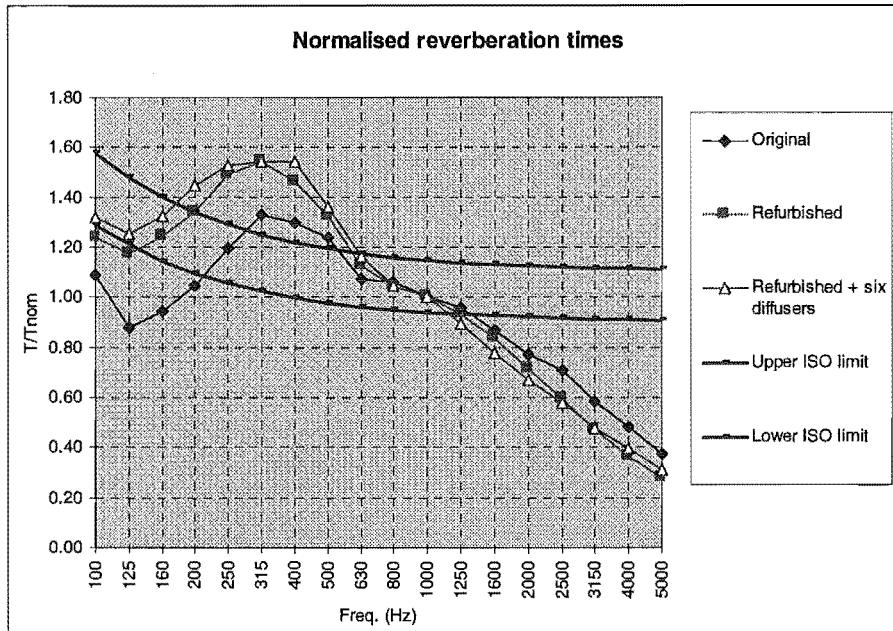


Figure 6.6 Normalised reverberation times in the original Room and refurbished Room.

### 6.3 Uniformity

The sound field uniformity is seen by the standard deviation of sound pressure in the Reverberation Room, Figure 6.7. The general increase of standard deviation with lower frequencies was again thought to be due to the variation of a function of a random variable increasing with lower frequencies. However, it does appear that the Room was less uniform at frequencies lower than 250 Hz.

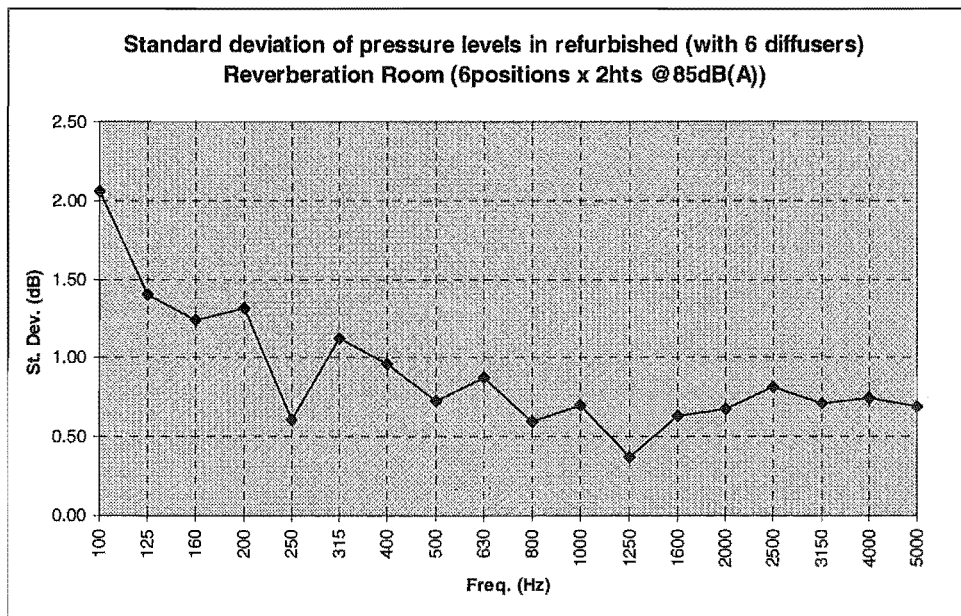


Figure 6.7 Variation of pressure levels in the refurbished Reverberation Room.

### 6.4 Benchmark

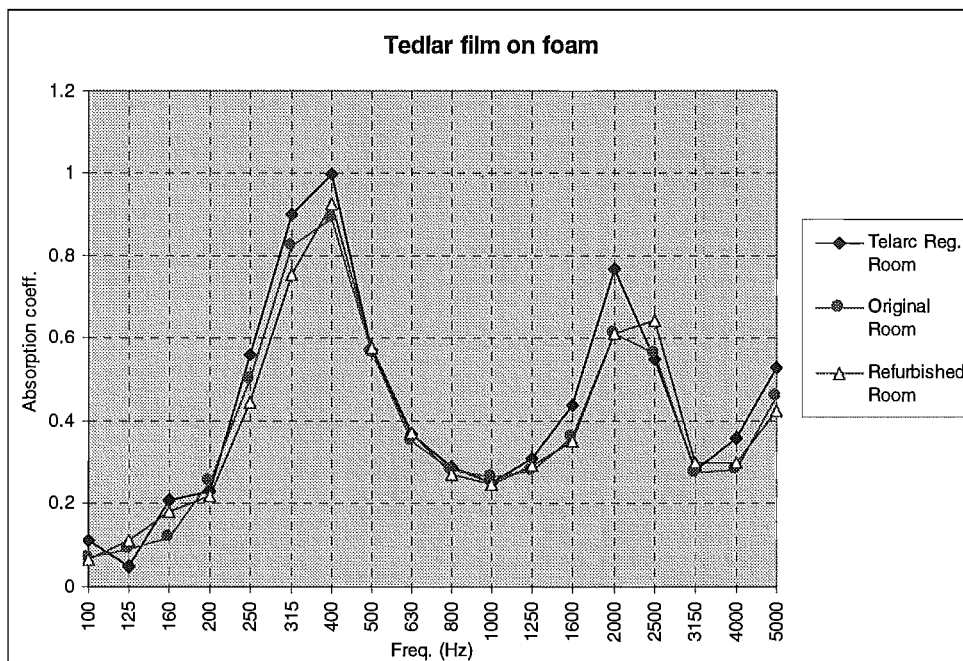


Figure 6.8 Benchmark absorption test for Tedlar™ film on foam.

The benchmark tests show very good comparison between the University of Canterbury, Department of Mechanical Engineering’s Reverberation Room and the Telarc registered Room. The test on Tedlar™, Figure 6.8, shows a very similar trend in absorption with approximately 10-15% difference between the results. For the most part the differences were less than 10%.

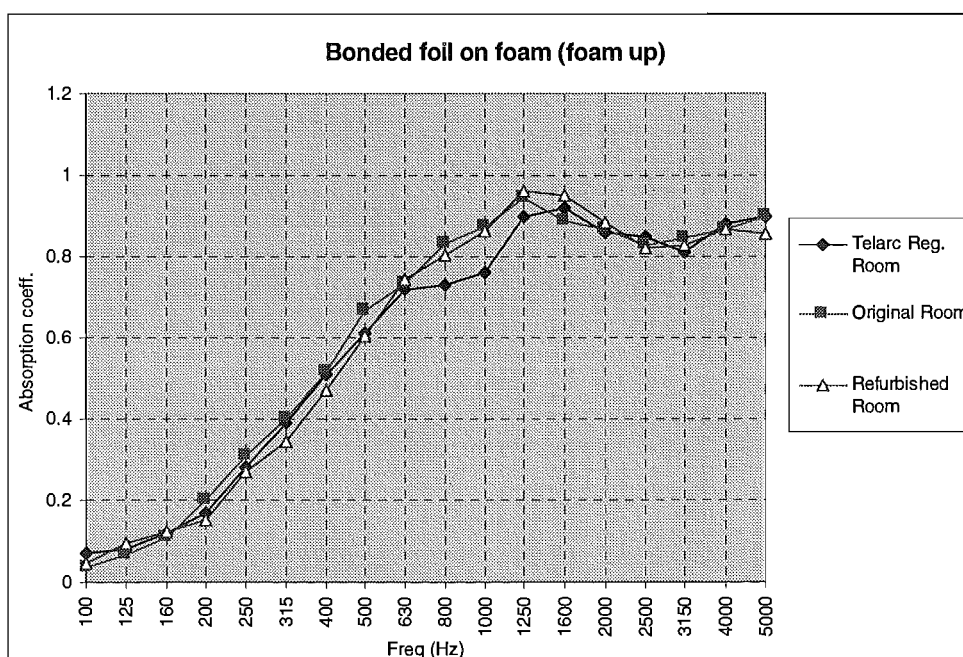


Figure 6.9 Benchmark absorption test for Bonded foil on foam (foam up).

The Bonded foil test, Figure 6.9, shows even closer results. The refurbished Room was at worst 10% different from the registered laboratory but was generally less than 5% different. The differences in results between the two laboratories will in part be due to different test specimen conditions. The specimen were rolled up for transport between laboratories and held some of this curvature in testing, Figure 6.10. The refurbished Room with diffusers gave very similar results to the original Room over the whole frequency range and in both tests. This gave a large amount of confidence in the absorption measurement procedures.



**Figure 6.10** Effect of curvature on test specimen.

## 7. Conclusions

In conclusion, it is clear that the Reverberation Room has been successfully calibrated. Its sound field diffusivity, reverberation and uniformity have been qualified and have improved with the Room's refurbishment. Reverberation time and sound pressure variations indicated poorer performance at lower frequencies but the benchmark tests showed good performance in all frequencies. Absorption tests in the Room were very repeatable and reliable.

## References

ISO 354:1988, "Acoustics - Measurement of sound absorption in a reverberation room", ISO, International Organisation for Standardisation, Switzerland, 1988.

Warnock, A.C.C. (1983), "Some practical aspects of absorption measurements in reverberation rooms", J. Acoust. Soc. Am., v74, 1983:1422-1432.



---

# 3

## Absorber Materials

---

### Summary

This chapter focuses on specifying fabrics, bulk porous absorbers and impervious films as acoustic absorbers. These materials have been tested in various combinations to determine their absorption characteristics – reported in chapter 4, Absorption Testing. To specify and compare the porous materials tested, it was necessary to measure their flow resistance. This is one of the single-most important acoustical parameters that characterises a porous material. It is simply the static pressure drop ( $N/m^2$ ) across a material divided by an air velocity (m/s) through the material. Apparatus was built to measure the flow resistance of fabrics, foams and fibrous materials. It has produced measurements with a repeatability of 5%. The fabrics and foams tested were inhomogeneous, giving variations from 17 to 32%. The fabrics had relatively low flow resistance, 5 to 67 mks rayls while the foams covered a range of flow resistance. It was found that the amount of reticulation, or number of closed cells, directly affected the flow resistivity (flow resistance normalised to thickness) of the foams. Crushing the foam, reduced the amount of reticulation, and hence reduced the flow resistivity. The fibreglass board tested had the largest flow resistivity (47000 mks rayls/m) and was closest to the theoretical optimum (51500 mks rayls/m at 24 mm). The flow resistance of a range of materials has been successfully measured with the new apparatus.

## Table of Contents

<b>Table of Contents.....</b>	<b>x</b>
<b>List of Figures .....</b>	<b>xi</b>
<b>List of Tables.....</b>	<b>xi</b>
<b>1. Introduction.....</b>	<b>32</b>
<i>1.1 Absorption.....</i>	<i>32</i>
<i>1.2 Parameters.....</i>	<i>32</i>
<b>2. Aims .....</b>	<b>32</b>
<b>3. Theory.....</b>	<b>33</b>
<i>3.1 Flow resistance .....</i>	<i>33</i>
<b>4. Equipment .....</b>	<b>33</b>
<i>4.1 Materials .....</i>	<i>33</i>
<i>4.2 Flow resistance Test Rig .....</i>	<i>34</i>
<i>4.3 Annubar calibration.....</i>	<i>36</i>
<b>5. Procedure.....</b>	<b>36</b>
<i>5.1 Annubar calibration.....</i>	<i>36</i>
<i>5.2 Flow resistance tests .....</i>	<i>37</i>
<b>6. Results and Discussion.....</b>	<b>37</b>
<i>6.1 Calibration.....</i>	<i>37</i>
<i>6.2 Fabrics .....</i>	<i>39</i>
<i>6.3 Bulk materials .....</i>	<i>40</i>
<b>7. Conclusions.....</b>	<b>42</b>
<b>References .....</b>	<b>43</b>
<b>Bibliography .....</b>	<b>43</b>

## List of Figures

<u>Figure No.</u>	<u>Page</u>
Figure 4.1 Zoomed view of crushed CMSG, (a); polyester board, (b); and fibreglass, (c).....	34
Figure 4.2 Flow resistance Test Rig, (a); enlargement of pipe section, (b); enlargement of annubar, (c).....	35
Figure 4.3 Annubar calibration .....	36
Figure 6.1 Fabric flow resistance. ....	39
Figure 6.2 Flow resistance of 23 mm and 46 mm CMSG. ....	40
Figure 6.3 Homogeneity test. ....	41

## List of Tables

<u>Table No.</u>	<u>Page</u>
Table 6.1 Flow resistance results .....	38

## **1. Introduction**

### **1.1 Absorption**

Porous materials, such as glass wools, foams and fabrics are commonly used to absorb sound. Typical examples of these materials include carpet, curtains and thermal insulation. They typically consist of a network of interlocking pores that convert incident sound energy into heat. Fibreglass has frequently been used for its absorption qualities. Recently, its adverse health effects have prompted a move toward other materials such as polyurethane foams, fibrous polyester boards and woollen blankets. Fibreglass can be encapsulated but this generally reduces its sound absorption. An acoustic material's worth depends not only on its absorption but also on its fire resistance, cost and health risk. Much research has been carried out on fibreglass based absorbers and their combination with perforated fibreboard. This study focused on polyurethane foams, and to a lesser extent polyester boards, in combination with impervious films and fabrics.

### **1.2 Parameters**

An acoustic material can be described by many parameters based on its physical properties. Density and thickness are two very basic but critical parameters used to describe these materials. More specialist acoustic parameters include porosity, flow resistance and stiffness. Of these, the flow resistance is considered the most characteristic of a porous material's acoustic absorption. It is also critical to the theoretical modelling of porous materials. Hence, apparatus was built to measure the flow resistance of porous materials such as foams and fabrics.

## **2. Aims**

The aims of the Materials study were to:

1. Establish important materials for use as absorbers (covered some-what in the Absorber Survey).
2. Investigate novel combinations of materials as absorbers.
3. Quantify the important acoustic parameters used to describe materials.

## 3. Theory

### 3.1 Flow resistance

The steady flow resistance of a porous layer is defined as the ratio of static pressure drop across the layer to mean velocity of flow through the layer. It is usually implied that the velocity is low enough so that the pressure drop is proportional to the velocity. Flow resistance is usually quoted in mks rayls (or  $\text{Ns/m}^3$ ). Flow resistivity is quoted in mks rayls per metre (or  $\text{Ns/m}^4$ ). Porous materials typically have a flow resistivity of 20,000 mks rayls/m.

At a microscopic scale, the flow resistance is determined by the equivalent width between fibres or pores and the number of these per unit area. In oscillatory flow, as is the case for sound waves, the pressure drop contains a component proportional to the velocity and also a component proportional to the acceleration. This second component becomes apparent in flow resistance measurements at higher velocities.

## 4. Equipment

### 4.1 Materials

#### 4.1.1 Fabrics

The three main fabrics used were Hessian, Charade and Spotlight. These fabrics were chosen more for their aesthetic value than acoustic characteristics. However, it will be shown in the Absorption Testing chapter that these fabrics can significantly improve the performance of bulk porous layers such as foams or fibrous boards. Other fabrics, named Fabric A, B and C, were used for comparing the Test Rig to another flow resistance apparatus.

The Hessian fabric was a rather open weave material with a surface density of  $275 \text{ g/m}^2$ . Charade was made of 100% polypropylene. Spotlight consisted of 92.5% wool and 7.5% viscose, with a surface density of  $265 \text{ g/m}^2$ .

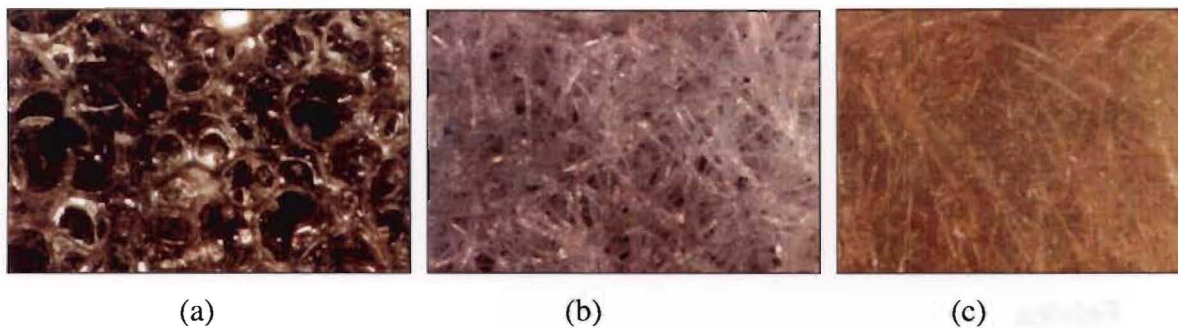
#### 4.1.2 Bulk materials

SPF foam is an open cell flexible polyurethane foam of the polyether type. It typically has 35–40 cells / 25 mm and a density of  $27\text{--}29 \text{ kg/m}^3$ . CMSG is a combustion modified foam based on the SPF foam. It is partially reticulated, meaning that some of its cells are closed,

and is loaded with melamine, Figure 4.1 (a). CMSG typically has 36-38 cells / 25 mm and a density of  $43 \text{ kg/m}^3$ . CMSG(c) refers to crushed CMSG foam. This foam had been run through nip-rollers to reduce the amount of closed cells. Otherwise it was exactly the same as standard CMSG foam.

The polyester board comprised many polyester fibres of varying density, Figure 4.1 (b). An average fibre density has been taken as  $1380 \text{ kg/m}^3$ . The board had a standard density of  $80 \text{ kg/m}^3$ .

The fibreglass board was tightly packed with a density of  $90 \text{ kg/m}^3$ , Figure 4.1 (c). The fibre density was taken as  $2600 \text{ kg/m}^3$ . Fibreglass board was included as it has been used extensively as a thermal insulator and acoustic absorber. It has been the object of indepth study but can pose a health problem when fibres are inhaled or touched. Hence it was used to compare against the other bulk materials mentioned above.



**Figure 4.1** Zoomed view of (a) crushed CMSG, (b) polyester board, and (c) fibreglass.

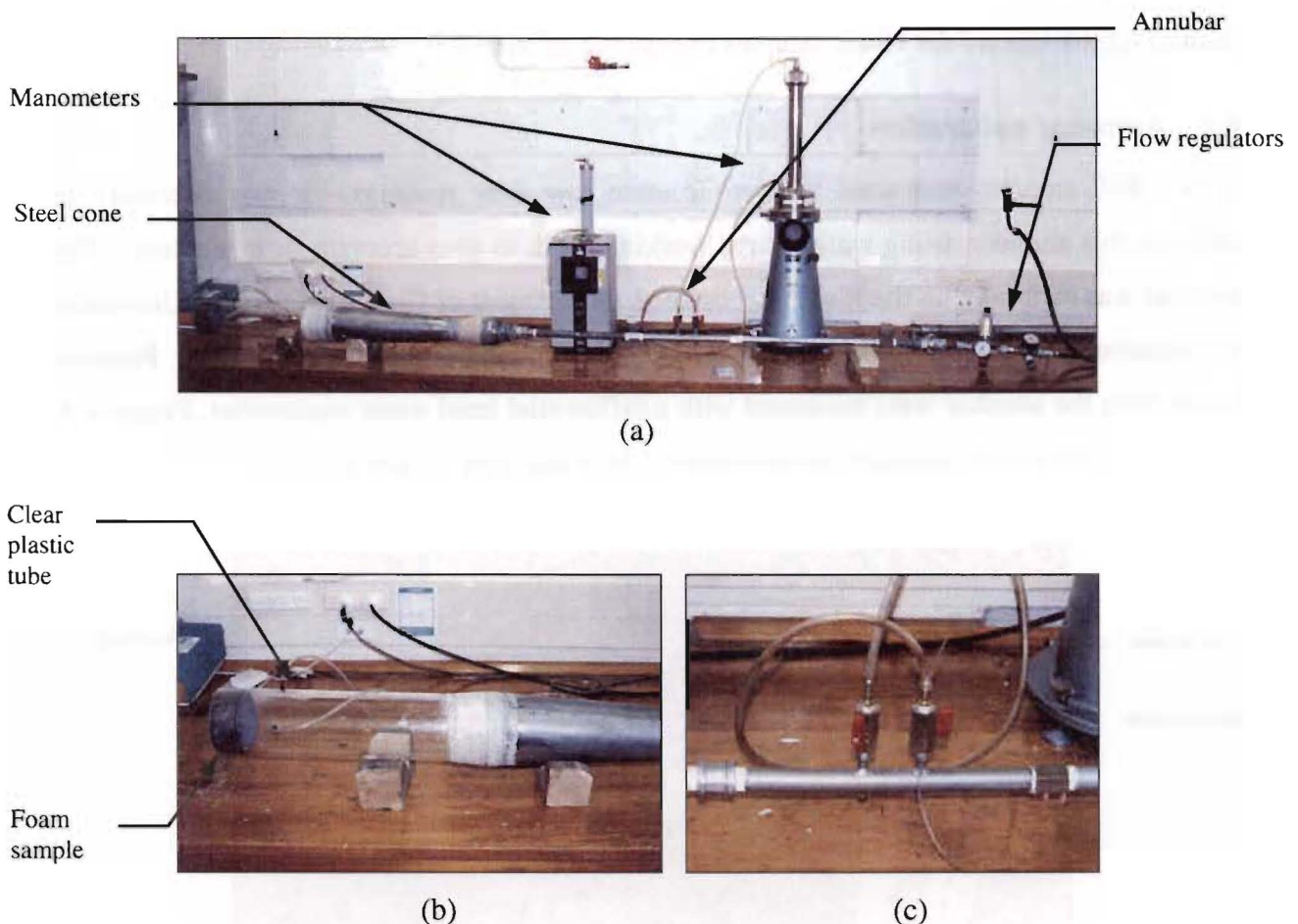
#### 4.1.3 Films

The impervious films used were made from Mylar™, Bonded foil and PVC. Mylar™ is a thin metallised polyester film. A range of film thicknesses and corresponding surface densities were used. Bonded foil is made of  $7 \mu\text{m}$  aluminium foil backed by a high density polyethylene mesh. It was  $120 \mu\text{m}$  thick with a surface density of  $70 \text{ g/m}^2$ . The PVC film was a relatively thick and heavy material. It had a surface density of  $1000 \text{ g/m}^2$ . The films used had a range of surface densities,  $35 \text{ g/m}^2$ ,  $140 \text{ g/m}^2$  and  $1000 \text{ g/m}^2$ ; covering approximately two orders of magnitude.

## 4.2 Flow resistance Test Rig

The Test Rig was built in the Department of Mechanical Engineering, University of Canterbury. The clear plastic tube used had an internal diameter of 100 mm and a wall

thickness of 5 mm. Two pressure taps, ninety degrees apart, were placed 100 mm from the open end. The pressures from these two pressure taps were combined to give the average static pressure inside the tube. A steel cone was used, as shown in Figure 4.2 (a, b), to increase the diameter from the annubar to the plastic tube. Two wire mesh screens, located at each end of the steel cone, were used as turbulence generators.



**Figure 4.2 (a) Flow resistance Test Rig, (b) enlargement of pipe section, (c) enlargement of annubar.**

#### 4.2.1 Annubar DNT-10, ½" SCH40, CB.

The annubar is a primary flow sensor designed to produce a differential pressure that is proportional to flow. The ½" model used had an internal diameter of 15 mm.

#### 4.2.2 Manometers

Two water manometers were used in the flow resistance Test Rig. One was a Betz manometer, model AVA, serial number 610132. This one was used to measure the static pressure drop across each sample. The second manometer, "Aerolab 38" - No. 4948, was used to measure the annubar pressure differentials.

### 4.2.3 Flow regulators

Two Norgren flow regulators were used in series to control and steady the air flow from the compressed air supply.

### 4.2.4 Pipe clip

A steel pipe clip was used to fasten fabric samples at the end of the pipe. The clip was secured tightly around the fabric samples to ensure a good seal.

## 4.3 Annubar calibration

A ½" BSP annubar was used to give accurate low flow readings. It was necessary to calibrate this annubar, using water as the working fluid, to give accurate flow readings. The annubar was calibrated in the Fluids Laboratory, Department of Civil Engineering, University of Canterbury. This Laboratory had the advantage of a constant head water source. Pressure levels from the annubar were measured with a differential head water manometer, Figure 4.3. Water flow rates were measured with a bucket, stopwatch and weight scales.

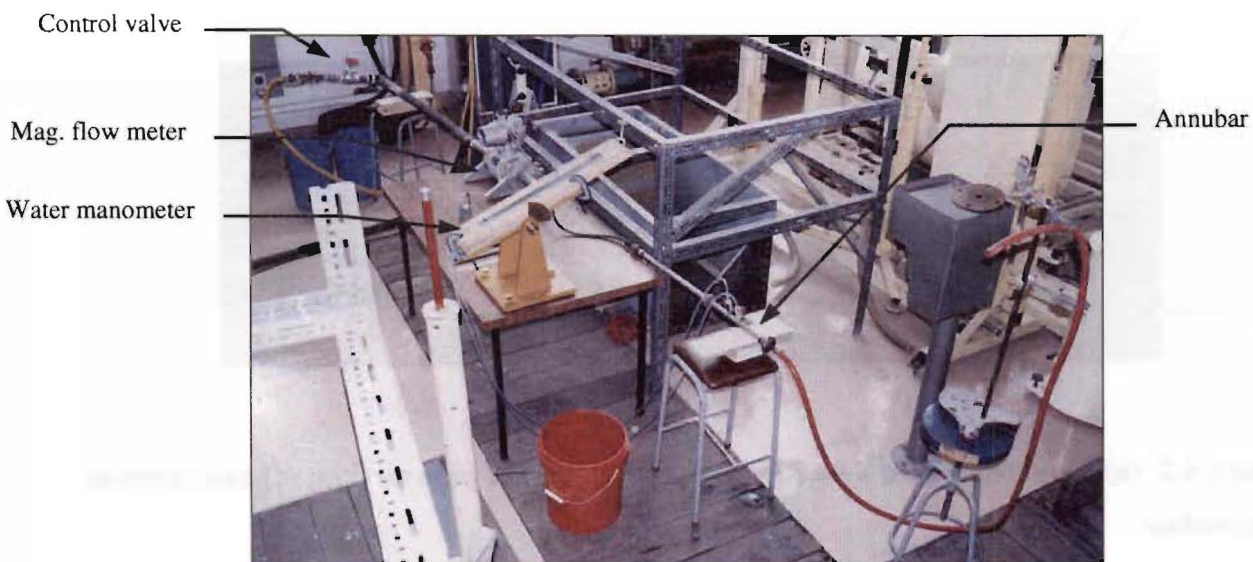


Figure 4.3 Annubar calibration

## 5. Procedure

### 5.1 Annubar calibration

Water from the constant head source was run through a control valve, magnetic flow meter, annubar and hose, Figure 4.3. Pressure levels from the annubar were measured with the differential head of water while the water flow rate was measured by the bucket and



stopwatch technique. The collected water was then weighed on scales and the water temperature checked. Pressure levels and flow rates were measured at six different flow rates. This data was graphed as water flow rate squared versus differential pressure in metres of water, see Figure B.1 in Appendix B. This comprised one test. Four tests were carried out to check the repeatability of the calibration procedure. Finally, the calibration was then converted to air, Figure B.2 in Appendix B.

## **5.2 Flow resistance tests**

Australian standard, AS 2284.14-1979<sup>1</sup> and ASTM C522-1987<sup>2</sup> were referred to with regard to the air flow resistance tests carried out. The procedures outlined in these standards were followed.

Fabrics were mounted at the end of the pipe with a steel pipe clip. Bulk porous materials were punched out at a 102 mm diameter to ensure a good fit inside the pipe. The bulk material's edge in contact with the pipe was sealed with a gel. Typically, six flow rates and the corresponding static pressures were measured for each sample. At least two different samples from the same material were measured to average out any inhomogeneity.

Repeatability tests were carried out on two CMSG foam samples. Five samples were taken from a 1.2 x 2.4m CMSG foam sheet and tested to ascertain the amount of inhomogeneity in a sheet. Six tests were carried out on one of the fabrics to measure its inhomogeneity. Fabrics previously tested in another laboratory were measured to benchmark the flow resistance equipment and procedures.

## **6. Results and Discussion**

### **6.1 Calibration**

The fabrics tested as part of the Test Rig calibration gave fairly similar results to the independent tests previously carried out. The closest result was that of Fabric B, with a difference of 15%, while the largest difference was with Fabric C, 53%, Table 6.1. Unfortunately it was uncertain if the exact same area of the fabric sample was used as it was not marked. ASTM C522 states that the tests should give a reproducibility of approximately 15% between laboratories. Some of the differences shown are attributed to inhomogeneities

---

<sup>1</sup> Porosity air flow test for flexible cellular polyurethane.

<sup>2</sup> Standard test method for airflow resistance of acoustical materials.

within the fabrics tested. There was a 16% flow resistance variation in a small area of Fabric A and a 32% variation in the 1.2 x 2.4m CMSG foam sheet. The independent tests were quoted at 5% accuracy.

**Table 6.1 Flow resistance results**

Material	Description	Flow resistance (mks rays)	Flow resistivity <sup>3</sup> (mks rays/m)
<b>Calibration</b>			
Fabric A	University of Canterbury	1100	
	Independent laboratory	1680	
Fabric B	University of Canterbury	170	
	Independent laboratory	200	
Fabric C	University of Canterbury	80	
	Independent laboratory	170	
<b>Fabrics</b>			
Hessian	275 g/m <sup>2</sup>	5	
Charade	230 g/m <sup>2</sup>	38	
Spotlight	265 g/m <sup>2</sup>	67	
<b>Bulk materials</b>			
46 CMSG	Combustion modified foam		18400
46 CMSG (c)	Crushed, combustion modified foam		13700
23 CMSG	Combustion modified foam		9800
23 CMSG (c)	Crushed, combustion modified foam		8800
46 Polyester	Fibrous board - 80 kg/m <sup>3</sup> , 46 mm		5300
25 Polyester	Fibrous board - 80 kg/m <sup>3</sup> , 25 mm		11700
25 Fibreglass	Fibrous board - 90 kg/m <sup>3</sup> , 25 mm		47000
SPF foam	Multi-purpose foam.		13800
<b>Homogeneity Test</b>			
24 CMSG NC1	Non-crushed CMSG foam 1.		10100
24 CMSG NC2	Non-crushed CMSG foam 2.		8600
24 CMSG NC3	Non-crushed CMSG foam 3.		9000
24 CMSG NC4	Non-crushed CMSG foam 4.		12780
24 CMSG NC5	Non-crushed CMSG foam 5.		10600

<sup>3</sup> Calculated according to Forchheimer equation,  $\Delta p = aV + bV^2$ , where  $a$  and  $b$  are constants,  $\Delta p$  = static pressure drop,  $V$  = flow speed. The constant  $a$  is equal to the viscous flow resistance.

Material	Description	Flow resistance (mks rayls)	Flow resistivity (mks rayls/m)
<b>Repeatability Test</b>			
24 CMSG NC2	Non-crushed CMSG foam 2.		7420
24 CMSG NC2r	Retest on Non-crushed CMSG foam 2.		7040
24 CMSG NC4	Non-crushed CMSG foam 4.		12780
24 CMSG NC4r	Retest on Non-crushed CMSG foam 4.		12760
<b>Impervious films</b>			
		<b>Surface density (g/m<sup>2</sup>)</b>	
Mylar™	Metallised polyester film	35	
		70	
		140	
PVC	Polyvinyl Chloride	1000	
Vapastop bonded foil	Aluminium foil	70	

See Appendix B for flow resistance plots.

### 6.2 Fabrics

The fabrics tested had relatively low flow resistances, 5 to 67 mks rayls, Figure 6.1.

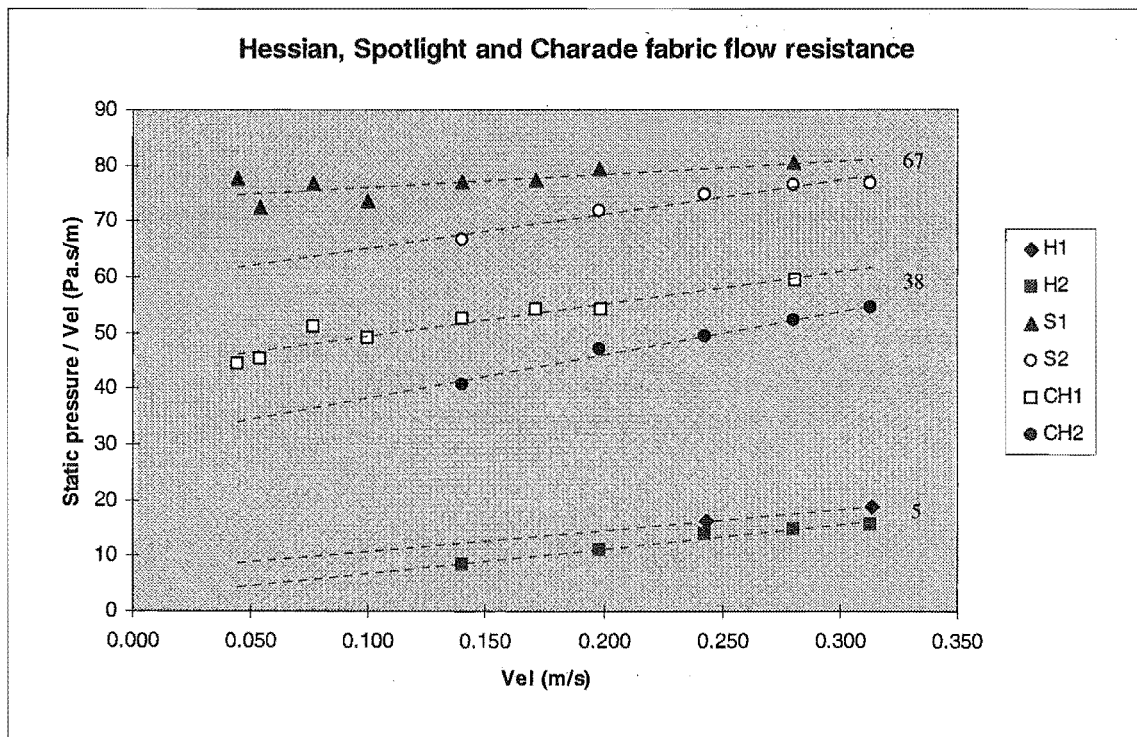


Figure 6.1 Fabric flow resistance.

However some fabrics, such as Fabric A in the calibration, had quite high flow resistance (1100 mks rays). Inhomogeneity of the fabric samples was typically within the experimental uncertainty. It has been shown by Ingard (1994), that 412 mks rays is an optimal flow resistance for fabric coverings. The closest material to this was Fabric B (170 mks rays).

### 6.3 Bulk materials

The 46 mm and 23 mm CMSG results were expected to collapse onto the same line when plotted, as the results were normalised to each sample's thickness. Similarly, this was expected for the crushed CMSG and polyester samples. This was not the case, as shown in Figure 6.2, for CMSG.

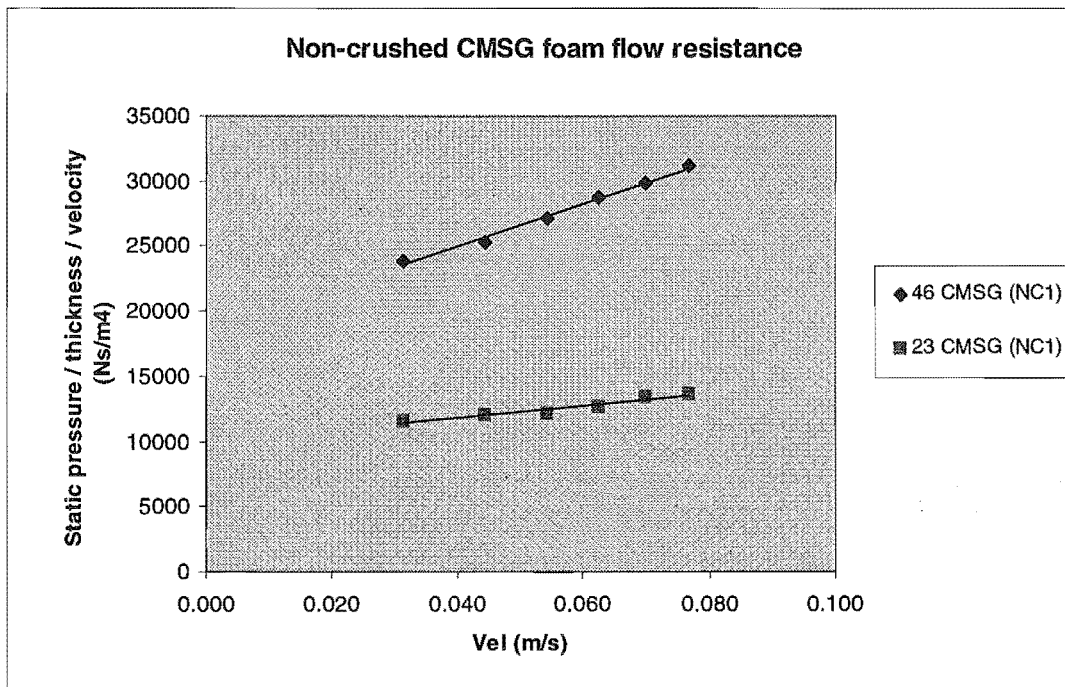


Figure 6.2 Flow resistance of 23 mm and 46 mm CMSG.

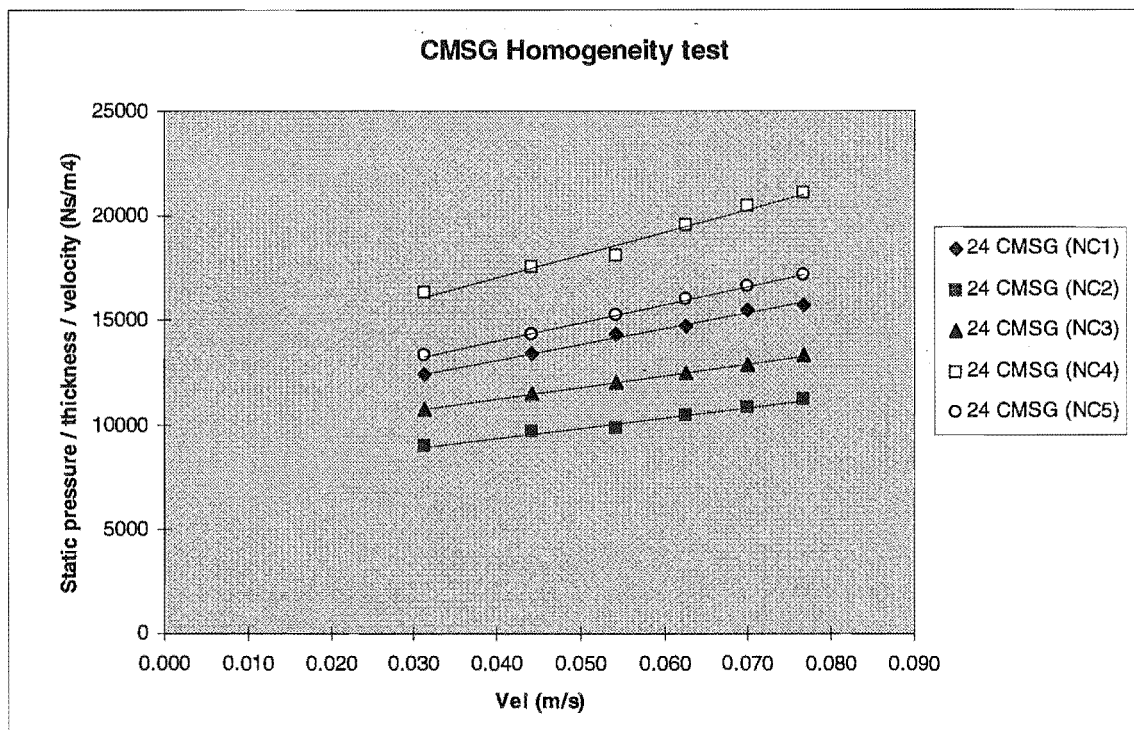
The thicker foams had larger flow resistivity. This was perhaps due to different flow regimes within the thicker samples producing more resistance. The thicker samples also had more contact area inside the pipe and hence had a better seal. However, the 46 mm polyester sample had a flow resistivity that was less than half of the 25 mm polyester sample. This may be due to its fibrous nature and the way it delaminated when punched out of a sheet.

Crushing the CMSG foam had a large effect on its flow resistivity. Crushed CMSG had a flow resistivity 25% less than the non crushed CMSG. Crushing the partially reticulated foam reduced the number of closed cells. This gave less resistance to air flow and hence a lower

flow resistivity. The difference was not as large for the 23 mm CMSG samples but was still apparent (10% reduction in flow resistivity).

It was interesting that the 25 mm polyester board ( $80 \text{ kg/m}^3$ ) had a flow resistivity of 11700 mks rayls/m while the 25 mm fibreglass board ( $90 \text{ kg/m}^3$ ) was 47000 mks rayls/m, when the materials had similar densities. The polyester fibres had a density of approximately  $1380 \text{ kg/m}^3$  while the fibreglass fibres were almost twice as dense at  $2600 \text{ kg/m}^3$ . The difference in flow resistivity implies that the fibreglass was packed significantly tighter than the polyester.

Repeatability tests carried out on two CMSG foam samples gave an experimental uncertainty of 5%. Most of the bulk materials were homogeneous within the experimental uncertainty. Five samples of CMSG foam from one sheet showed a 32% variation in flow resistivity, Figure 6.3. This variation is thought to be related to the manufacturing process.



**Figure 6.3 Homogeneity test.**

Bies and Hansen (1979) and Ingard (1994) have shown that there exists an optimal flow resistance for porous absorbing materials. This value is approximately 1235 mks rayls. The closest material to this was the fibreglass at 1175 mks rayls. All of the materials tested were below the optimum. It is worth noting that the optimum flow resistance was calculated from theoretical models. These predictions assume that the porous material's frame is rigid, as in the case of fibreglass and polyester board. They are also applicable to some elastic framed

materials such as open cell polyurethane foams. The models are less accurate for stiff or partially reticulated foams.

## **7. Conclusions**

A range of materials have been studied and their important acoustic parameters identified. Impervious films have been specified by their surface density and thickness. The flow resistance of fabrics, foams and fibrous materials has been quantified with the flow resistance apparatus. This equipment has given repeatability of 5% on CMSG foam. This was small in comparison to the inhomogeneity in the test materials. A range of up to 32% was found for five CMSG foam samples taken from a standard sheet. Fabrics showed a smaller variation of approximately 16%.

## References

Bies, D.A., Hansen, C.H. (1979), "Flow resistance information for acoustical design", *Applied Acoustics*, 13, 1980:357-391.

## Bibliography

QC            Ingard, U., "Notes on sound absorption technology", Noise control  
233            Foundation, 1994.  
.I44

---

# 4

## Absorption Testing

---

### Summary

This chapter details the absorption measurements carried out in the Reverberation Room. The effect of various absorber parameters were to be determined with the aims of producing “tunable” and wideband absorbers. Parameters such as material thickness, flow resistance and film weight were investigated. Different absorber characteristics such as the effect of film location, adhesive bonding, material type and air cavities were also studied. It was found that an increase in material thickness shifted absorption curves to lower frequencies. The addition of impervious films to bulk materials gave high absorption peaks at mid to low frequencies. Different film locations, on top of the substrate or sandwiched between it, gave quite different results across the frequency range but showed similar trends at each thickness. The fibreglass board had the most consistent high frequency absorption while the CMSG foams and the polyester board performed better at mid to low frequencies. The absorption of film faced foams was quite sensitive to the type of bonding between the film and foam and between the foam and backing surface; absorption peaks moved between 315, 800 and 1000 Hz. Air cavities between absorbers and the backing surface moved the absorption curves to low frequencies, giving results similar to a solid layer of the same total thickness. The absorption of porous substrates with fabric coverings increased with the fabric's flow resistance. Miscellaneous tests included the effect of different foams, homogeneity of foam and polyester sheets and the effect of contoured foam. The measured results had a repeatability of 5%. The effect of a number of significant parameters has been qualified allowing absorbers to be tuned for certain frequencies and for broad band absorption.



## Table of Contents

<b>Table of Contents.....</b>	<b>xii</b>
<b>List of Figures .....</b>	<b>xiii</b>
<b>List of Tables.....</b>	<b>xiii</b>
<b>1. Introduction.....</b>	<b>44</b>
<i>1.1 Testing.....</i>	<i>44</i>
<i>1.2 Materials .....</i>	<i>44</i>
<b>2. Aims .....</b>	<b>45</b>
<b>3. Theory.....</b>	<b>45</b>
<i>3.1 Calculation of absorption .....</i>	<i>45</i>
<b>4. Equipment .....</b>	<b>45</b>
<i>4.1 Modular precision sound analyser, Type 2260B.....</i>	<i>45</i>
<i>4.2 JBL EON Power 10.....</i>	<i>45</i>
<b>5. Procedure.....</b>	<b>46</b>
<b>6. Results.....</b>	<b>46</b>
<i>6.1 Conventions.....</i>	<i>46</i>
<i>6.2 Examples .....</i>	<i>47</i>
<i>6.3 Thickness variations.....</i>	<i>48</i>
<i>6.4 Film position .....</i>	<i>51</i>
<i>6.5 Materials .....</i>	<i>53</i>
<i>6.6 Impervious films.....</i>	<i>54</i>
<i>6.7 Air cavities .....</i>	<i>61</i>
<i>6.8 Fabrics .....</i>	<i>62</i>
<i>6.9 Miscellaneous Tests .....</i>	<i>63</i>
<i>6.10 Repeatability.....</i>	<i>67</i>
<b>7. Conclusions.....</b>	<b>68</b>
<b>References .....</b>	<b>69</b>
<b>Bibliography .....</b>	<b>69</b>

## List of Figures

<u>Figure No.</u>	<u>Page</u>
Figure 6.1 Cardboard honeycomb used to an achieve air cavity.....	47
Figure 6.2 Alternating foam and bonded film strips, (a); Contoured SPF foam with fabric covering, (b).....	48
Figure 6.3 Absorption variation with thickness for CMSG.....	49
Figure 6.4 Absorption variation with thickness for Mylar™ film bonded to CMSG.....	50
Figure 6.5 Absorption variation with thickness for Mylar™ film sandwiched between two layers of CMSG. ...	51
Figure 6.6 Film position variation at 30 mm thickness. ....	52
Figure 6.7 CMSG and CMSG (crushed) at 24 mm thickness. ....	52
Figure 6.8 Fibrous bulk absorbers at 24 mm thickness. ....	53
Figure 6.9 Effect of bonded and loose-laid films on CMSG (crushed).....	54
Figure 6.10 Effect of bonded and loose-laid films on polyester. ....	55
Figure 6.11 Effect of rear surface bonding on absorption peaks.....	56
Figure 6.12 150 mm strip adhered film on crushed CMSG. ....	57
Figure 6.13 Alternating bonded film and foam absorption for 150 mm strips. ....	58
Figure 6.14 Effect of film weight when loose-laid on crushed CMSG.....	59
Figure 6.15 Effect of film weight when bonded to crushed CMSG.....	60
Figure 6.16 Effect of crushed CMSG thickness with a bonded film.....	60
Figure 6.17 Air cavity behind polyester board.....	61
Figure 6.18 Loose-laid fabrics on top of polyester board.....	62
Figure 6.19 Loose-laid fabric and bonded fabric on top of polyester board. ....	63
Figure 6.20 Effect of different foams on the absorption of foam and film systems.....	64
Figure 6.21 Effect of crushed foam on a sandwiched film system.....	64
Figure 6.22 Effect of bonding multiple layers.....	65
Figure 6.23 Homogeneity test on CMSG.....	66
Figure 6.24 Homogeneity test on polyester.....	66
Figure 6.25 Contoured foam with fabric covering.....	67
Figure 6.26 Repeatability test on film faced CMSG.....	68

## List of Tables

<u>Table No.</u>	<u>Page</u>
Table 5.1 Speaker and microphone positions.....	46

## 1. Introduction

### 1.1 Testing

The sound absorption of acoustical materials such as ceiling or wall treatments, furniture, people and space absorbers can only be accurately measured in a reverberation room. International standard, ISO 354-1985, details test procedures and room requirements for the measurement of sound absorption in a reverberation room. Sound absorption coefficients in a reverberation room represent the ratio of non-reflected-to-incident sound energy over all angles of incidence. Absorption coefficients may be larger than unity due to diffraction effects at a specimen's edges. This effect is minimised by the use of frames that enclose the specimen being tested.

### 1.2 Materials

It is generally difficult to absorb sound at low frequencies. Materials of a similar size to the noise wavelength are usually required to interfere with the noise and hence absorb it. The most common approach is to apply thick absorbers, up to 100 mm thick. Another approach is to use a resonator based absorber (see Absorber Survey) which can be tuned to certain frequencies but within a very narrow bandwidth. The Reverberation Room calibration results serendipitously showed a large absorption peak at 300-400 Hz and again at 2000-2500 Hz, for a relatively thin 24 mm foam layer coated with a thin impervious film. Some of the testing work that followed the calibration was aimed at "tuning" these absorption peaks and making them more broad-band.

Most of the tests were carried out on absorber thicknesses of 24 and 50 mm. Larger thicknesses were not tested. These are usually impractical due to the amount of room volume used and the high material costs. Polyurethane, partially reticulated foams and fibrous polyester board were predominantly used as the bulk absorbing materials. It was thought that these materials would be fairly representative of most elastic (foam based) and rigid framed (fibre based) porous, sound absorbing materials. Fibreglass was also tested as a comparison because it has been the most prevalent and traditional sound absorbing material used.

## 2. Aims

The aims of the testing section were to determine the effects of the following material parameters and layer combinations on absorption:

1. Bulk material thickness: alone and in combination with impervious films.
2. Different bulk absorbing materials.
3. Film weight for various bonding types when fixed to a foam or fibrous substrate.
4. Air cavities on bulk materials and on foams with impervious films.
5. Fabric flow resistance and bonding type in combination with bulk materials.
6. Contoured foam, bonded layers and bulk material homogeneity.

## 3. Theory

### 3.1 Calculation of absorption, ISO 354:1988

$$\alpha = 55.3 \frac{V}{cA} \left( \frac{1}{T_2} - \frac{1}{T_1} \right) \quad (3.1)$$

$\alpha$  = absorption coefficient.

$V$  = volume of empty reverberation room,  $m^3$ .

$c$  = speed of sound in air (343 m/s).

$A$  = area of test specimen,  $m^2$ .

$T_1$  = reverberation time of empty reverberation room (s).

$T_2$  = reverberation time of reverberation room with test specimen present (s).

## 4. Equipment

### 4.1 Modular precision sound analyser, Type 2260B.

See section 4.3 in Chapter 2, Reverberation Room Calibration.

### 4.2 JBL EON Power 10

A 110W portable speaker and amplifier (tilted at 30 degrees).

## 5. Procedure

The 2260 sound analyser, building acoustics software and JBL speaker were used to measure reverberation times in the Reverberation Room, with and without the test specimen present. The 2260 analyser was calibrated externally and internally before each set of measurements. A variety of speaker and microphone positions were used within the Room as shown in Table 5.1. The JBL amplifier and speaker were set to produce approximately 85 dB(A). Reverberation times were measured with the 2260 analyser's microphone at 1m and 1.5m heights for each speaker and microphone combination. Two reverberation decays were measured at each microphone height. A total of 12 reverberation decays were measured for each test specimen.

**Table 5.1 Speaker and microphone positions**

Speaker	Microphone
Pt 4 South	Pt 23
Pt 17 East	Pt 6
Pt 38 Northwest	Pt 30

See Figure A.1 in Appendix A for the point locations in the Room.

Test specimen comprised four sheets of 1.2 x 2.4 m absorber. Each sheet was enclosed by a MDF frame, Figure C.1 in Appendix C. Absorption coefficients were calculated from the averaged reverberation times of the empty Room and averaged reverberation times with a test specimen present according to ISO 354:1988 (see section 3.1, Calculation of absorption).

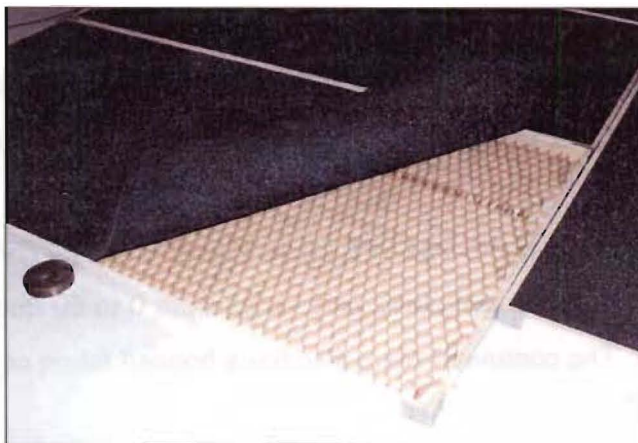
## 6. Results

Absorption coefficients and NRCs are given in Appendix C for each absorber tested.

### 6.1 Conventions

Diagrams were used in the key of each absorption plot to represent the absorbers being tested. The lowest layer in each diagram is against the Reverberation Room's floor. The left hand side number indicates the thickness in mm for bulk porous materials and Gib board; surface density in  $\text{g/m}^2$  for impervious films; and flow resistance in mks rayls for fabric coverings. The 35 and 140  $\text{g/m}^2$  films are made from Mylar™ while the 1000  $\text{g/m}^2$  film is PVC. The wording inside the boxed layers indicates the bulk material type; "CMSG" for combustion modified foam; "CMSG(c)" for crushed combustion modified foam; "POLY" for fibrous polyester board; "FIBG" for fibreglass board; and "SPF" for SPF foam. Bonded foams, films

and fabrics are indicated by a “B” on the right hand side or above the layer. The arrow points to the layer that the foam, film or fabric is bonded to. Loose-laid films, foams and fabrics do not have a “B” and in some cases are indicated by a “L” above the layer. Air cavities are indicated by “CAV” and were achieved with cardboard honeycomb, Figure 6.1. “Th. Avg.” indicates that the result was not measured but is a theoretical average of other measured results.



**Figure 6.1** Cardboard honeycomb used to achieve an air cavity.

**6.2 Examples**

$$\begin{matrix} 24 \\ 35 \\ 24 \end{matrix} \begin{matrix} \text{CM} \\ \text{MSG} \\ \text{CM} \end{matrix} \begin{matrix} \text{L} \\ \text{L} \\ \text{B} \end{matrix} \downarrow$$
 Represents a 24 mm thick layer of CMMSG foam with a 35 g/m<sup>2</sup> Mylar™ film coating. The top layer of 24 mm CMMSG foam is loose-laid on top of the film faced foam.


$$\begin{matrix} 140 \\ 24 \end{matrix} \begin{matrix} \text{L} \\ \text{L} \\ \text{CM} \\ \text{MSG(c)} \end{matrix} \begin{matrix} \text{L} \\ \text{L} \\ \text{B} \end{matrix} \downarrow$$
 This is a 24 mm thick layer of crushed CMMSG foam, faced with a strip adhered 140 g/m<sup>2</sup> Mylar™ film.

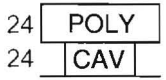
$$\begin{matrix} 140 \\ 24 \end{matrix} \begin{matrix} \text{B} \\ \text{CM} \\ \text{Th. Avg.} \\ \text{SG(c)} \end{matrix} \begin{matrix} \text{L} \\ \text{L} \\ \text{B} \end{matrix} \downarrow$$
 This is the arithmetic average of two measured results. One half of the specimen’s area is crushed CMMSG faced with a 140 g/m<sup>2</sup> bonded Mylar™ film. The other half is crushed CMMSG with loose-laid 140 g/m<sup>2</sup> Mylar™ film.

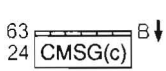
$$\begin{matrix} 140 \\ 24 \end{matrix} \begin{matrix} \text{CM} \\ \text{MSG(c)} \end{matrix} \begin{matrix} \text{L} \\ \text{L} \\ \text{B} \end{matrix} \downarrow$$
 Represents 24 mm thick crushed CMMSG foam with alternating strips of foam and 140 g/m<sup>2</sup> bonded film, Figure 6.2 (a). The strips are 150 mm wide.

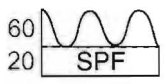
$$\begin{matrix} 140 \\ 24 \end{matrix} \begin{matrix} \text{B} \\ \text{CM} \\ \text{Th. Avg.} \\ \text{SG(c)} \end{matrix} \begin{matrix} \text{L} \\ \text{L} \\ \text{B} \end{matrix} \downarrow$$
 This is the arithmetic average of two measured results. One half of the specimen is crushed CMMSG faced with a 140 g/m<sup>2</sup> bonded Mylar™ film. The

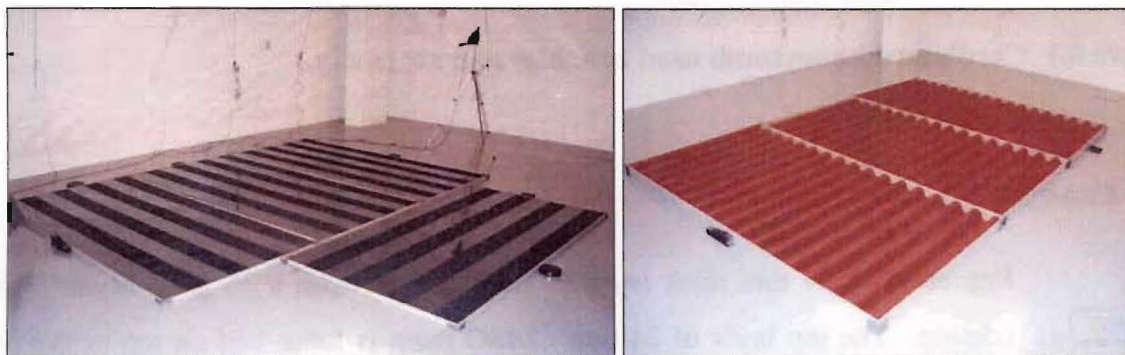
other half is crushed CMSG by itself.

 This shows a 6 mm thick layer of Gib board with crushed CMSG foam and a bonded Mylar™ film. The foam is bonded to the Gib as is the film to the foam.

 Shows a 24 mm thick air cavity with 24 mm thick loose-laid polyester board.

 Represents a layer of crushed CMSG foam covered by a fabric. The fabric has a flow resistance of 63 mks rays and is bonded to the foam.

 This represents a contoured SPF foam, Figure 6.2 (b). The base foam thickness is 20 mm while the contoured part varies from 0 to 60 mm. The peaks are 150 mm apart. The contoured foam also has a bonded fabric covering.



(a)

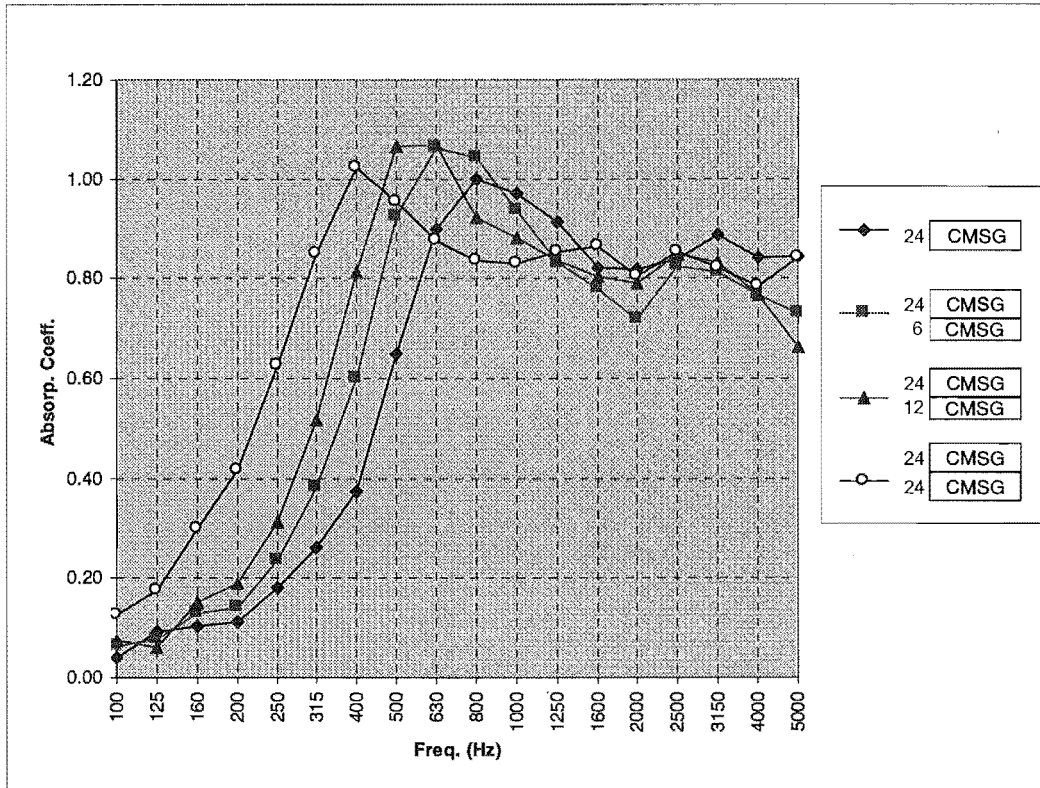
(b)

**Figure 6.2 (a) Alternating foam and bonded film strips, (b) Contoured SPF foam with fabric covering.**

### 6.3 Thickness variations

Impervious films are usually applied to porous absorbers to protect the material from harmful environments. The films were bonded with a spray-on contact adhesive to the substrate. Initial tests were carried out on CMSG foam by itself and in combination with a light impervious film at various foam thicknesses. These were tested to obtain a preliminary set of results and to determine the effect of thickness variation on each system's absorption.

The effect of bulk absorber thickness on absorption is well known. Figure 6.3 shows typical trends of absorption for a porous material at different thicknesses.

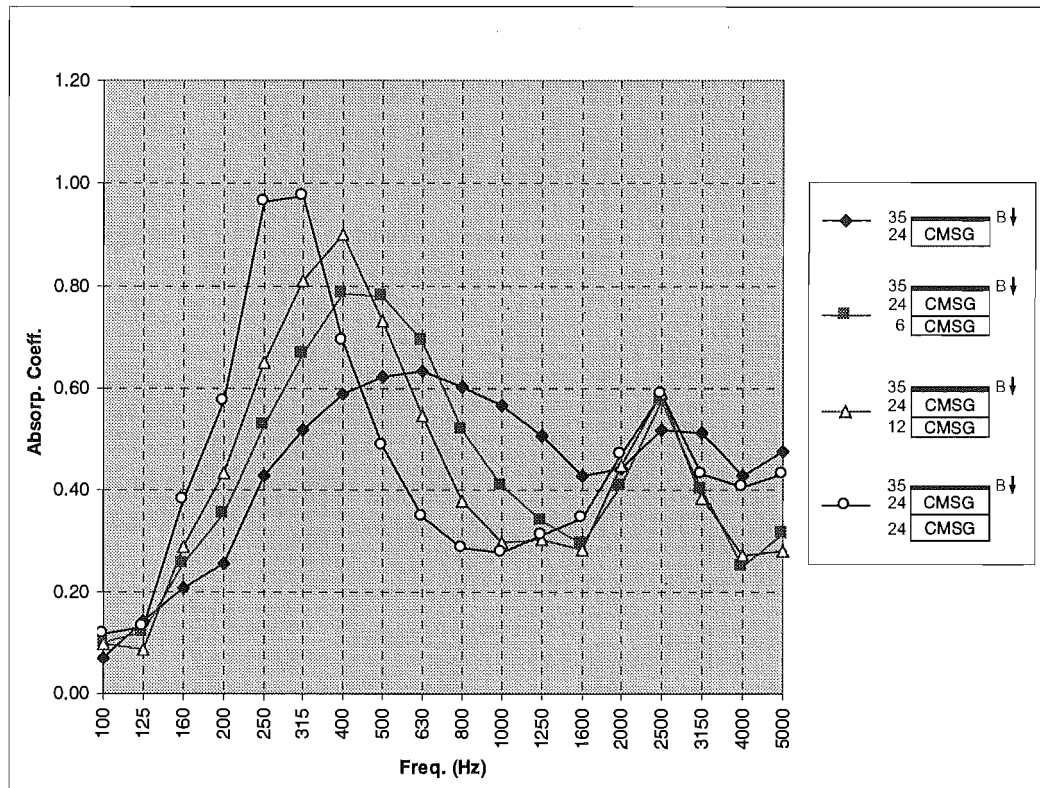


**Figure 6.3 Absorption variation with thickness for CMSG.**

Some of the results exceed unity. This seems to be a characteristic of reverberation room absorption measurements and is usually attributed to diffraction effects around the specimen's edges. The absorption peak moved from 800 Hz for 24 mm CMSG through to 400 Hz for 48 mm CMSG. These peaks were lower than expected. This seems to be due to the amount of reticulation in the CMSG. Reticulation is thought to affect the flow resistance as well as the tortuosity of the foam. It would appear that increased tortuosity moves absorption peaks to lower frequencies for bulk materials but also reduces absorption at higher frequencies.

When CMSG foam was faced by an impervious Mylar™ film the absorption was observed to increase in frequencies under 500 Hz. The absorption decreased in frequencies above 500 Hz. The film, bonded directly to the foam, causes incident sound to vibrate the frame of the foam as well as the air within the foam. This appears to create a low frequency resonance from 250 to 400 Hz and a secondary resonance from 2000 to 2500 Hz. These absorption peaks are shown clearly with the increase in foam thickness, Figure 6.4.





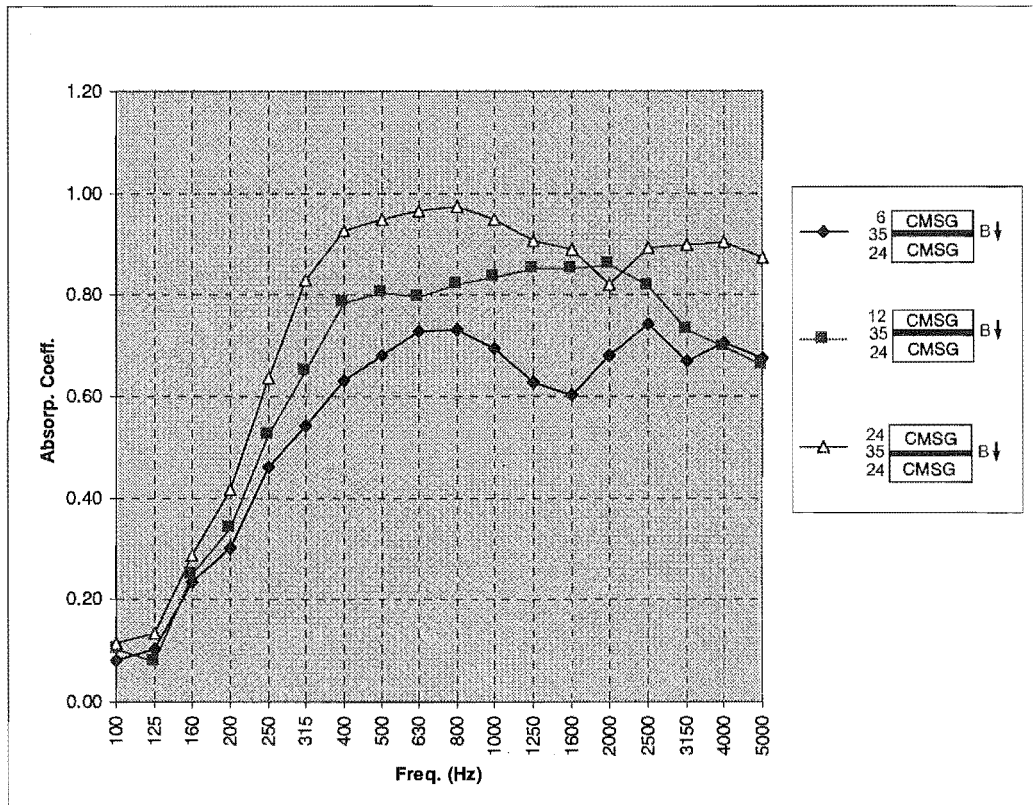
**Figure 6.4** Absorption variation with thickness for Mylar™ film bonded to CMSG.

It is also clear that the change in thickness had a larger effect on the low frequency peak than the high frequency one. It is thought that the foam's stiffness and the film weight have more of an effect on the second peak while the foam's thickness and stiffness relate to the low frequency peak. This is discussed further in section 6.6. It is worth noting that the absorption trends for this system, at 36 and 48 mm foam thicknesses, were also produced with 24 mm of foam in the Reverberation Room Calibration chapter and are reproduced later in this chapter.

CMSG foam was tested with bonded foil to identify which material, foam or film, caused the large peak at 315 Hz. This result is shown in Figure C.3 in Appendix C. The foam was found to be more significant than the film. The large absorption peak at low frequencies appeared again when the 24 mm CMSG was crushed. SPF foam and crushed CMSG foam both have lower flow resistance than CMSG. This indicates that foam stiffness and flow resistance affect the low frequency resonance. Next, an attempt was made to combine the absorption at low frequencies of the film faced CMSG, with the absorption at high frequencies of the plain CMSG.

CMSG foam was loose-laid on top of a film faced CMSG foam. The top foam layer thickness was increased and the absorption measured, Figure 6.5. Thicker layers of loose-laid foam

increased the absorption across most of the frequency range. Anomalies occurred at 2000 Hz, 4000 and 5000 Hz. These anomalies may be characteristic of the sandwiched film system. It is useful to compare the results at each thickness to ascertain the optimal position of the film.



**Figure 6.5** Absorption variation with thickness for Mylar™ film sandwiched between two layers of CMSG.

#### 6.4 Film position

The three film positions - on top of the foam, sandwiched between the foams and the foam alone, showed similar trends at each thickness. Figure 6.6 shows the typical trend for a 30 mm thickness. See Figures C.4 to C.6 in Appendix C for the results at 24, 36 and 48 mm thicknesses. Each position seems to have its own advantages and disadvantages. No single position out-performs the others across the whole frequency range. A fairly consistent trend for each thickness was that the sandwiched film gave a "quasi-average" of the other two. An exception occurred between 315 and 500 Hz where the other two systems cross over. Comparisons were made between different bulk absorbers to simplify the systems involved

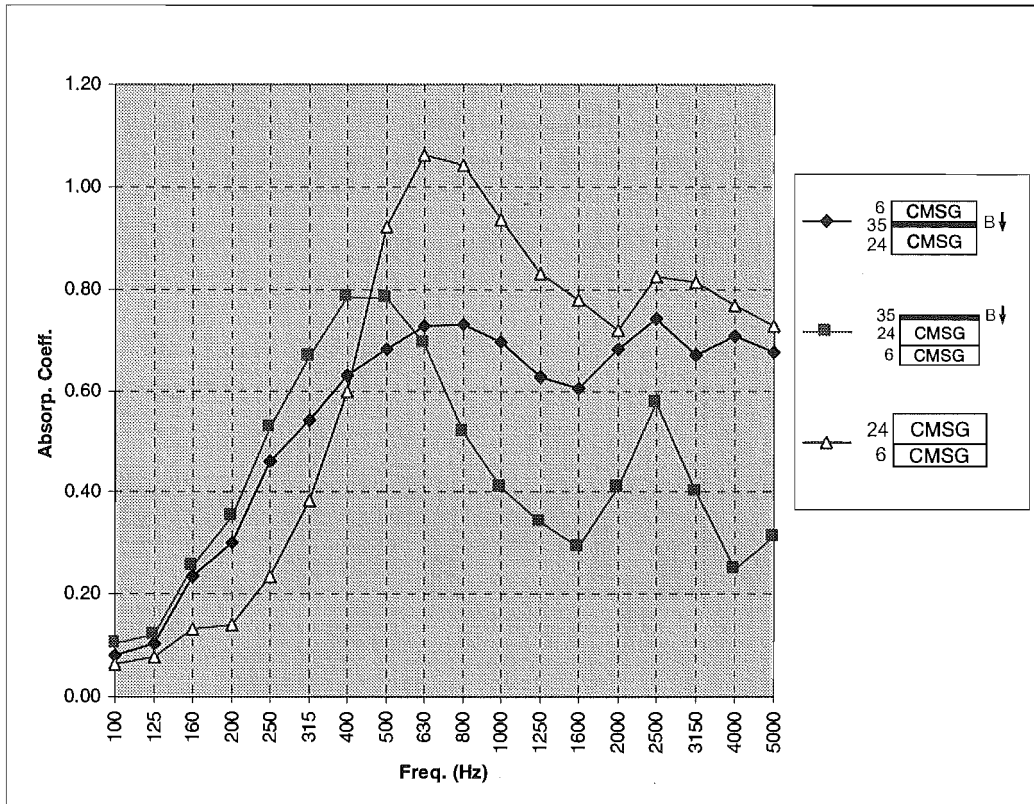


Figure 6.6 Film position variation at 30 mm thickness.

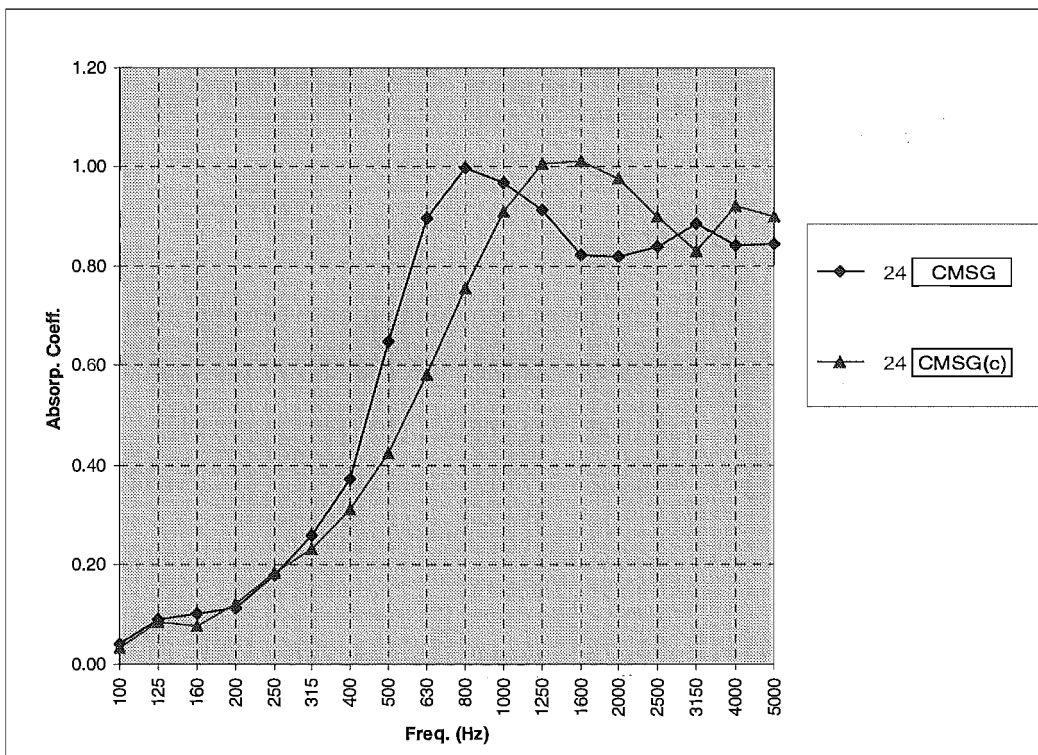


Figure 6.7 CMSG and CMSG (crushed) at 24 mm thickness.

## 6.5 Materials

Four different bulk absorbers were tested by themselves to compare their acoustic absorption. CMSG foam was crushed by running it through nip rollers. This was done to reduce the amount of closed cells (reticulation) and to give a lower flow resistance. This moved the absorption peak of the CMSG from 800 Hz to 1250-1600 Hz, as shown in Figure 6.7. Neither system is more advantageous than the other unless a certain “problem” frequency is known; in which case the appropriate foam can be selected. Similar trends were found for polyester and fibreglass absorbers.

The fibrous absorbers showed typical porous absorber trends, Figure 6.8. Polyester board performed better at some low frequencies but generally has less absorption than the fibreglass. This will be due to the large difference in flow resistivity; 11700 mks rays/m for polyester and 47000 mks rays/m for fibreglass. The fibreglass had very wide band absorption with consistently high values in frequencies above 1000 Hz. This indicates that the theoretical optimum flow resistance, which the 24 mm thick fibreglass was very close to, does give high absorption. The 24 mm polyester’s absorption could be improved by increasing its flow resistance.

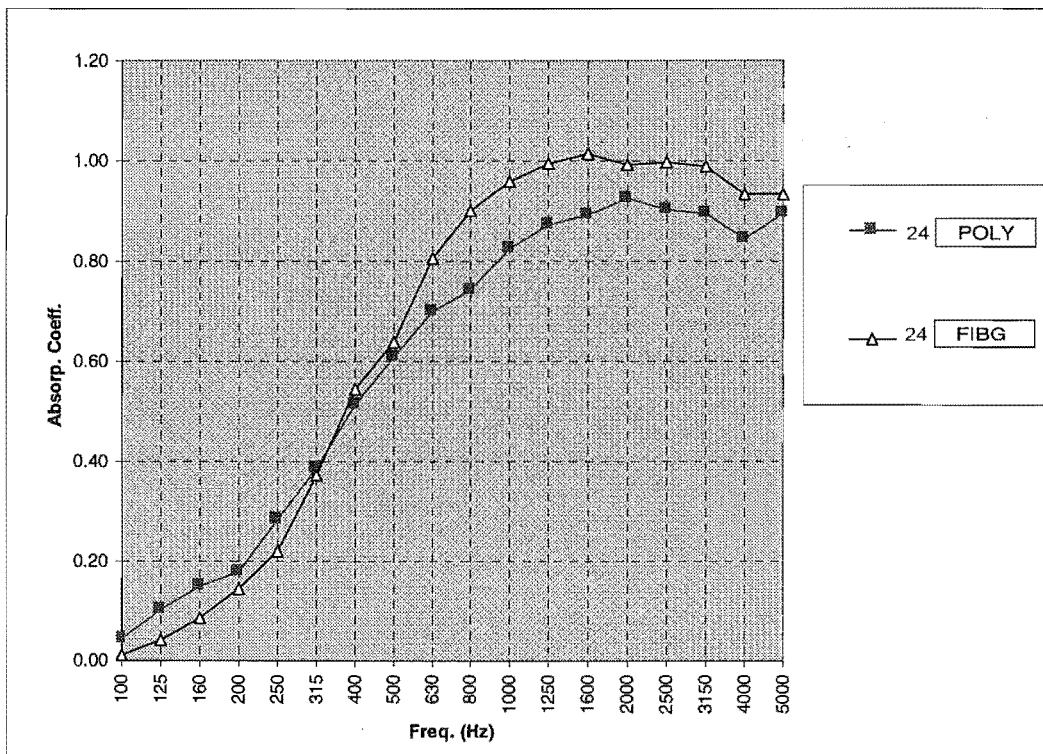
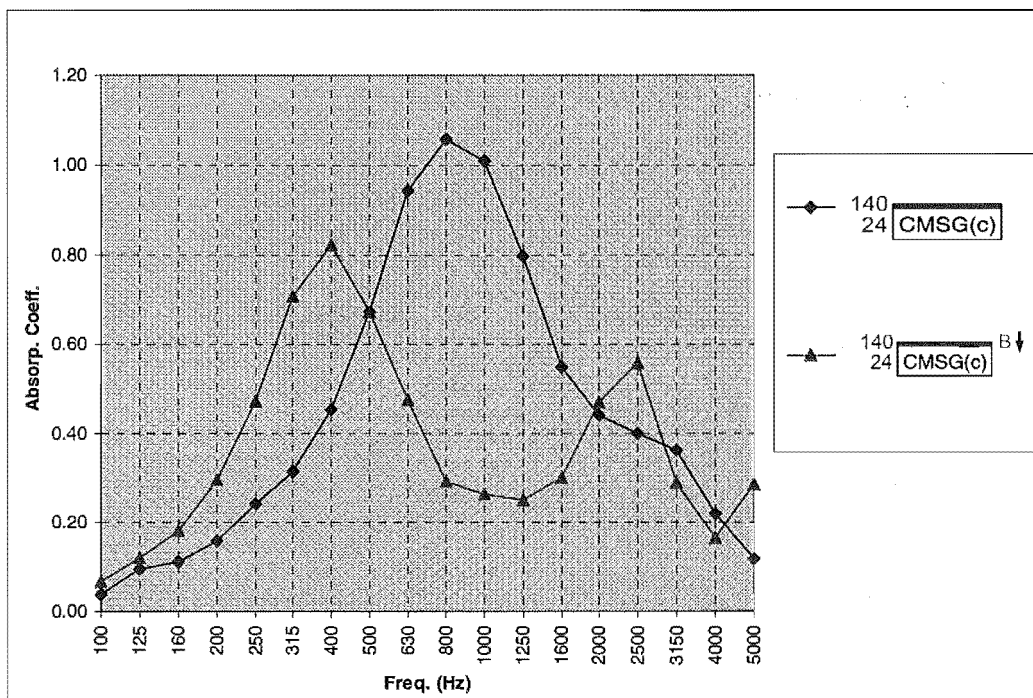


Figure 6.8 Fibrous bulk absorbers at 24 mm thickness.

Figure C.7 in Appendix C shows the typical increase in absorption at low frequencies, from 24 to 50 mm thickness. The increase in absorption for the thicker polyester board was approximately 30% at mid to low frequencies (200 to 500 Hz). The increase in absorption for the same change in thickness of CMSG, shown in Figure 6.3, was approximately 60% in the same frequency range. The total flow resistance of 46 mm thick CMSG was 850 mks rays while 46 mm polyester had flow resistance of 240 mks rays. The change in absorption was greater for CMSG because it moved closer to the optimum flow resistance of 1235 mks rays. It is clear though, that thicker polyester performed better at almost all frequencies while thicker CMSG only performed better at frequencies less than 500 Hz.

### 6.6 Impervious films

Impervious films are usually applied to porous absorbers to protect the absorbent from harmful environments. The films are typically bonded with contact adhesive to the porous material. The effect of bonded film, as opposed to loose-laid film, was investigated to determine the system's sensitivity to bonding. Figure 6.9 shows the large difference in absorption between loose-laid Mylar™ film and bonded Mylar™ film on crushed CMSG. The loose-laid film produced a single large and quite wide peak centred on 800 Hz while the bonded film produced a large peak at 400 Hz and a smaller one at 2500 Hz.

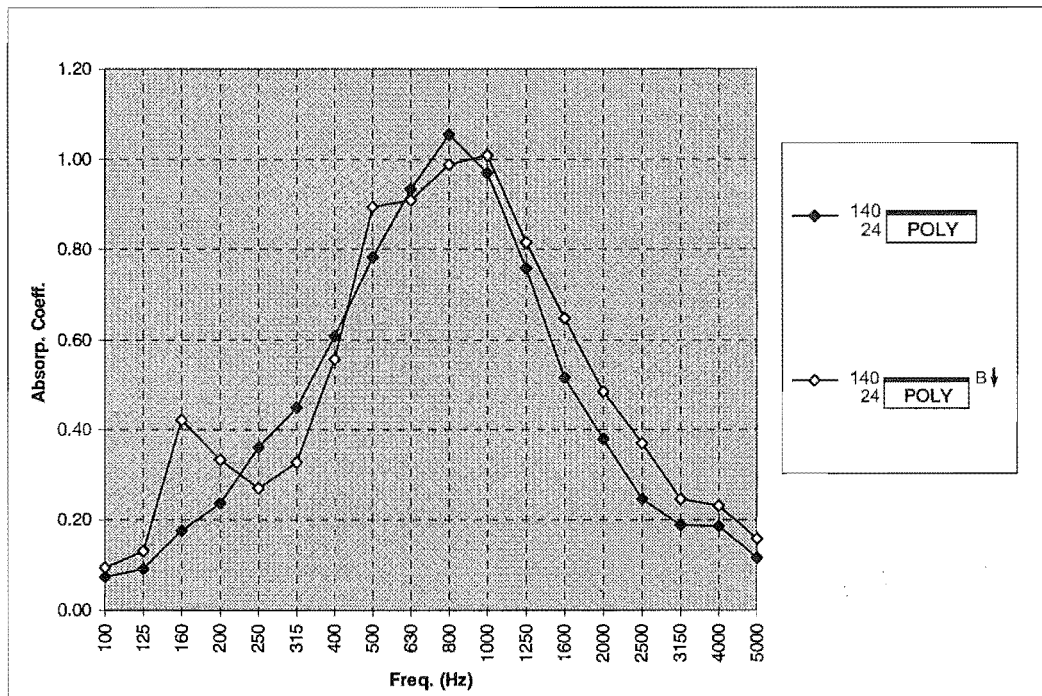


**Figure 6.9** Effect of bonded and loose-laid films on CMSG (crushed).

It would appear that incident sound energy excited the loose-laid impervious film, which transmitted the vibration to air within the pores of the substrate. Sound waves seemed to

resonate between the film and floor, giving an absorption peak at 800 Hz. The substrate's frame will have little or no excitation compared to the fluid surrounding it. Bonding the film to the substrate can have a large effect.

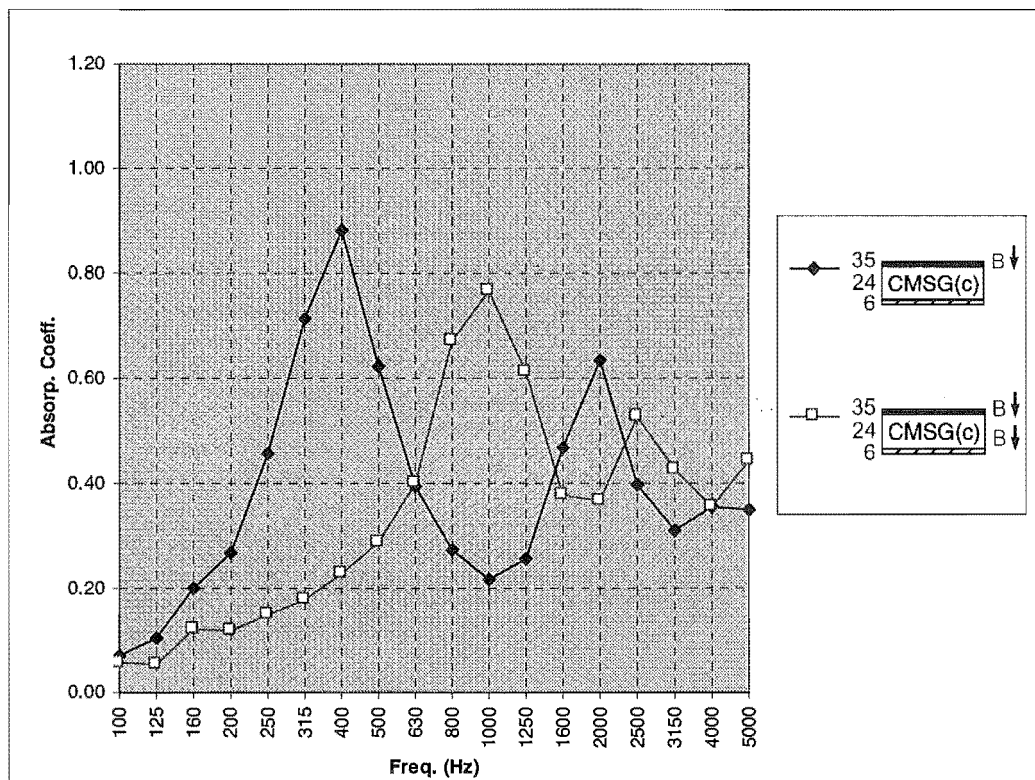
Figure 6.9 and Figure 6.10 show that bonding the film to the substrate layer dramatically changed the foam system but had a small effect on the polyester system. Two absorption peaks, centred on 315 Hz and 2500 Hz, are clear in Figure 6.9 for the foam substrate. The bonded film on polyester gave the same predominant peak at 800 Hz and produced a smaller peak at 160 Hz, Figure 6.10.



**Figure 6.10** Effect of bonded and loose-laid films on polyester.

The difference in results can be explained by examining each substrate's stiffness. Bonding the film to the lower layer induced vibration in the frame of the material. An elastic material, such as the CMSG foam, can "carry" this wave and in doing so produced quite different resonances from the loose-laid case. There was a combination of fluid borne sound waves in the foam's pores and frame borne waves in the foam's structure. This gave the characteristic 315 and 2500 Hz absorption peaks. Fibrous materials are relatively stiff compared to most foams and hence, are less able to support frame borne waves. The absorption characteristic remained almost unchanged when the film was bonded to the polyester substrate. These bonding effects were investigated further.

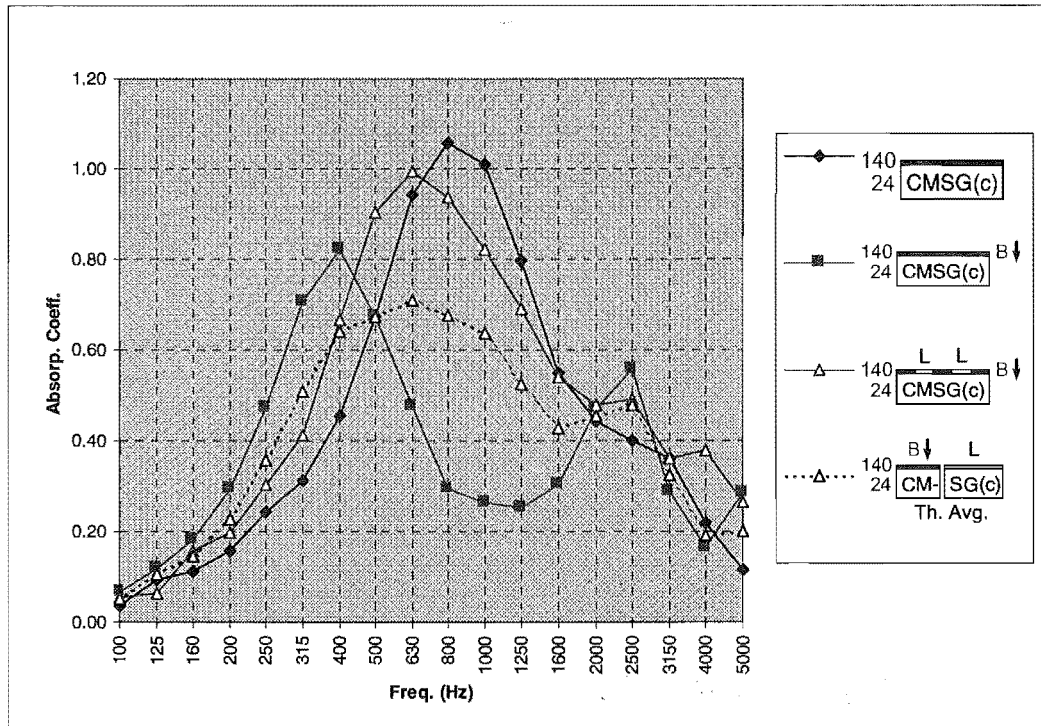
It became apparent from the modelling work that the bonding conditions between foams, impervious films and the backing surface were critical to the system's absorption. The effect of bonded and loose-laid films have been described above. The effect of bonding the foam (with an impervious film facing) to its backing surface was investigated. Most absorbers are fixed to walls by adhesives. All of the previous tests were carried out with loose-laid materials on the Reverberation Room floor as it was impractical to bond each specimen to the floor. Four sheets of Gib board were painted and then placed in the Reverberation Room. Mylar™ faced CMSG was tested - loose-laid on Gib board and then bonded to the Gib. The loose-laid system performed similarly to the situation where it was loose-laid on the Reverberation Room floor, Figure C.8 in Appendix C. Bonding the rear surface of the foam to the Gib shifted the peak absorption from 400 to 1000 Hz, Figure 6.11. The high frequency peak was also observed to move but less dramatically.



**Figure 6.11 Effect of rear surface bonding on absorption peaks.**

Clearly, the loose-laid system's absorption peaks were dependant on it being decoupled from the backing surface. This has significant implications on the absorption test method for film faced systems. Measured results for these systems may not give the same installed results unless care is given to match the test conditions to the installation conditions. Different amounts of bonding were examined next.

Another film bonding test was carried out to determine the effect of strip adhered film. It can be seen from Figure 6.12 that the 150 mm alternating, adhered film and loose-laid film gave a quasi-average of the two previous tests – loose-laid film and bonded film on crushed CMSG. This result is somewhat similar to the trend shown in film position, section 6.4. For example, where the two previous absorption curves cross over at 500 Hz, the strip adhered specimen gave more absorption than the other two specimen, Figure 6.12. The strip adhered film gave quite a wide peak, centred on 630 Hz. Strip adhered film had other interesting characteristics.



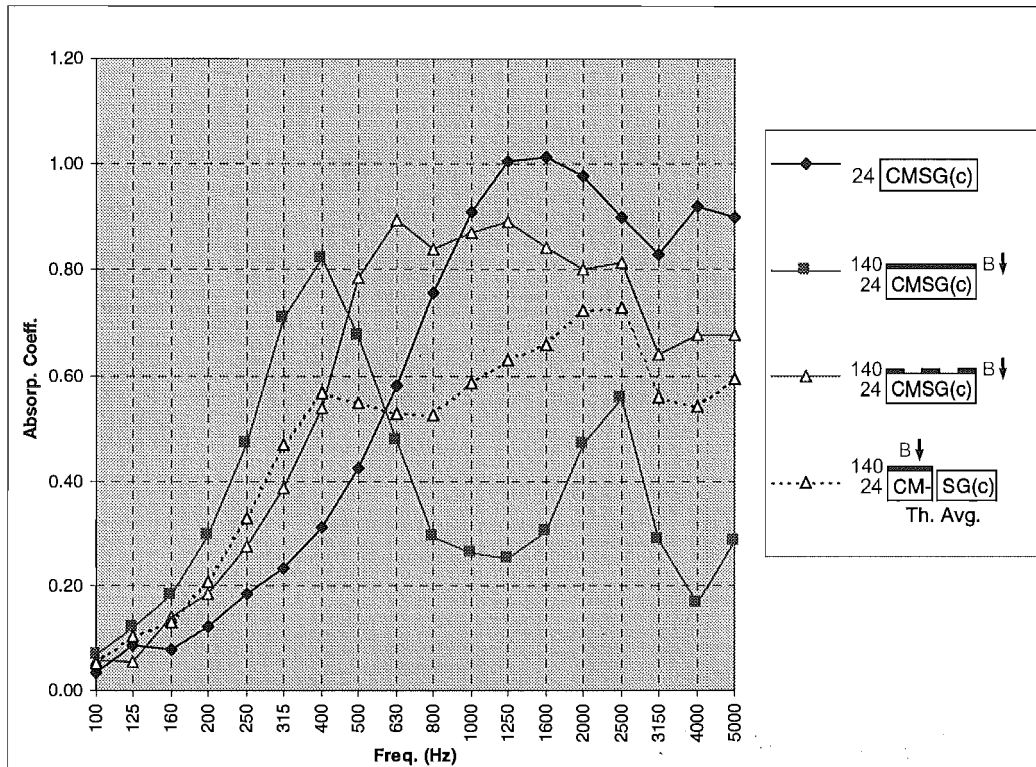
**Figure 6.12** 150 mm strip adhered film on crushed CMSG.

It is worth noting that this strip adhered film generally gave more absorption than the theoretical average of the loose-laid film and the bonded film on crushed CMSG. This average would be the result of testing say four absorbers, two with loose-laid film and two with bonded film. Strip adhered film combines the differently bonded films into four absorbers, giving more absorption than the average of bonded and loose-laid films. These curves had the same peak, centred on 630 Hz, but very different magnitudes. This is thought to be due to a diffraction effect produced by the varying impedance across the surface. This phenomenon was found and modelled, albeit for quite different materials, by Takahashi (1989).

Increased absorption due to diffraction was examined for alternating strips of film and foam. A similar trend was found to strip adhered films which showed increased absorption (more



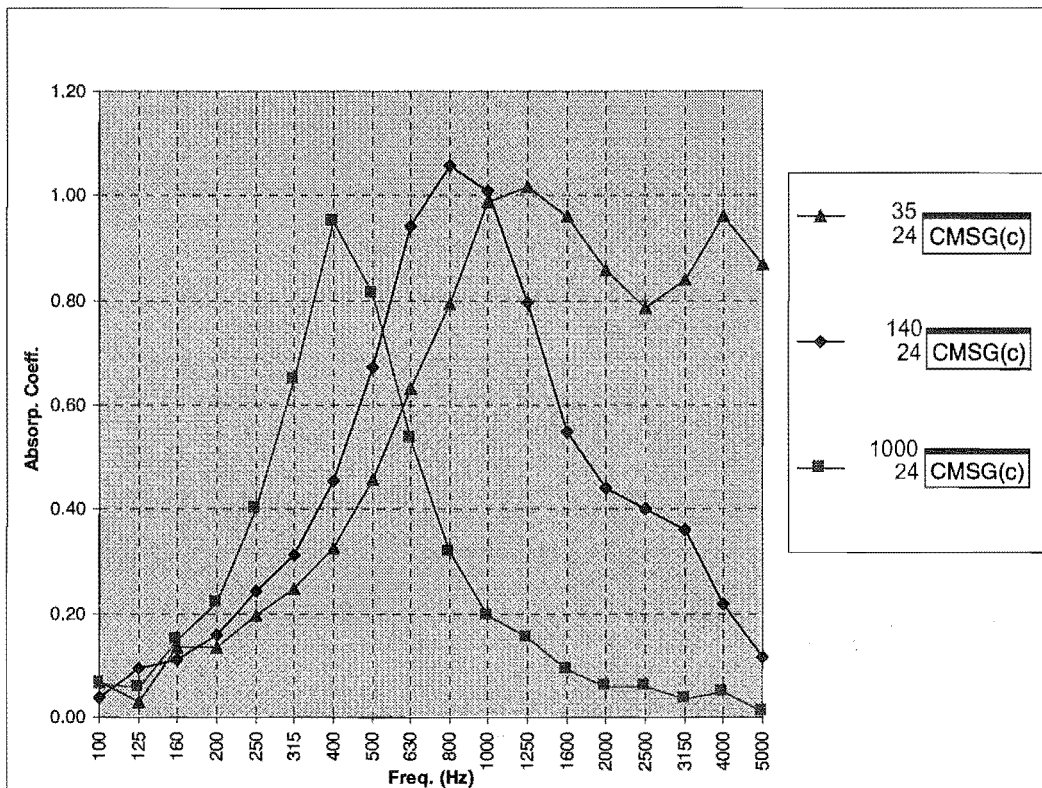
than the average of foam and film faced foam) above 400 Hz, Figure 6.13. Again, where the foam by itself and the foam/film system curves crossed over at 630 Hz, the strip combination had significantly more absorption than the theoretical average. The effect was also shown with a thicker foam substrate in Appendix C, Figure C.9. It is clear that careful use of films can produce increased absorption. However, comparing this system at 24 mm thickness with the fibreglass and crushed CMSG yields interesting results.



**Figure 6.13** Alternating bonded film and foam absorption for 150 mm strips.

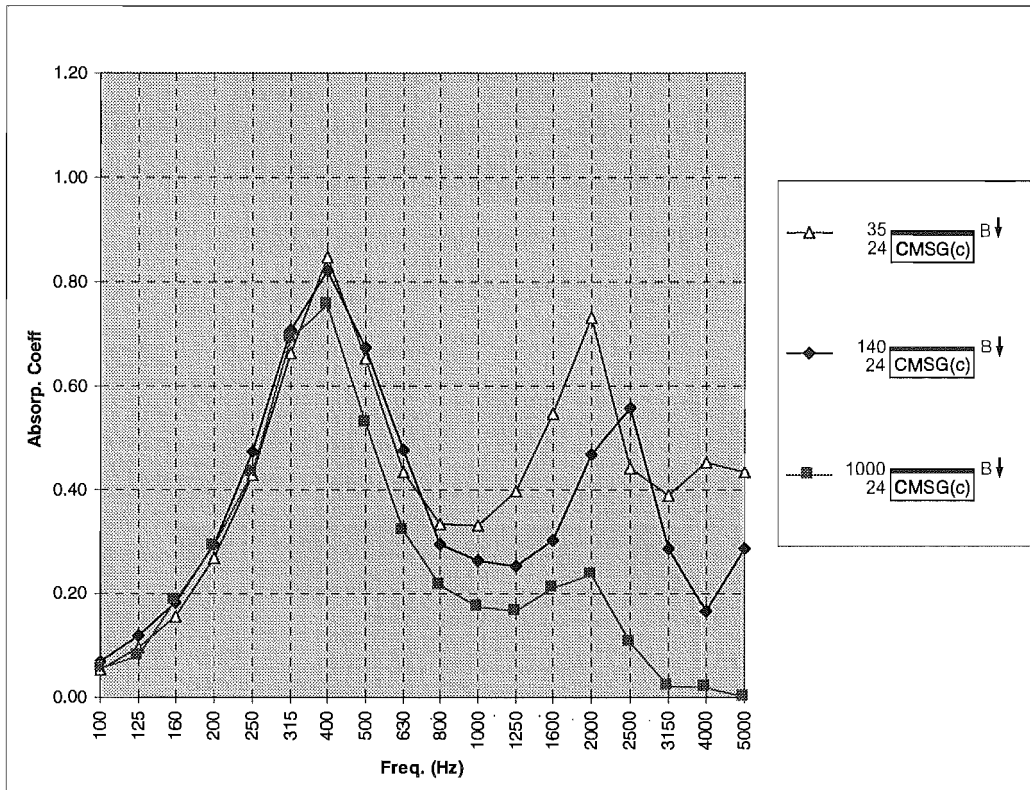
It can be seen from Figure C.10 in Appendix C that alternating strips of film performed better than CMSG at frequencies less than 630 Hz but not as well between 630 and 1250 Hz and above 2500 Hz. It performed only marginally better than the fibreglass at low frequencies. It has been shown that the 24 mm fibreglass specimen had an almost optimum theoretical flow resistance of 1175 mks rays while the foam was considerably lower at 225 mks rays. The CMSG foam, faced with film strips and indeed the foam by itself, would absorb appreciably more sound if they were optimised for flow resistance. The flow resistance should be increased by reducing the cell size or other means but not by increasing the amount of reticulation. Increased reticulation has been shown to reduce the foam's absorption at high frequencies, Figure 6.7. The discussion thus far has focussed somewhat on the effect of film bonding type. The sensitivity of these systems to film weight is discussed next.

A range of film weights were tested, bonded and loose-laid, on CMSG and polyester. It was believed that the frequency dependence of the absorption peaks for this system was generally proportional to the square root of foam stiffness and inversely proportional to the square root of film weight. Film weights covering a range of two orders of magnitude were tested to facilitate measurable shifts in frequency. It was clear that the heavier films did indeed shift the peak absorption to lower frequencies, Figure 6.14, when the film was loose-laid. This trend was also apparent for loose-laid films on polyester substrate, Figure C.11 in Appendix C. Quite a different trend was found when the films were bonded to the foam structure.



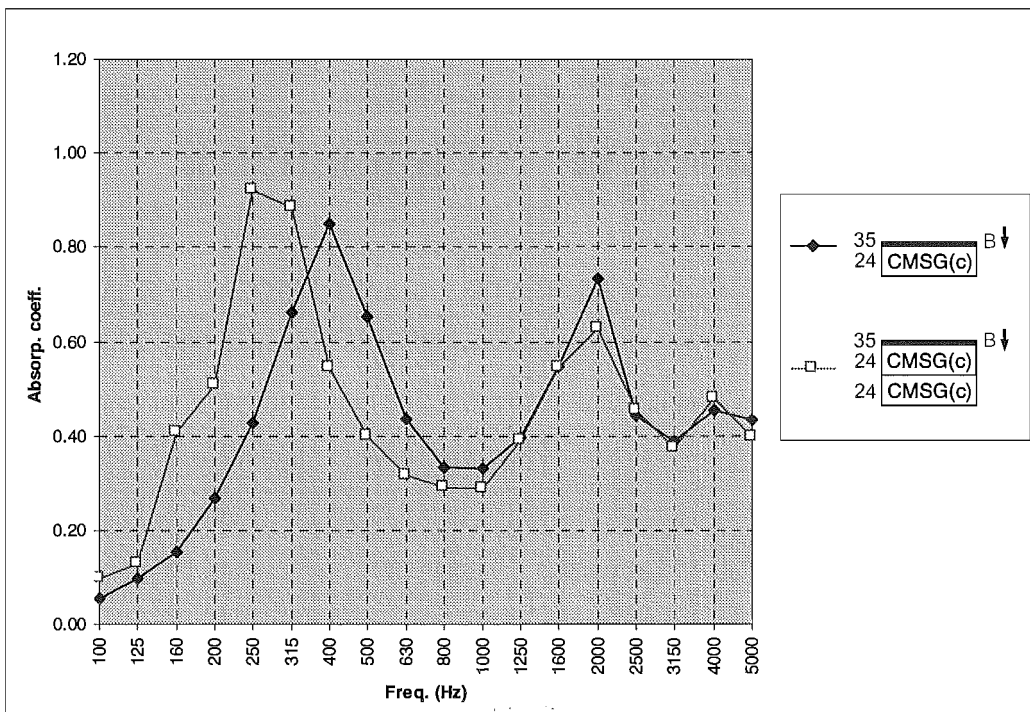
**Figure 6.14** Effect of film weight when loose-laid on crushed CMSG.

The same films were tested but now bonded to the crushed CMSG. It was apparent that the heavier films reduced the high frequency peak's magnitude and had little effect on the low frequency peak, Figure 6.15. The heavier films affected the foam's frame motion at higher frequencies. These films, especially the 1000 g/m<sup>2</sup> PVC, may have affected the foam's stiffness. This set of tests was not carried out on polyester as previous tests showed that bonded films had a small effect on polyester. Throughout these tests on polyester, the low frequency peak at 300 to 400 Hz did not shift in frequency and only slightly in magnitude.



**Figure 6.15 Effect of film weight when bonded to crushed CMSG.**

Theoretical modelling indicated that foam thickness beneath a film would shift the characteristic low frequency peak. Figure 6.16 shows that indeed, this was the case. A clear frequency shift, from 400 to 250 Hz, can be seen. The high frequency peak was observed to not shift.

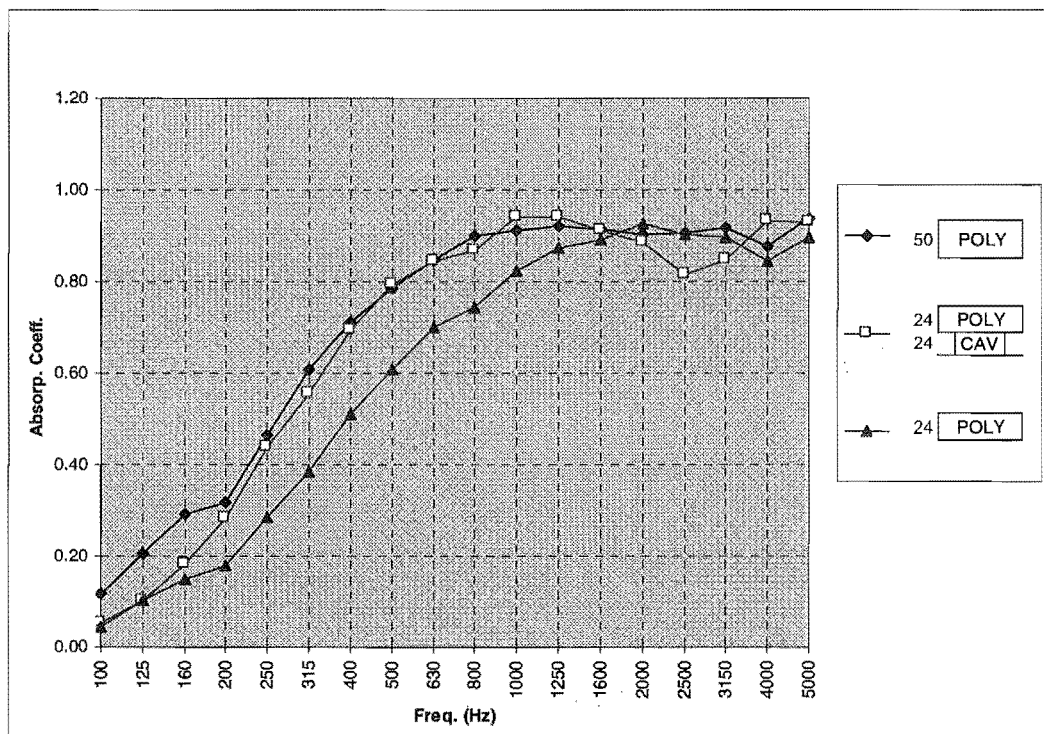


**Figure 6.16 Effect of crushed CMSG thickness with a bonded film.**

The sensitivity of the two absorption peaks to different material parameters can be summarised. The low frequency peak was sensitive to substrate thickness and stiffness. It did not change with film weight when the film was bonded to the foam. This peak did not appear for rigid framed substrates. The high frequency peak was sensitive to film weight and insensitive to foam thickness.

### 6.7 Air cavities

A range of tests were performed on CMSG alone, film faced CMSG and polyester to determine the advantages of including an air cavity with the material. It was found that moving a material away from its backing floor significantly improved its low frequency absorption. It appeared to shift the absorption curves to lower frequencies not too dissimilar to increasing the thickness of porous substrate. This effect was shown for polyester in Figure 6.17 and crushed CMSG in Figure C.12 in Appendix C.



**Figure 6.17 Air cavity behind polyester board.**

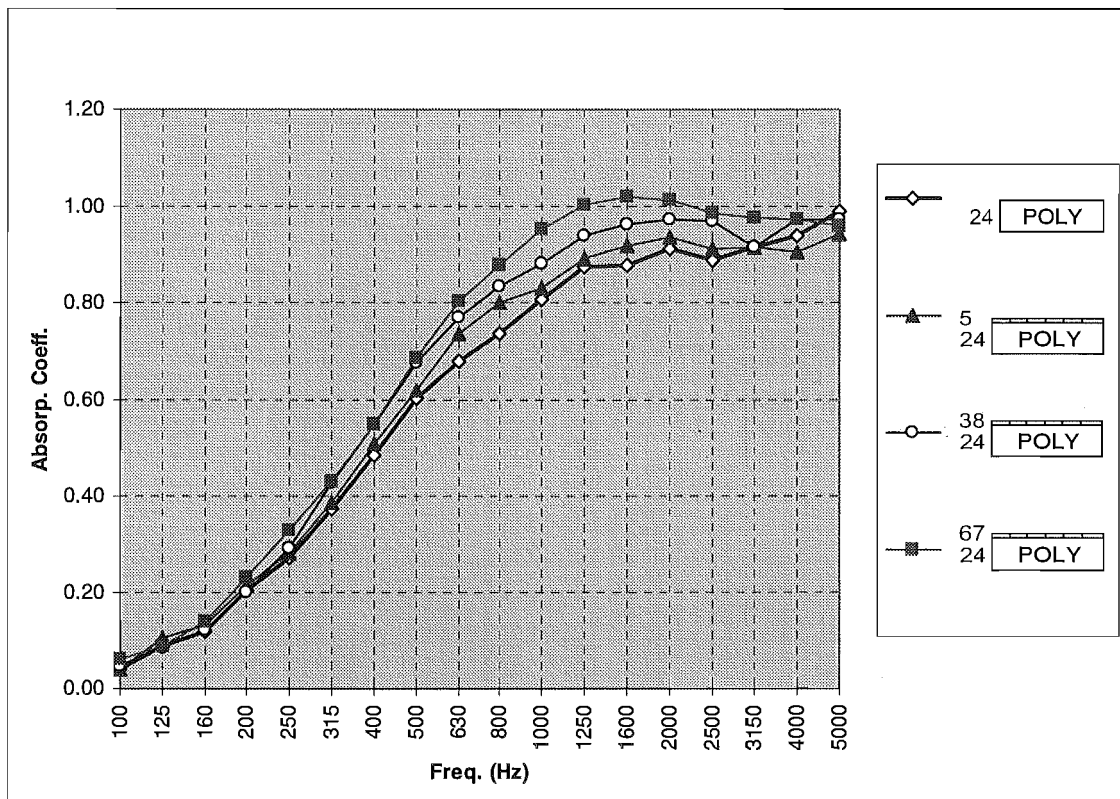
This result was again apparent for film faced CMSG, Figures C.13 and C.14 in Appendix C. In each case, the materials with air cavities were quite similar to their companions with the cavity filled by bulk absorbent.

Sound is absorbed through an air cavity by impedance mismatch. At the interface between a porous material and an air cavity some sound is reflected and then absorbed in the material

and some is transmitted into the cavity. The speed of propagation of transmitted sound is different in air than in porous material. Energy is used in this transition, appearing as absorption. Waves will also resonate between the floor and the substrate surfaces. A practical consideration is that installed absorbers often need to meet aesthetic requirements as well as acoustic ones.

### 6.8 Fabrics

Bulk absorbers installed in commercial premises are usually covered with fabric to improve their appearance. These fabrics can also improve the acoustic performance of the absorber. Tests were carried out on crushed CMSG and polyester with three different fabrics coverings. The effect of bonded and loose-laid fabrics was also investigated. Figure 6.18 shows that each loose-laid fabric improved the absorption of polyester.



**Figure 6.18** Loose-laid fabrics on top of polyester board.

This was also found for a loose-laid fabric on crushed CMSG, Figure C.15 in Appendix C. The absorption increased with fabric flow resistance. Ingard (1994) showed theoretically that an optimal flow resistance for fabric coverings was around 410 mks rays. These fabrics had considerably lower flow resistance, 5 to 67 mks rays, but still increased the absorption of the substrate. It would appear that higher flow resistance fabrics are required to gain the most absorption from the coverings.

Figure 6.19 shows that bonding the fabric to polyester had very small effect when compared to the loose-laid fabric. This was similarly found for CMSG, Figure C.16 in Appendix C. This result can be expected as the fabrics are porous, allowing incident sound waves to travel through into the substrate layer. Wave motion in the substrate's frame was not induced as much as in the case of an impervious film facing, discussed in section 6.6.

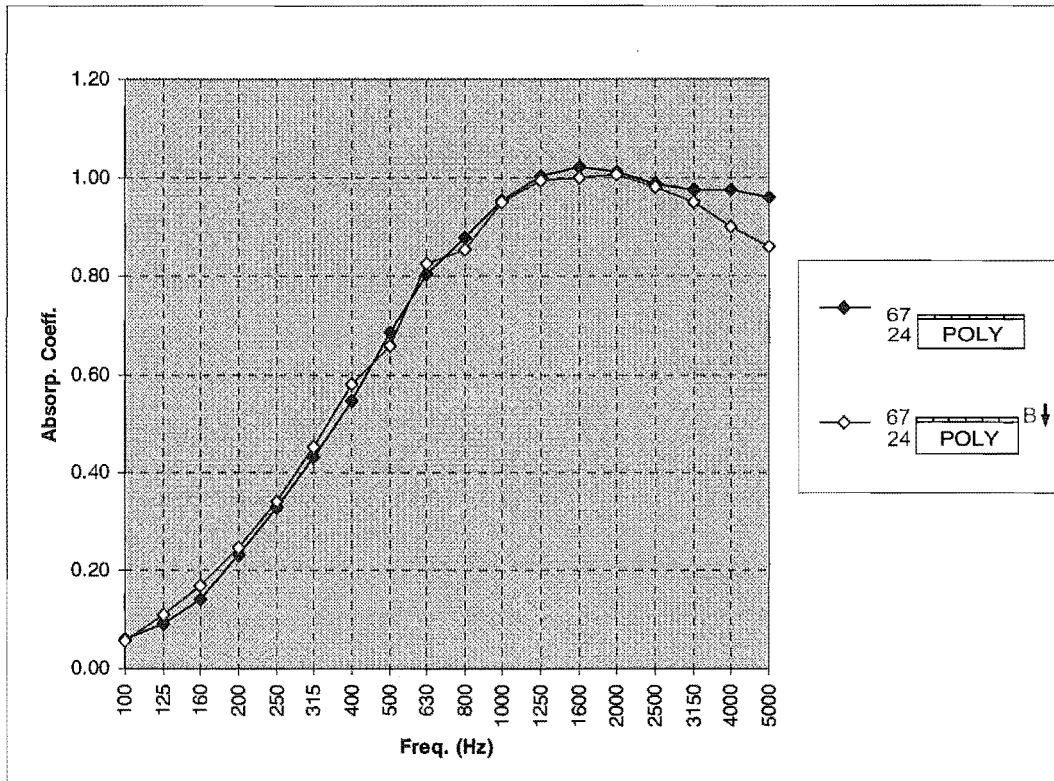


Figure 6.19 Loose-laid fabric and bonded fabric on top of polyester board.

### 6.9 Miscellaneous Tests

Aluminium foil was tested, bonded to three foams – SPF, CMSG and crushed CMSG. The results are shown in Figure 6.20. SPF and crushed CMSG gave similar low frequency absorption peaks at 400 Hz but slightly different at higher frequencies. The CMSG system did not appear to give any significant absorption peaks. SPF and crushed CMSG both had lower flow resistance than CMSG. They also had less reticulation and were less stiff. It is not clear which parameter, or combination of parameters, produced the very different results.

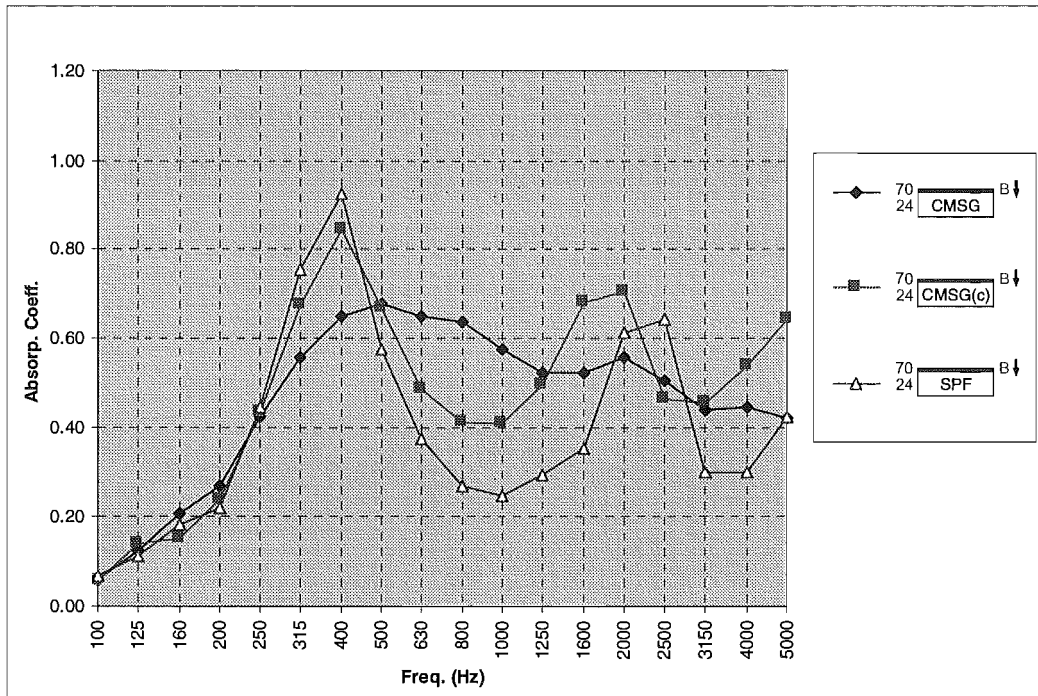


Figure 6.20 Effect of different foams on the absorption of foam and film systems.

Previous tests showed that MSG performed quite differently from crushed MSG when combined with bonded films. A film sandwiched between two layers of MSG was tested. The specimen was then crushed and retested. The difference in results is clear, Figure 6.21. MSG absorbed much more sound than crushed MSG between 630 and 2500 Hz. The foam only affected this system at frequencies greater than 630 Hz.

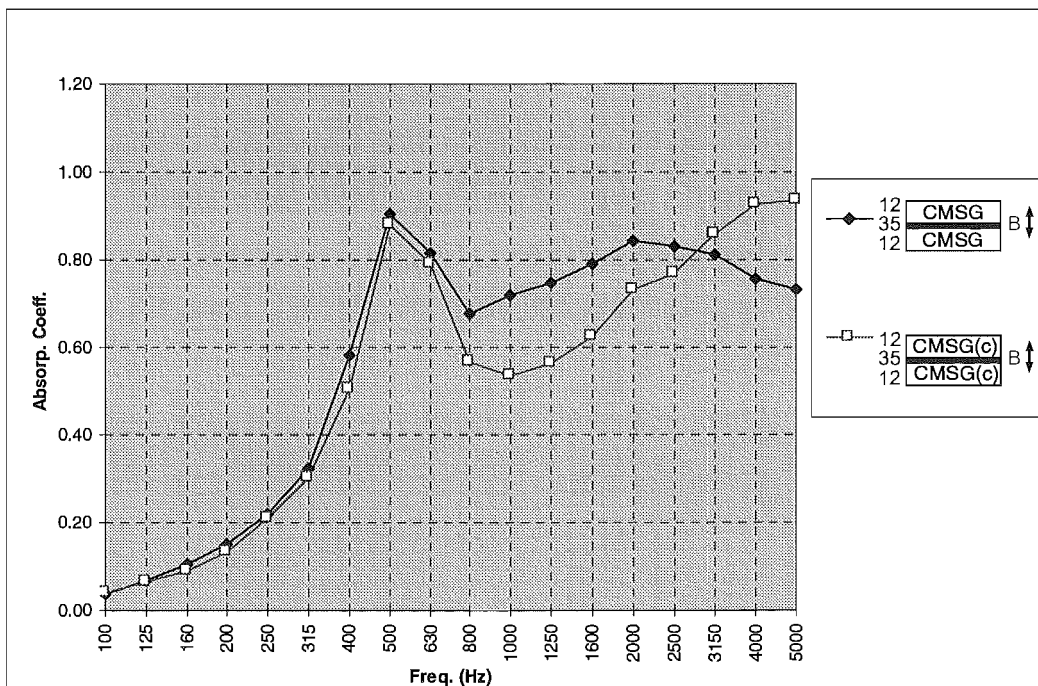
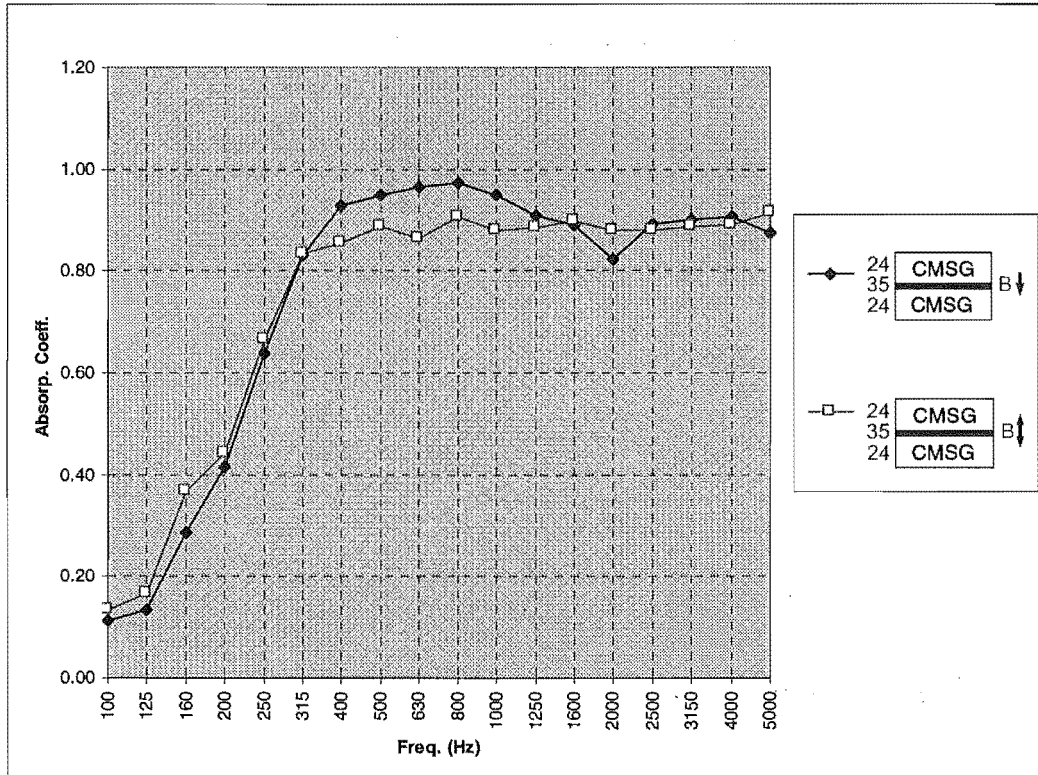


Figure 6.21 Effect of crushed foam on a sandwiched film system.

All of the layers of installed absorbers are usually bonded together. For convenience, most tests were carried out with loose-laid bulk materials. A comparison was made to determine the effect of bonding the top layer of foam. Figure 6.22 shows that there is a significant difference in the results between 400 and 1250 Hz. The loose-laid foam was decoupled from the bottom film and foam layers and hence had different absorption. This difference was small because the self weight of the loose-laid foam provided good contact between the foam and the lower film.



**Figure 6.22** Effect of bonding multiple layers.

Flow resistance measurements have shown that CMSG foam had a large variation in homogeneity, up to 50%. Tests were carried out on two different CMSG specimen and two different polyester specimen. The results for CMSG, Figure 6.23, reflected the fairly large amount of inhomogeneity in a sheet of CMSG. Figure 6.24 shows only slight variations for the polyester specimen. It would appear that the polyester tested was more homogeneous than the CMSG foam. Flow resistance homogeneity tests have not been carried out on polyester at this time.



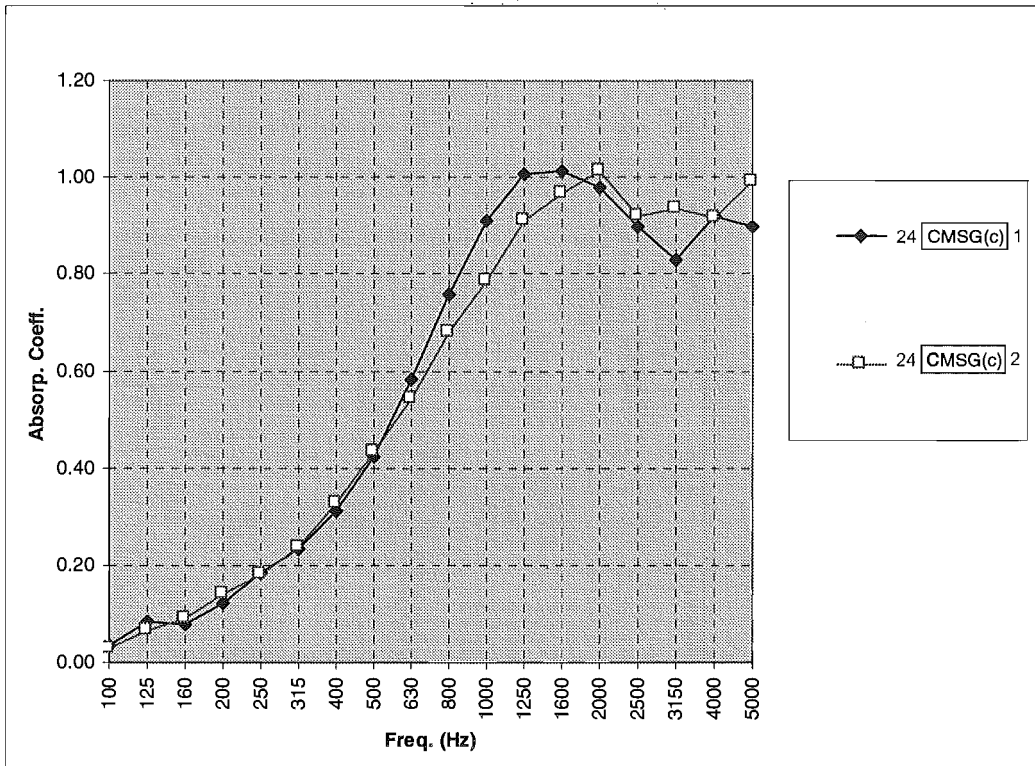


Figure 6.23 Homogeneity test on CMSG

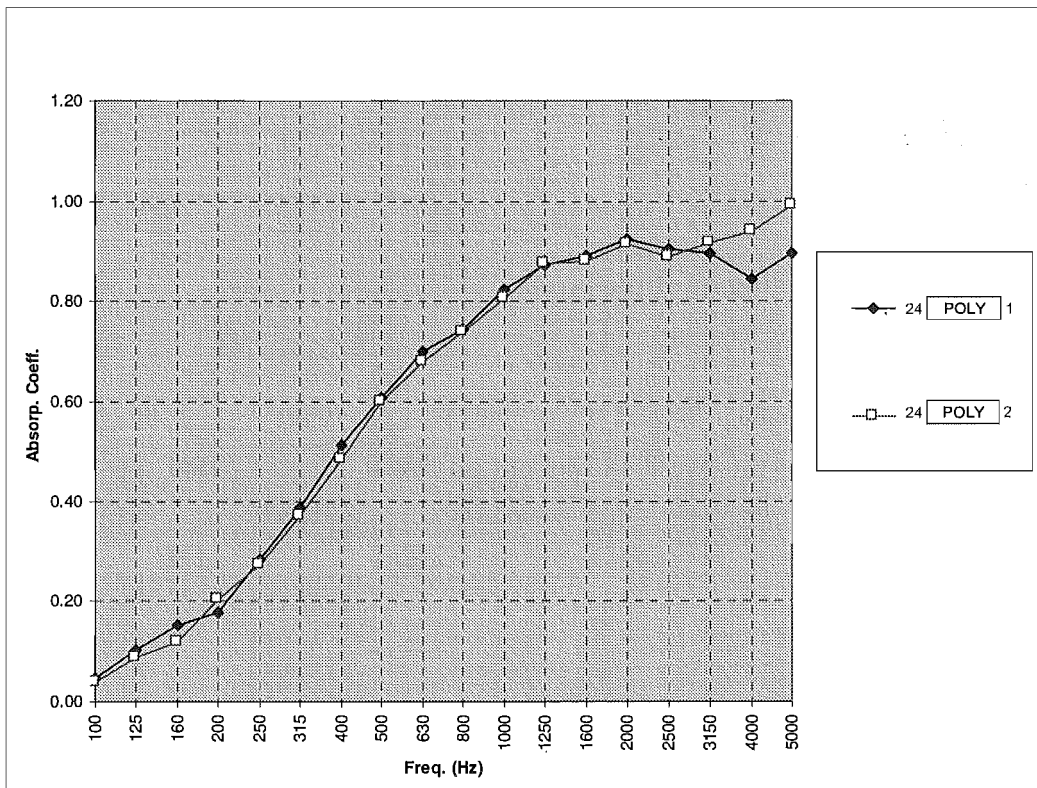


Figure 6.24 Homogeneity test on polyester

All of the tests carried out so far have been on plane bulk absorbers. A single comparative test was performed on a contoured foam. Two mating specimens were cut from a 100 mm thick sheet of SPF foam, Figure 6.2 (b). Hence, the contoured specimen was compared to materials of 50 mm thickness as this represents the same amount of material. The contoured foam absorbed more sound than CMSG at frequencies less than 1600 Hz, Figure 6.25. It absorbed more than the film faced foam system except at 250 Hz. A precise comparison cannot be made here as the contoured foam had a fabric covering while the other two specimen did not. It has been shown previously that fabric coverings can increase the absorption considerably. The two dimensional surface causes incident sound waves to propagate at right angles to the surface through the foam. This causes more wave dispersion, interaction and hence absorption than regular shaped foams.

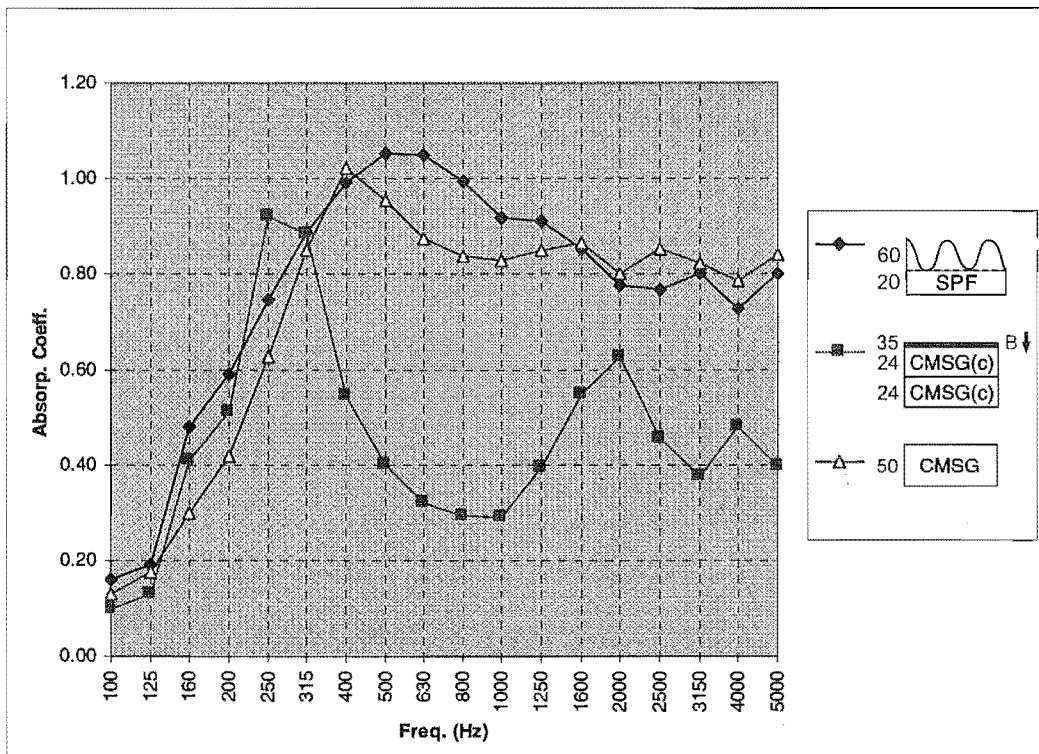


Figure 6.25 Contoured foam with fabric covering.

### 6.10 Repeatability

A repeatability test was carried out on a film faced CMSG foam. The tests were carried out on different days but with the same specimen, equipment and test procedures. The results, Figure 6.26, show very repeatable measurements. On average there was a 5% difference between the results. The repeatability test gives a good indication of the reliability of the Reverberation Room, measurement procedures and the equipment used. Clearly, confidence can be placed in the measured results.

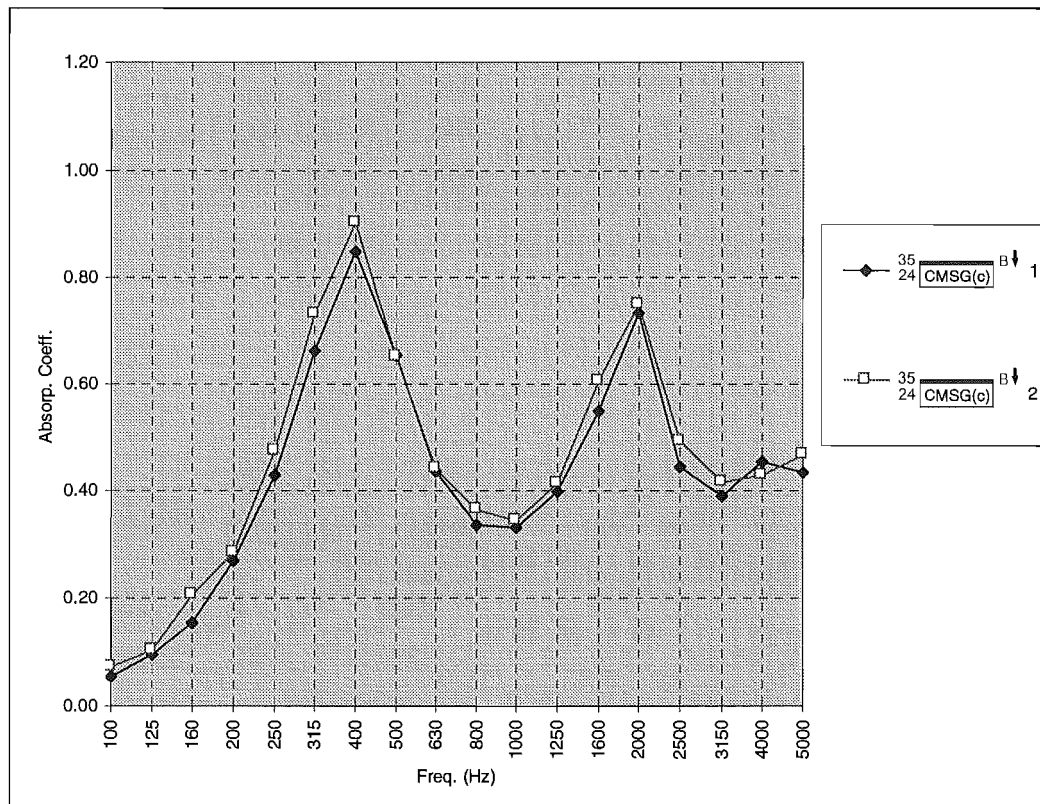


Figure 6.26 Repeatability test on film faced CMSG.

## 7. Conclusions

The effect of various absorber parameters have been determined, facilitating the design of “tunable” and wideband absorbers. Parameters including material thickness, flow resistance, film weight and fabric flow resistance were investigated. Absorber characteristics such as the effect of film position, layer bonding, material type and air cavities were similarly studied. The effect of thicker materials gave the expected result of increasing low frequency absorption. Impervious films added to bulk materials produced large absorption peaks at mid to low frequencies but were very sensitive to the type of film bonding used. Out of the bulk porous materials tested, fibreglass gave the most consistent high frequency absorption while CMSG foams and polyester board gave more mid to low frequency absorption. Air cavities behind an absorber gave similar results to a solid absorber of the same total thickness. Fabric coverings improved the absorption of porous substrates and were insensitive to bonding type. Tests were also performed on SPF foam, contoured foam and the homogeneity of foam and polyester sheets.

## References

Takahashi, D., (1989), "Excess sound absorption due to periodically arranged absorptive materials", J. Acoust. Soc. Am., v86, 1990:2215-2222.

## Bibliography

QC            Ingard, U., "Notes on sound absorption technology", Noise Control  
233            Foundation, 1994.  
.I44

---

# 5

## Modelling

---

### Summary

This chapter describes the modelling that was used to predict the absorption characteristics of tested materials. The aim was to model most of the materials and combinations of materials that were tested in the previous chapter. Two empirical models (Delany and Bazley, Qunli) and two theoretical models (Allard and Champoux, Allard et al) were used to predict the sound absorption. All four models gave similar absorption trends to the measured results for the rigid framed fibrous materials tested - fibreglass and polyester. The more complicated theoretical model of Allard et al gave the best correlation between measured and predicted results for all of the foam based absorbers. It typically gave the same trend as the measured results but with lower absorption coefficients. Allard's model was best suited to modelling system's of several layers including impervious films, fabric coverings and air cavities. Optimisation of absorber material parameters could be carried out with this model.

## Table of Contents

<b>Table of Contents</b> .....	<b>xiv</b>
<b>List of Figures</b> .....	<b>xv</b>
<b>List of Tables</b> .....	<b>xv</b>
<b>1. Introduction</b> .....	<b>70</b>
<b>2. Aims</b> .....	<b>70</b>
<b>3. Rigid Framed Fibrous Materials</b> .....	<b>70</b>
<b>4. Elastic Framed Porous Materials</b> .....	<b>71</b>
4.1 <i>Introduction</i> .....	71
4.2 <i>Fluid filled porous materials</i> .....	72
4.3 <i>Propagation constants in an elastic porous material</i> .....	73
4.4 <i>Material parameters</i> .....	75
<b>5. Layered Porous Materials</b> .....	<b>76</b>
5.1 <i>Matrix description of a porous material</i> .....	76
<b>6. A Matrix Representation of Layered Materials</b> .....	<b>78</b>
6.1 <i>Transfer matrices of fluid and porous layers</i> .....	78
6.2 <i>Interface matrices</i> .....	80
6.3 <i>The acoustic field in a layered material</i> .....	83
<b>7. Model Comparisons</b> .....	<b>84</b>
7.1 <i>Rigid framed fibrous materials</i> .....	84
7.2 <i>Elastic framed porous materials</i> .....	86
<b>8. Conclusion</b> .....	<b>93</b>
<b>References</b> .....	<b>94</b>
<b>Bibliography</b> .....	<b>95</b>

## List of Figures

<u>Figure No.</u>	<u>Page</u>
Figure 5.1 Sound waves in a porous material .....	76
Figure 6.1 Acoustic field in porous media and air layers .....	78
Figure 6.2 Impervious film in combination with air and porous layers. ....	81
Figure 7.1 Measured and predicted absorption for fibreglass. ....	85
Figure 7.2 Measured and predicted absorption for polyester. ....	86
Figure 7.3 Measured and predicted absorption for CMSG foam. ....	87
Figure 7.4 Measured and predicted absorption for crushed CMSG foam. ....	88
Figure 7.5 Measured and predicted absorption for loose-laid Mylar™ (35g/m <sup>2</sup> ). ....	89
Figure 7.6 Measured and predicted absorption for film faced crushed CMSG. ....	90
Figure 7.7 Measured and predicted absorption for film faced crushed CMSG which is bonded to the backing surface. ....	90
Figure 7.8 Measured and predicted absorption of fabric coverings on polyester. ....	91

## List of Tables

<u>Table No.</u>	<u>Page</u>
Table 7.1 Material flow resistivity .....	85
Table 7.2 Fibreglass material parameters for Allard et al, elastic frame model in Figure 7.1. ....	85
Table 7.3 Polyester material parameters for Allard et al, elastic frame model in Figure 7.2. ....	86
Table 7.4 CMSG foam material parameters for Allard et al, elastic frame model in Figure 7.3. ....	87
Table 7.5 Crushed CMSG foam material parameters for Allard et al, elastic frame model in Figure 7.4. ....	88
Table 7.6 Mylar™ film parameters for use in Allard et al, elastic frame model in Figure 7.5. ....	89
Table 7.7 Material parameters for Allard et al, elastic frame models in Figure 7.8. ....	92

## 1. Introduction

The modelling work was carried out to complement the tested results and ultimately to be used to optimise for different absorption characteristics. Rigid frame theoretical and empirical models were initially used but were difficult to modify and correlate to measured results. Hence more complicated elastic framed models were implemented. These were easier to modify and to model complicated layered systems but required more input parameters.

## 2. Aims

To predict the absorption of the different absorber systems that had been tested.

## 3. Rigid Framed Fibrous Materials

In general, sound propagation in isotropic materials is determined by two complex quantities, the characteristic impedance  $Z_0 = R + jX$  and the propagation constant  $\gamma = \alpha + j\beta$ . Delany and Bazley (1969) measured the acoustic properties of many fibrous absorbent materials. They found that the characteristic impedance and propagation constant of these materials normalised as a function of frequency divided by flow resistance. Their power laws are presented below:

$$\frac{R}{\rho_0 c_0} = 1 + 9.08 \left( \frac{f}{\sigma_c} \right)^{-0.75}, \quad \frac{X}{\rho_0 c_0} = -11.9 \left( \frac{f}{\sigma_c} \right)^{-0.73} \quad (3.1)$$

$$\alpha = 10.3 \frac{\omega}{c_0} \left( \frac{f}{\sigma_c} \right)^{-0.59}, \quad \beta = \frac{\omega}{c_0} \left[ 1 + 10.8 \left( \frac{f}{\sigma_c} \right)^{-0.70} \right] \quad (3.2)$$

with a suggested range of:

$$100 < \frac{f}{\sigma_c} < 10000 \quad (3.3)$$

$R$ ,  $X$ ,  $\alpha$  and  $\beta$  are coefficients in the characteristic impedance  $Z_0$  and propagation constant  $\gamma$  above. The symbols  $f$  and  $\sigma_c$  are the frequency in Hz and flow resistivity in cgs rays/m.  $\rho_0$  is the density of air and  $c_0$  is speed of sound in air. These can be used to calculate the normal incidence absorption coefficients of rigidly backed porous materials:



$$Z = Z_0 \coth(\gamma l), \quad \alpha_n = 1 - \frac{|Z - \rho_0 c_0|^2}{|Z + \rho_0 c_0|^2} \quad (3.4, 3.5)$$

$Z$  is the surface impedance of the porous layer,  $\alpha_n$  is the normal incidence absorption coefficient and  $l$  is the layer thickness in metres. The diffuse field absorption coefficient can be calculated by taking a statistical average over all angles of incidence, Ingard (1994):

$$\alpha_{sf} = 2 \int_0^{\pi/2} \alpha(\theta) \sin(\theta) \cos(\theta) d\theta \quad (3.6)$$

This can be expressed in closed form for locally reacting, rigidly backed porous layers, Ingard (1994).

Empirical expressions, similar to those of Delany and Bazley, describing porous plastic, open cell foams were found by Qunli (1988).

New expressions to model sound propagation in fibrous materials were developed by Allard and Champoux (1991). These theoretical equations are based on the general frequency dependence of viscous forces in porous materials.

These models were used to predict the sound absorption of the materials tested in Chapter 4, Absorption Testing.

## 4. Elastic Framed Porous Materials

### 4.1 Introduction

The previous section described the calculation of absorption for rigid framed porous materials. In many cases an incident sound wave will cause movement in the material's frame and movement of air in the material's pores. Materials with bonded, impervious film facings have significant frame motion. Rigid frame theory does not allow for frame motion and hence cannot be used for film faced materials. The elastic frame theory is based on the work by Biot (1955) who developed a theory for the propagation of elastic waves in fluid-saturated porous materials. Allard et al (1989a, 1989b, 1993, 1994) have developed this theory and applied it to the absorption and transmission loss of layered porous media. The theory has been published and is summarised in the following sections for completeness, as it covers many years, papers and differing notations. This section details the equations of motion, propagation constants and material parameters of an elastic framed porous material.

## 4.2 Fluid filled porous materials

### 4.2.1 Equations of motion

Let  $u$  be the average displacement of the frame and  $U$  the average displacement of the fluid in a volume element  $dV$  of the porous material. It is assumed that the pore size is small compared to the volume element  $dV$  and that  $dV$  is small compared to the wavelength of sound. The equations of motion for the porous material are:

$$\rho_{11} \frac{\partial^2 u}{\partial t^2} + \rho_{12} \frac{\partial u}{\partial t^2} = P \nabla (\nabla \cdot u) + Q \nabla (\nabla \cdot U) - N \nabla \times \nabla \times u + bF(\omega) \left( \frac{\partial U}{\partial t} - \frac{\partial u}{\partial t} \right) \quad (4.1)$$

$$\rho_{22} \frac{\partial^2 U}{\partial t^2} + \rho_{12} \frac{\partial u}{\partial t^2} = R \nabla (\nabla \cdot U) + R \nabla (\nabla \cdot u) - bF(\omega) \left( \frac{\partial U}{\partial t} - \frac{\partial u}{\partial t} \right) \quad (4.2)$$

With

$$\rho_{11} = \rho_1 + \rho_a \quad (4.3)$$

$$\rho_{12} = -\rho_a \quad (4.4)$$

$$\rho_{22} = h\rho_f + \rho_a \quad (4.5)$$

$\rho_1$  is the density of the frame and  $\rho_f$  the density of air.  $\rho_a$  is a mass coupling term, which is related to the structure factor  $k_s$  and the porosity  $h$  by the equation

$$\rho_a = h\rho_f(k_s - 1) \quad (4.6)$$

The coefficient  $bF(\omega)$  in (4.1) and (4.2) is a frequency-dependent viscous coupling term. It can be calculated for parallel pores of different shapes:

$$bF(\omega) = -\frac{h^2 \sigma}{4} \frac{\mu \sqrt{-i} \frac{J_1(\mu \sqrt{-i})}{J_0(\mu \sqrt{-i})}}{1 - 2 \frac{J_1(\mu \sqrt{-i})}{J_0(\mu \sqrt{-i})}} \quad (4.7)$$

$J_0$  and  $J_1$  are the Bessel functions of zero and first order respectively.  $\sigma$  is the flow resistivity in mks rays/m and  $\mu$  is given by:

$$\mu^2 = C \left( \frac{8k_s \eta}{h\sigma} \right) \quad (4.8)$$

The parameter  $C$  is a shape factor, equal to 1 for cylindrical pores and equal to  $2/3$  for parallel slits. Low flow resistivity materials typically have  $C = 1$  and high flow resistance foams require  $C = 2$ .

The parameters  $P$ ,  $Q$ ,  $R$ , and  $N$  in (4.1) and (4.2) are experimentally determined elastic constants. For a plastic foam, these parameters can be approximated by:

$$N = \text{complex shear modulus of the frame} \quad (4.9)$$

$$P = K_b + \frac{4}{3}N + \frac{(1-h)^2}{h}K_f \quad (4.10)$$

$$Q = (1-h)K_f \quad (4.11)$$

$$R = hK_f \quad (4.12)$$

$K_f$  is the compressibility of the air in the porous material. The compressibility of the air in the porous material is approximately isothermal at low frequencies. At high frequencies it is adiabatic.  $K_f$  of the air in the porous material takes this transition into account:

$$K_f = \frac{\mathcal{P}_0}{\left[ 1 + \frac{2(\gamma-1) J_1(Npr^{\frac{1}{2}}\mu\sqrt{-i})}{Npr^{\frac{1}{2}}\mu\sqrt{-i} J_0(Npr^{\frac{1}{2}}\mu\sqrt{-i})} \right]} \quad (4.13)$$

where  $\gamma = C_p/C_v$ , the ratio of the specific heats of air at constant pressure and constant volume.  $p_0$  is the equilibrium pressure of air.  $Npr$  is the Prandtl number of air (0.71).

#### 4.2.2 Stress-strain relations in an elastic porous material

The stresses used are forces per unit area acting on the frame of the fluid of the porous material.  $\tau_{ij}^s$  is the stress in the frame (s = solid) and  $\tau_{ij}^f$  is the stress in the fluid (f = fluid) of the porous material. These relations are given by

$$\tau_{ij}^s = [(P - 2N)\nabla \cdot u + Q\nabla \cdot U]\delta_{ij} + N\left(\frac{\partial u_i}{\partial \chi_j} + \frac{\partial u_j}{\partial \chi_i}\right) \quad (4.14)$$

$$\tau_{ij}^f = -hp\delta_{ij} = [R\nabla \cdot U + Q\nabla \cdot u]\delta_{ij} \quad (4.15)$$

$\delta_{ij}$  is the Kronecker delta.

#### 4.3 Propagation constants in an elastic porous material

The average displacement vectors of the frame and gas can be written as a function of scalar and vector potentials:

$$u = \nabla\phi + \nabla \times H \quad (4.16)$$

$$U = \nabla\chi + \nabla \times G \quad (4.17)$$

Inserting (4.16) and (4.17) into (4.1) and (4.2) gives one set of equations for longitudinal displacements and one set for transverse displacements. Harmonic time dependence is assumed for the longitudinal displacements:

$$\Phi = \varphi_1 + \varphi_2 \quad (4.18)$$

$$\chi = \mu_1 \varphi_1 + \mu_2 \varphi_2 \quad (4.19)$$

with

$$(\nabla^2 + k_1^2)\varphi_1 = 0 \quad (4.20)$$

$$(\nabla^2 + k_2^2)\varphi_2 = 0 \quad (4.21)$$

In these equations, the propagation constants are

$$k_{1,2} = \frac{\omega^2}{2(PR - Q^2)} \left[ (\tilde{\rho}_{11}R + \tilde{\rho}_{22}P - 2\tilde{\rho}_{12}Q) \pm \sqrt{\Delta} \right] \quad (4.22)$$

$$\Delta = (\tilde{\rho}_{11}R + \tilde{\rho}_{22}P - 2\tilde{\rho}_{12}Q)^2 - 4(PR - Q^2)(\tilde{\rho}_{11}\tilde{\rho}_{22} - \tilde{\rho}_{12}^2) \quad (4.23)$$

$$\tilde{\rho}_{11} = \rho_{11} - i \frac{bF(\omega)}{\omega} \quad (4.24)$$

$$\tilde{\rho}_{22} = \rho_{22} - i \frac{bF(\omega)}{\omega} \quad (4.25)$$

$$\tilde{\rho}_{12} = \rho_{12} + i \frac{bF(\omega)}{\omega} \quad (4.26)$$

and in (4.19)  $\mu_1$  and  $\mu_2$  are given by

$$\mu_1 = \frac{\tilde{\rho}_{11}R - \tilde{\rho}_{12}Q - (PR - Q^2) \frac{k_1^2}{\omega}}{\tilde{\rho}_{22}Q - \tilde{\rho}_{12}R} \quad (4.27)$$

$$\mu_2 = \frac{\tilde{\rho}_{11}R - \tilde{\rho}_{12}Q - (PR - Q^2) \frac{k_2^2}{\omega}}{\tilde{\rho}_{22}Q - \tilde{\rho}_{12}R} \quad (4.28)$$

It can be seen that two longitudinal waves  $\varphi_1$  and  $\varphi_2$ , with different propagation constants,  $k_1$  and  $k_2$ , propagate in the porous material. These are called slow ( $P_1$ ) and fast ( $P_2$ ) waves. It can be shown that for the slow wave, frame and air move approximately in phase opposition, whereas for the fast wave they move in phase. Consequently, the slow wave has much higher attenuation than the fast wave. The parameter  $\mu_1$  is the ratio of slow wave amplitudes in the air and frame.  $\mu_2$  is the ratio of fast wave amplitudes in the air and frame.

For the shear wave (S):

$$G = \mu_3 H \quad (4.29)$$

with

$$\nabla^2 H + k_3^2 H = 0$$

The propagation constant is:

$$k_3^2 = \frac{\omega^2}{N} \frac{\tilde{\rho}_{11}\tilde{\rho}_{22} - \tilde{\rho}_{12}^2}{\tilde{\rho}_{22}} \quad (4.30)$$

and

$$\mu_3 = -\frac{\tilde{\rho}_{12}}{\tilde{\rho}_{22}} \quad (4.31)$$

#### 4.4 Material parameters

For a detailed description of the procedures and equipment to measure the porosity, shear modulus, frame compressibility and tortuosity of porous materials see Lauriks (1994).

##### 4.4.1 Porosity

Porosity  $h$  is the amount of air in a porous material that can participate in sound propagation. For open cell reticulated foams, the porosity can be determined if the density  $\rho$  of the frame material is known:

$$h = 1 - \frac{m}{V\rho} \quad (4.32)$$

where  $V$  is the volume and  $m$  the total mass of the sample. Open cell foams typically have porosity greater than 0.90. The determination of porosity for partially reticulated foams is more difficult. The porosity of reticulated foams is usually greater than 0.95.

##### 4.4.2 Shear modulus

The dynamic shear modulus  $N$  can be measured with two foam samples of equal thickness, a shaker and an impedance head. The shaker creates shear waves in the samples while the impedance head measures the forces and velocity between the samples. The frequency response of the force and velocity outputs can be measured with a two-channel FFT analyser.

##### 4.4.3 Frame compressibility

The frame compressibility  $K_b$  can be evaluated from the shear modulus and the Poisson ratio:

$$K_b = \frac{2}{3} N \frac{1+\nu}{1-2\nu} \quad (4.33)$$

##### 4.4.4 Tortuosity

The tortuosity  $k_s$  of a foam can be measured if the frame is an electrical insulator. Air in the pores is filled with a conducting fluid, and the electrical resistivity  $r$  of the material is measured. The tortuosity is then given by:

$$k_s = h \frac{r}{r_f} \quad (4.34)$$

where  $r_f$  is the electrical resistivity of the conducting fluid. Reticulated foams typically have a tortuosity close to 1, while non-reticulated foams can have values as high as 4.

## 5. Layered Porous Materials

### 5.1 Matrix description of a porous material

This section describes the propagation of a sound field in an elastic framed porous material. This theory is based on the work by Biot (1955) and has been presented in matrix form by Allard et al (1989a, 1993) and Lauriks (1994). A porous material of thickness  $d$  is represented in Figure 5.1. An incident plane wave in the air above the layer generates a  $P_1$ ,  $P_2$  and an  $S$  wave in the porous layer. Each wave is reflected and generates a  $P_1$ ,  $P_2$  and  $S$  wave at the interface  $x_3 = 0$ . The three incident waves can be represented by:

$$\phi_j' = A_j' e^{-ik_j(x_1 w_{j1} + x_3 w_{j3}) + i\alpha t} \quad j=1,2,3 \quad (5.1)$$

$\omega_3$  is the component of the vector potential  $H$  of the  $S$  wave. For the reflected waves:

$$\phi_j'' = A_j'' e^{-ik_j(x_1 w_{j1} - x_3 w_{j3}) + i\alpha t} \quad j=1,2,3 \quad (5.2)$$

Application of the law of Snell-Descartes gives:

$$w_{j1} k_j = k \sin \theta \quad (5.3)$$

$$w_{j3} = \sqrt{(1 - w_{j1}^2)} \quad (5.4)$$

where  $k$  is the wave number in air and  $\theta$  the angle of incidence.

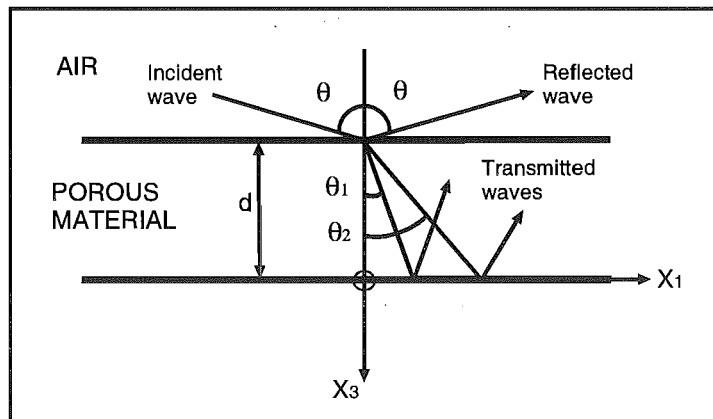


Figure 5.1 Sound waves in a porous material

The wavenumbers of the  $P_1$ ,  $P_2$  and  $S$  wave are complex and hence the  $w_{j1}$  are complex too. Consequently the waves represented in (5.1) and (5.2) are inhomogeneous plane waves. The total sound field in the layer is given by:

$$\varphi_j = \varphi'_j + \varphi''_j = \bar{\varphi}'_j e^{-i\alpha_j x_3} + \bar{\varphi}''_j e^{i\alpha_j x_3} \quad (5.5)$$

$$\bar{\varphi}'_j = A'_j e^{-i\zeta_j x_1 + i\alpha x} \quad (5.6)$$

$$\bar{\varphi}''_j = A''_j e^{-i\zeta_j x_1 + i\alpha x} \quad (5.7)$$

$$\alpha_j = k_j w_{j3} \quad \zeta_j = k_j w_{j1} \quad (5.8)$$

This sound field is determined by the six amplitudes  $A'_j$  and  $A''_j$ . If six independent stresses and displacements are known at one of the two faces of the layer then the amplitudes can be calculated. The six stresses and displacements that are typically used are  $u_1$ ,  $u_3$ ,  $U_3$ ,  $\tau_{33}^s$ ,  $\tau_{13}^s$  and  $\tau_{33}^f$ .

Let  $V$  be the vector

$$V = [u_1, u_3, U_3, \tau_{33}^s, \tau_{13}^s, \tau_{33}^f] \quad (5.9)$$

The displacement and stress components can be written as a function of the potentials with the aid of (4.14 - 4.19)

$$u_1 = \frac{\partial \varphi_1}{\partial x_1} + \frac{\partial \varphi_2}{\partial x_1} - \frac{\partial \varphi_3}{\partial x_3} \quad (5.10)$$

$$u_3 = \frac{\partial \varphi_1}{\partial x_3} + \frac{\partial \varphi_2}{\partial x_3} + \frac{\partial \varphi_3}{\partial x_1} \quad (5.11)$$

$$U_3 = \mu_1 \frac{\partial \varphi_1}{\partial x_3} + \mu_2 \frac{\partial \varphi_2}{\partial x_3} + \mu_3 \frac{\partial \varphi_3}{\partial x_1} \quad (5.12)$$

$$\tau_{33}^s = (P - 2N) \nabla \cdot u + 2N \frac{\partial u_3}{\partial x_3} \quad (5.13)$$

$$\tau_{12}^s = N \left( \frac{\partial u_3}{\partial x_1} + \frac{\partial u_1}{\partial x_3} \right) \quad (5.14)$$

$$\tau_{33}^f = R \nabla \cdot U + Q \nabla \cdot u \quad (5.15)$$

These can be expressed in matrix form:

$$V = [G(x_3)] \phi \quad (5.16)$$

with the vector  $\phi$  given by:

$$\phi = \begin{bmatrix} \varphi_j'' + \varphi_j' \\ \varphi_j'' - \varphi_j' \\ \varphi_j'' + \varphi_j' \\ \varphi_j'' - \varphi_j' \\ \varphi_j'' + \varphi_j' \\ \varphi_j'' - \varphi_j' \end{bmatrix} \quad (5.17)$$

The elements of the matrix  $[G(x_3)]$  are given in Appendix D. The vector  $V$  at the two faces of the porous layer can be determined by setting  $x_3$  equal to 0 and  $-d$ :

$$V(x_3 = -d) = [G(-d)]\phi \quad (5.18)$$

$$V(x_3 = 0) = [G(0)]\phi \quad (5.19)$$

A relationship between the values of  $V$  at the faces of the layer is found by inverting  $[G(0)]$ :

$$V(x_3 = -d) = [G(-d)][G(0)]^{-1}V(x_3 = 0) \quad (5.20)$$

The matrix  $[T^p] = [G(-d)][G(0)]^{-1}$  is an acoustic transfer matrix for the porous layer.

## 6. A Matrix Representation of Layered Materials

### 6.1 Transfer matrices of fluid and porous layers

A general method for determining the absorption and transmission loss of layered materials has been presented by Allard et al (1993). This included fluid, porous and solid layers in various combinations. Porous media and air layers of a stratified material are shown in Figure 6.1. The acoustic field is generated by a plane wave at angle of incidence  $\theta$ .

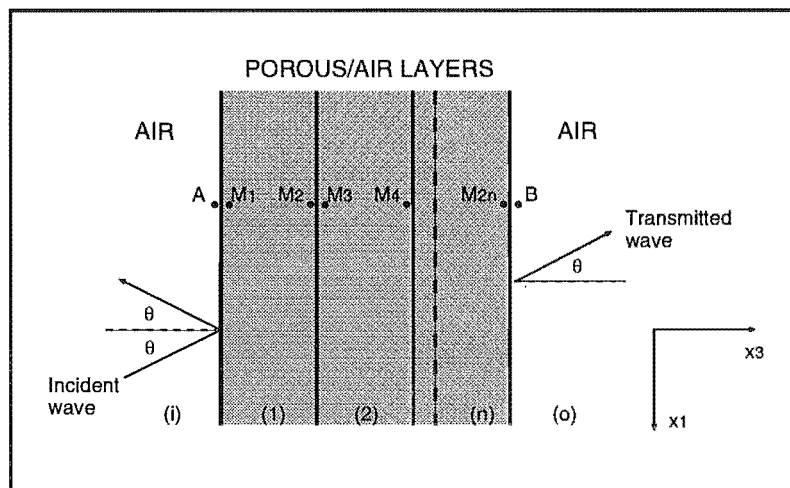


Figure 6.1 Acoustic field in porous media and air layers.



The component of the wavenumber vector  $k_1$  in the  $x_1$  direction in each layer is given by:

$$k_1 = k \sin \theta \quad (6.1)$$

where  $k$  is the wavenumber in air. Let  $v_3^s(M)$ ,  $v_1^s(M)$  be the  $x_3$  and  $x_1$  velocity components of the porous material's frame at  $M$ . Also, let  $v_3^f(M)$ ,  $v_1^f(M)$  be the  $x_3$  and  $x_1$  velocity components of the fluid at  $M$  (in the case of a fluid, or of the air in a porous material). Let  $\sigma_{33}^s$ ,  $\sigma_{13}^s$  and  $\sigma_{33}^f$ ,  $\sigma_{13}^f$  be the normal and the tangential stresses. These stresses are related to forces acting per unit area of material. In a fluid:

$$\sigma_{13}^f = 0, \quad \sigma_{33}^f = -p \quad (6.2, 6.3)$$

where  $p$  is the pressure. In a porous medium, equation (6.3) becomes

$$\sigma_{33}^f = -\phi p \quad (6.4)$$

where  $\phi$  is the porosity. In a fluid layer, the acoustic field is known if the quantities  $(p(M), v_3^f(M))$  are known. A 2 x 2 matrix is used to relate the pressure and the  $x_3$  velocity component at either side of the layer ( $M_2$  and  $M_1$  if the first layer of the stratified material in Figure 6.1 is a fluid):

$$V^f(M_1) = [T^f] V^f(M_2) \quad (6.5)$$

with

$$V^f(M_2) = [p(M_2), v_3^f(M_2)]^T \quad (6.6)$$

The superscript  $T$ , in equation (6.6) indicates the transposition from line to column vector.

$$\begin{aligned} T_{11}^f &= \cos k_3 L & T_{12}^f &= (\omega \rho / k_3) j \sin k_3 L \\ T_{21}^f &= (k_3 / \omega \rho) j \sin k_3 L & T_{22}^f &= \cos k_3 L \end{aligned} \quad (6.7)$$

$\rho$  is the density,  $L$  the thickness of the layer, and the symbol  $j$  represents  $\sqrt{-1}$ .

$$k_3 = (k_f^2 - k_1^2)^{1/2} \quad (6.8)$$

where  $k_f$  is the wavenumber in the fluid.

Three different kinds of waves can propagate in a porous material according to the Biot theory. If the first layer in Figure 6.1 is a porous layer, two vectors  $V^p(M_1)$  and  $V^p(M_2)$  are related by a 6 x 6 transfer matrix  $[T^p]$ :

$$V^p(M_1) = [T^p] V^p(M_2) \quad (6.9)$$

where

$$V^p(M) = [v_1^s, v_3^s, v_3^f, \sigma_{33}^s, \sigma_{13}^s, \sigma_{33}^f]^T \quad (6.10)$$

The transfer matrix  $[T^p]$  is given in equation (5.20) above.

## 6.2 Interface matrices

The points  $M_2$  and  $M_3$  in Figure 6.1 are close to each other but on different sides of the boundary. Interface matrices relate the acoustic fields at  $M_2$  and  $M_3$ .

### 6.2.1 Fluid layers

For two fluids, the boundary conditions are

$$V^f(M_2) = V^f(M_3) \quad (6.11)$$

Two interface matrices  $[I_{f,f}]$  and  $[J_{f,f}]$  exist, such that:

$$[I_{f,f}]V^f(M_2) + [J_{f,f}]V^f(M_3) = 0 \quad (6.12)$$

where  $[I_{f,f}]$  and  $[J_{f,f}]$  are opposite and  $[I_{f,f}]$  is any diagonal matrix – for example, the 2 x 2 unit matrix.

### 6.2.2 Porous layers

For two porous layers, the boundary conditions are:

$$\sigma_{13}^s(M_2) = \sigma_{13}^s(M_3), \quad \sigma_{33}^f(M_2) + \sigma_{33}^s(M_2) = \sigma_{33}^f(M_3) + \sigma_{33}^s(M_3) \quad (6.13, 6.14)$$

$$v_1^s(M_2) = v_1^s(M_3), \quad v_3^s(M_2) = v_3^s(M_3) \quad (6.15, 6.16)$$

$$\phi_1(v_3^f(M_2) - v_3^s(M_2)) = \phi_2(v_3^f(M_3) - v_3^s(M_3)), \quad \sigma_{33}^f(M_2)/\phi_1 = \sigma_{33}^f(M_3)/\phi_2 \quad (6.17, 6.18)$$

where  $\phi_1$  and  $\phi_2$  are the porosities at  $M_2$  and  $M_3$ . Equation (6.12) can be rewritten as

$$[I_{p,p}]V^p(M_2) + [J_{p,p}]V^p(M_3) = 0 \quad (6.19)$$

where  $[I_{p,p}]$  is the 6 x 6 unit matrix, and  $[J_{p,p}]$  is given by

$$[J_{p,p}] = - \begin{bmatrix} 1 & 0 & 0 & 0 & 0 & 0 \\ 0 & 1 & 0 & 0 & 0 & 0 \\ 0 & 1 - \phi_2/\phi_1 & \phi_2/\phi_1 & 0 & 0 & 0 \\ 0 & 0 & 0 & 1 & 0 & (1 - \phi_1/\phi_2) \\ 0 & 0 & 0 & 0 & 1 & 0 \\ 0 & 0 & 0 & 0 & 0 & \phi_1/\phi_2 \end{bmatrix} \quad (6.20)$$

### 6.2.3 Porous, fluid layers

For a fluid and a porous layer, the boundary conditions are:

$$v_3^f(M_2) = (1 - \phi_2)v_3^s(M_3) + \phi_2v_3^f(M_3), \quad -\phi_2p(M_2) = \sigma_{33}^f(M_3) \quad (6.21, 6.22)$$

$$-(1 - \phi_2)p(M_2) = \sigma_{33}^s(M_3), \quad 0 = \sigma_{13}^s(M_3) \quad (6.23, 6.24)$$

These equations can be rewritten as:

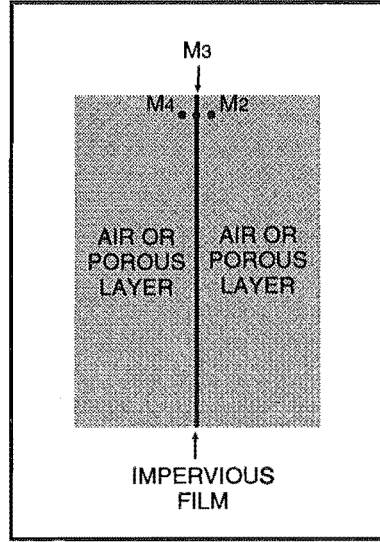
$$[I_{f,p}]V^f(M_2) + [J_{f,p}]V^p(M_3) = 0 \quad (6.25)$$

where

$$[I_{f,p}] = \begin{bmatrix} 0 & -1 \\ \phi_2 & 0 \\ (1-\phi_2) & 0 \\ 0 & 0 \end{bmatrix}, [J_{f,p}] = \begin{bmatrix} 0 & (1-\phi_2) & \phi_2 & 0 & 0 & 0 \\ 0 & 0 & 0 & 0 & 0 & 1 \\ 0 & 0 & 0 & 1 & 0 & 0 \\ 0 & 0 & 0 & 0 & 1 & 0 \end{bmatrix} \quad (6.26, 6.27)$$

#### 6.2.4 Film faced layers

The system of equations governing an impervious film facing are given by Allard et al (1989b).



**Figure 6.2** Impervious film in combination with air and porous layers.

For a fluid ( $M_4$ ), film ( $M_3$ ) and porous layer ( $M_2$ ) combination, Figure 6.2, the Newton law for the film can be written as:

$$i\omega\rho_1 v_3(M_3) = \sigma_{33}^s(M_2) + \sigma_{33}^f(M_2) - \sigma_{33}^f(M_4) \quad (6.28)$$

$$i\omega\rho_2 v_1(M_3) = \sigma_{13}^s(M_2) \quad (6.29)$$

with

$$\rho_1 = \rho - tk^2 \frac{\sin^2 \theta}{\omega^2} \quad \text{and} \quad \rho_2 = \rho - Sk^2 \frac{\sin^2 \theta}{\omega^2} \quad (6.30, 6.31)$$

and  $\rho$  is the mass per unit area of the film,  $t$  is the tension of the film and  $S$  the stiffness of the film. The film is assumed to be perfectly flexible. The boundary conditions are:

$$v_3^f(M_4) = v_3^f(M_2), \quad v_3^f(M_4) = v_3^s(M_2), \quad v_3^f(M_4) = v_3(M_3) \quad (6.32, 6.33, 6.34)$$

$$v_1^s(M_2) = v_1(M_3) \quad (6.35)$$

Inserting equation (6.34) into (6.28) and equation (6.35) into (6.29) yields:

$$i\omega\rho_1 v_3^f(M_4) = \sigma_{33}^s(M_2) + \sigma_{33}^f(M_2) - \sigma_{33}^f(M_4) \quad (6.36)$$

$$i\omega\rho_2 v_1^s(M_2) = \sigma_{13}^s(M_2) \quad (6.37)$$

These equations can be expressed, with the aid of equation (6.3), as:

$$[I_{f,s,p}]V^f(M_4) + [J_{f,s,p}]V^p(M_2) = 0 \quad (6.38)$$

where

$$[I_{f,s,p}] = \begin{bmatrix} -1 & i\omega\rho_1 \\ 0 & 0 \\ 0 & 1 \\ 0 & 1 \end{bmatrix}, [J_{f,s,p}] = \begin{bmatrix} 0 & 0 & 0 & -1 & 0 & -1 \\ i\omega\rho_2 & 0 & 0 & 0 & -1 & 0 \\ 0 & 0 & -1 & 0 & 0 & 0 \\ 0 & -1 & 0 & 0 & 1 & 0 \end{bmatrix} \quad (6.39, 6.40)$$

For a fluid ( $M_4$ ), film ( $M_3$ ) and fluid ( $M_2$ ) combination, Figure 6.2, the Newton law for the film can be written as:

$$i\omega\rho_1 v_3(M_3) = \sigma_{33}^f(M_2) - \sigma_{33}^f(M_4) \quad (6.41)$$

where  $\rho_1$  has the same meaning as in equation (6.30).

The boundary conditions are now:

$$v_3^f(M_4) = v_3^f(M_2), \quad v_3^f(M_4) = v_3(M_3) \quad (6.42, 6.43)$$

Inserting equations (6.43) and (6.3) into (6.41) yields:

$$i\omega\rho_1 v_3^f(M_2) - \sigma_{33}^f(M_2) = p(M_4) \quad (6.44)$$

These equations can be expressed as:

$$[I_{f,s,f}]V^f(M_4) + [J_{f,s,f}]V^f(M_2) = 0 \quad (6.45)$$

where

$$[I_{f,s,f}] = \begin{bmatrix} -1 & 0 \\ 0 & -1 \end{bmatrix}, [J_{f,s,f}] = \begin{bmatrix} 1 & i\omega\rho_1 \\ 0 & 1 \end{bmatrix} \quad (6.46, 6.47)$$

For a porous layer ( $M_4$ ), film ( $M_3$ ) and porous layer ( $M_2$ ) combination, Figure 6.2, the Newton law for the film can be written as:

$$i\omega\rho_1 v_3(M_3) = \sigma_{33}^s(M_2) + \sigma_{33}^f(M_2) - \sigma_{33}^f(M_4) - \sigma_{33}^s(M_4) \quad (6.48)$$

$$i\omega\rho_2 v_1(M_3) = \sigma_{13}^s(M_2) - \sigma_{13}^s(M_4) \quad (6.49)$$

where  $\rho_1$  and  $\rho_2$  have the same definitions as in equations (6.30) and (6.31). The boundary conditions are:

$$v_3^f(M_4) = v_3^s(M_2), \quad v_3^s(M_4) = v_3^s(M_2) \quad (6.50, 6.51)$$

$$v_3^s(M_4) = v_3^f(M_2), \quad v_3^f(M_2) = v_3(M_3) \quad (6.52, 6.53)$$

$$v_1^s(M_2) = v_1(M_3), \quad v_1^s(M_4) = v_1^s(M_2) \quad (6.54, 6.55)$$

These equations can be expressed as:

$$[I_{p,s,p}]V^p(M_4) + [J_{p,s,p}]V^p(M_2) = 0 \quad (6.56)$$

where

$$[I_{p,s,p}] = \begin{bmatrix} 0 & 0 & 0 & 1 & 0 & 1 \\ 0 & 0 & 0 & 0 & 1 & 0 \\ 0 & 1 & 0 & 0 & 0 & 0 \\ 0 & 0 & 1 & 0 & 0 & 0 \\ 0 & 1 & 0 & 0 & 0 & 0 \\ 1 & 0 & 0 & 0 & 0 & 0 \end{bmatrix}, [J_{p,s,p}] = \begin{bmatrix} 0 & 0 & i\omega\rho_1 & -1 & 0 & -1 \\ i\omega\rho_2 & 0 & 0 & 0 & -1 & 0 \\ 0 & -1 & 0 & 0 & 0 & 0 \\ 0 & -1 & 0 & 0 & 0 & 0 \\ 0 & 0 & -1 & 0 & 0 & 0 \\ -1 & 0 & 0 & 0 & 0 & 0 \end{bmatrix} \quad (6.57, 6.58)$$

Other interface matrices can easily be obtained from the previous equations.

### 6.3 The acoustic field in a layered material

The acoustic field at the boundaries of the layers in Figure 6.1 is defined by the vectors  $V(M_1)$ ,  $V(M_2), \dots, V(M_{2n})$ . It has been shown that interface matrices exist such that:

$$[I_{i,1}]V(A) + [J_{i,1}]V(M_1) = 0 \quad (6.59)$$

A transfer matrix can be used to describe the acoustic field through a layer:

$$V(M_1) = [T_{(1)}]V(M_2) \quad (6.60)$$

These can be combined by inserting equation (6.60) into (6.59) to describe a combination of many layers:

$$[I_{i,1}]V(A) + [J_{i,1}][T_{(1)}]V(M_2) = 0 \quad (6.61)$$

$$[I_{1,2}]V(M_2) + [J_{1,2}][T_{(2)}]V(M_4) = 0 \quad (6.62)$$

$$[I_{n,o}]V(M_{2n}) + [J_{n,o}]V(B) = 0 \quad (6.63)$$

This set of equations can be rewritten as:

$$[D]V_D = 0 \quad (6.64)$$

where

$$V_D = [p(A), v^f(A), V(M_2), \dots, V(M_{2n}), p(B), v^f(B)]^T \quad (6.65)$$

The acoustic field at each side of the layered material must be defined to enable the system's surface impedance to be determined. If the air layer at the right hand side of the material is semi-infinite, the impedance at  $B$  is given by:

$$Z_b = p(B)/v_3^f(B) = Z_c / \cos\theta \quad (6.66)$$

where  $Z_c$  is the characteristic impedance of air ( $Z_c = \rho_0 c_0$ ). Similarly, if the layered material is backed by a rigid wall of infinite impedance:

$$v(B) = 0 \quad (6.67)$$

This boundary condition is combined with equation (6.64):

$$\begin{bmatrix} & [D] & & & \\ 0 & \dots & 0 & 0 & 1 \end{bmatrix} V_D = [D'] V_D = 0 \quad (6.68)$$

Finally, the impedance  $Z_a$  of the layered material can be calculated by adding one more condition to the set of equations (6.68):

$$p(A) - Z_a v_3^f(A) = 0 \quad (6.69)$$

This gives a complete set of homogenous equations represented by the matrix  $[D'']$ :

$$[D''] V_D = \begin{bmatrix} -1 & Z_a & 0 & \dots & 0 \\ & & [D] & & \\ 0 & \dots & 0 & -1 & Z_b \end{bmatrix} V_D = 0 \quad (6.70)$$

For non-trivial solutions to this set of homogenous equations the determinant of matrix  $D''$  must be equal to zero. Expansion of  $D''$  along the top row gives:

$$Z_a = -|D_1'|/|D_2'| \quad (6.71)$$

where  $|D_1'|$  is the determinant of the matrix  $[D']$  with the first column removed.  $|D_2'|$  is the determinant of the matrix  $[D']$  with the second column removed. Hence, the surface impedance at the left hand side of a layered system can be determined. The absorption coefficient follows from:

$$\alpha(\theta) = 1 - \left| \frac{Z_a \cos \theta - \rho_0 c_0}{Z_a \cos \theta + \rho_0 c_0} \right|^2 \quad (6.72)$$

The diffuse field absorption coefficient can then be calculated by integrating over all angles of incidence, equation (3.6).

## 7. Model Comparisons

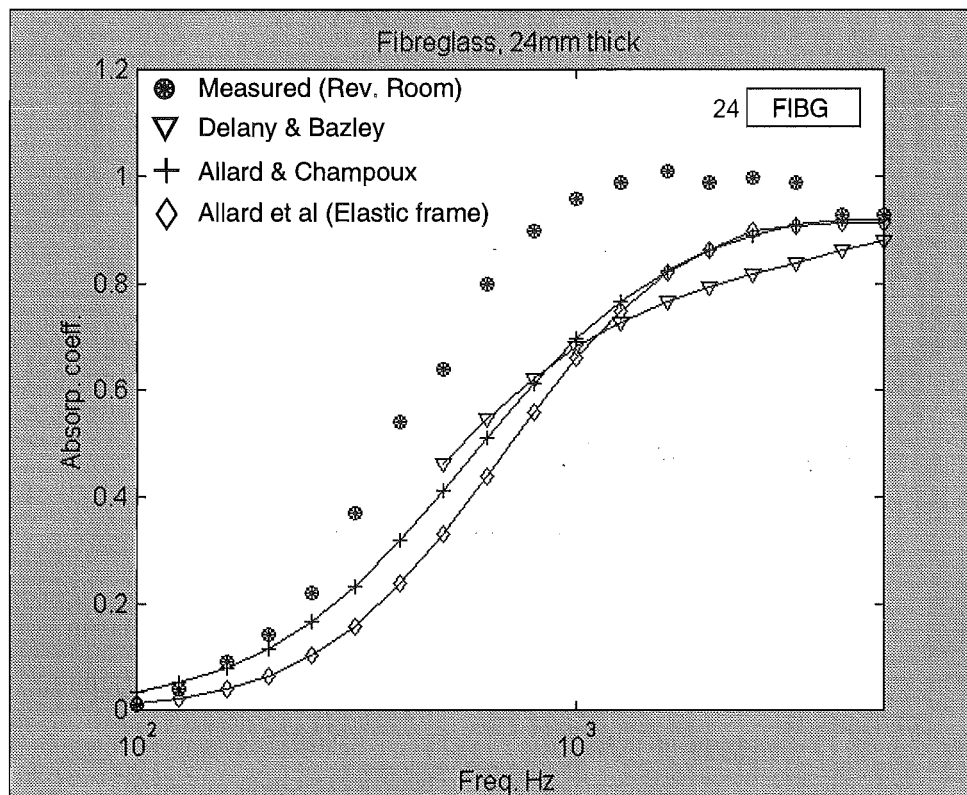
### 7.1 Rigid framed fibrous materials

In this section the measured absorption of fibreglass and polyester board is compared to that predicted by the empirical model of Delany and Bazley (1969) and the theoretical model presented by Allard and Champoux (1991). A comparison with the elastic framed porous material model, Allard et al (1989a, 1989b, 1993), is also included. This elastic framed model was more complicated than the previous ones and required more material parameters. Some of these were not measured but estimated, indicated by a “\*”. Each material’s flow resistivity is shown in Table 7.1. All of the modelled absorption coefficients presented below are the statistical average over all angles of incidence.

**Table 7.1 Material flow resistivity**

Material	Flow resistivity (mks rays/m)
Fibreglass	47000
Polyester	11700
CMSG foam	9800
Crushed CMSG foam	8800

Figure 7.1 shows the measured and predicted absorption of rigidly backed fibreglass. Each model gave similar trends and were consistently less than the measured data for all frequencies.

**Figure 7.1 Measured and predicted absorption for fibreglass.****Table 7.2 Fibreglass material parameters for Allard et al, elastic frame model in Figure 7.1.**

Material	Tortuosity, $k_s$	Frame density, $\rho_1$ ( $\text{kg/m}^3$ )	Porosity, $h$	Shear modulus, $N$ ( $\text{N/m}^2$ )	Poisson coefficient, $\nu$	Form factor, $c$
Fibreglass	1*	90	0.97	$10^6(1+0.1j)^*$	0.3*	1.4*

The measured and predicted absorption of polyester is shown in Figure 7.2. Most of the modelled results were less than the measured results. In this case, the predictions from the Delany and Bazley model and the Allard et al model were closest to the measured data.

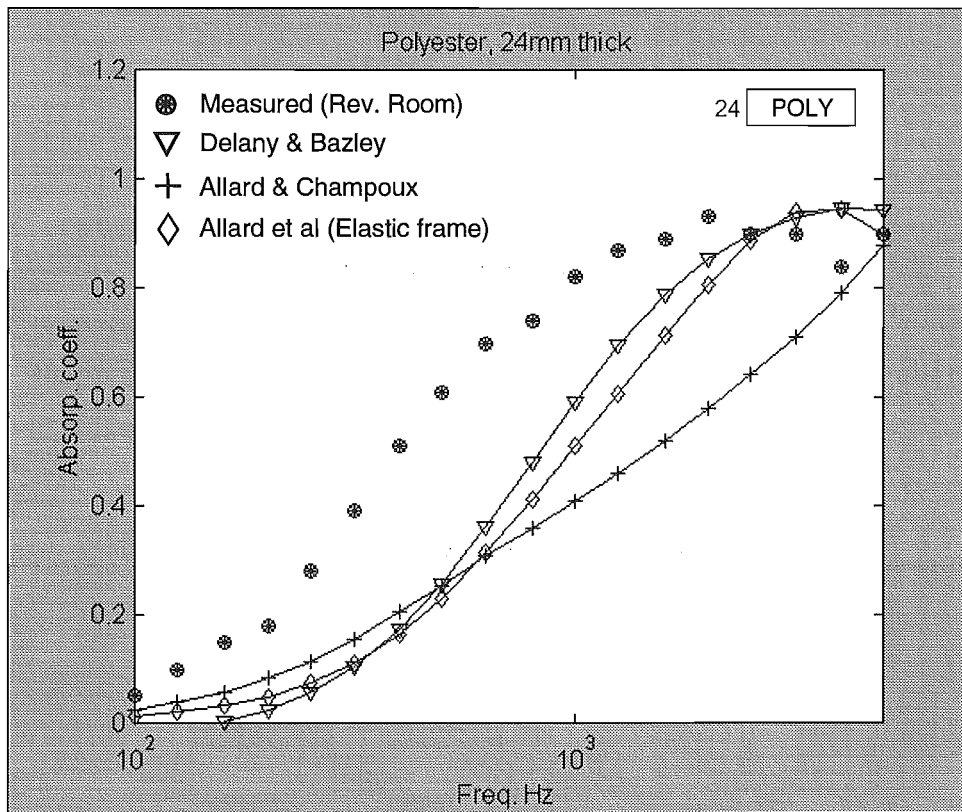


Figure 7.2 Measured and predicted absorption for polyester.

Table 7.3 Polyester material parameters for Allard et al, elastic frame model in Figure 7.2.

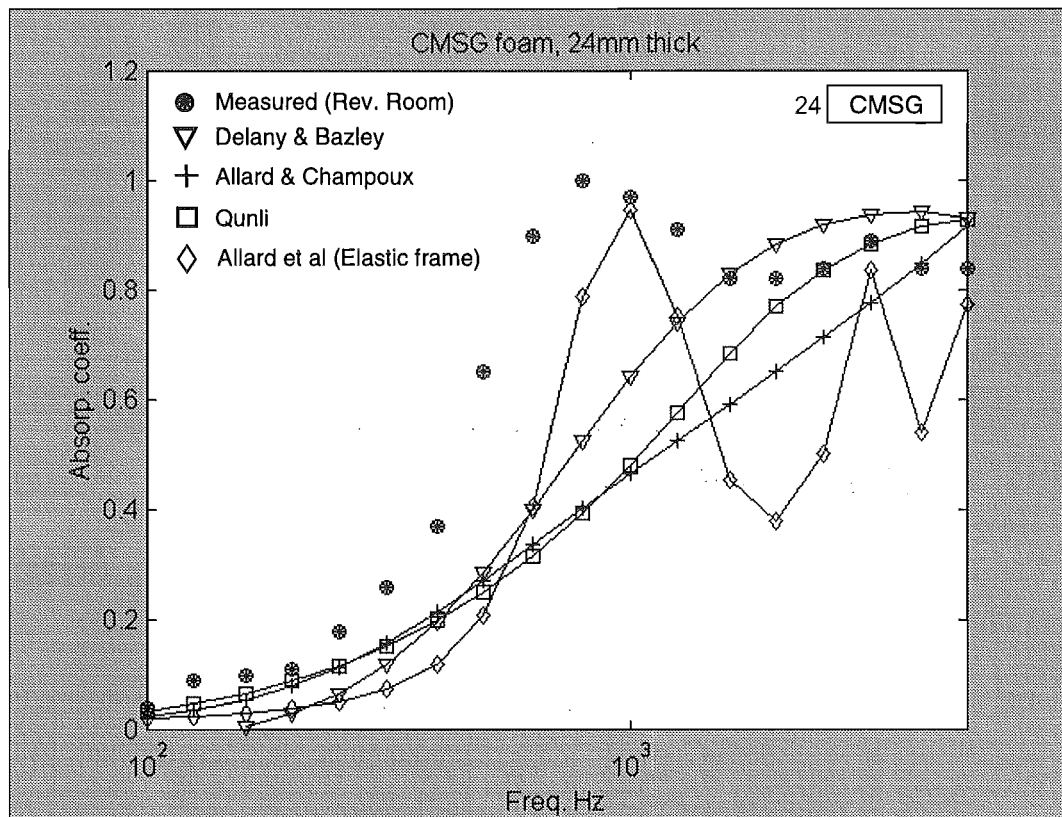
Material	Tortuosity, $k_s$	Frame density, $\rho_1$ ( $\text{kg/m}^3$ )	Porosity, $h$	Shear modulus, N ( $\text{N/m}^2$ )	Poisson coefficient, $\nu$	Form factor, $c$
Polyester	1*	80	0.94	$10^6(1+0.1j)^*$	0.3*	1.4*

### 7.2 Elastic framed porous materials

A comparison was also made between the measured absorption of CMSG foam and the empirical model presented by Qunli and the elastic framed porous model of Allard et al. The rigid framed fibrous predictions of Delany, Bazley, Allard and Champoux above are also shown as these are often used to approximate the absorption of foams.



The four models are shown in the prediction of CMSG foam absorption, Figure 7.3. The first three models, Delany and Bazley, Allard and Champoux and Qunli gave similar trends across the frequency range but were quite different from the measured results. In particular, these models did not account for closed cells in the foam and hence did not predict the lower frequency peak at 800Hz. The model of Allard et al gave a similar trend to the measured data when the tortuosity was set quite high. However, it seems that the Allard et al model was underdamped – evidenced by the large swings in absorption coefficient. The CMSG foam was produced from standard SPF foam by loading it with a Melamine powder. This loading was not accounted for in any of the models and may have contributed to the low frequency peak at 800 Hz.



**Figure 7.3** Measured and predicted absorption for CMSG foam.

**Table 7.4** CMSG foam material parameters for Allard et al, elastic frame model in Figure 7.3.

Material	Tortuosity, $k_s$	Frame density, $\rho_1$ ( $\text{kg/m}^3$ )	Porosity, h	Shear modulus, N ( $\text{N/m}^2$ )	Poisson coefficient, $\nu$	Form factor, c
CMSG	10*	43	0.96	$10^5(1+0.1j)^*$	0.3*	3*

Figure 7.4 shows the measured and modelled absorption coefficients for crushed CMSG foam backed by a rigid wall. The first three models did not predict the absorption peak at 1600 Hz. Again, this will be due to the amount of reticulation in the CMSG foam. The model of Allard et al with high tortuosity showed the measured trend but with lower absorption coefficients.

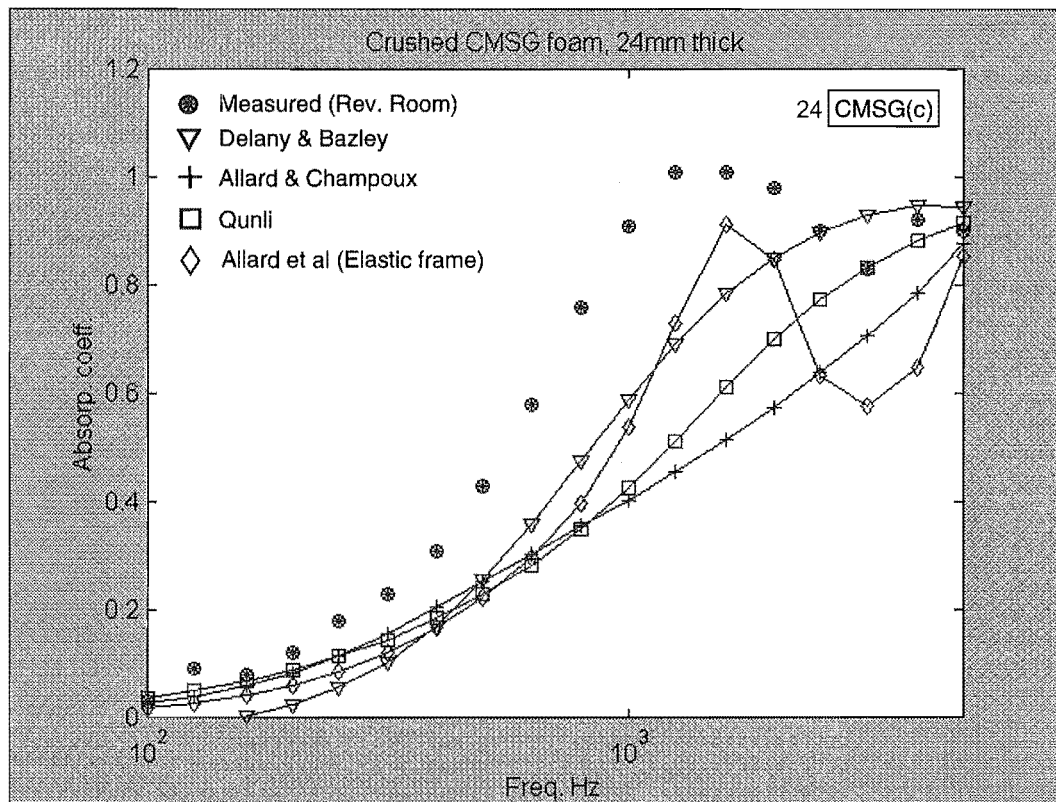
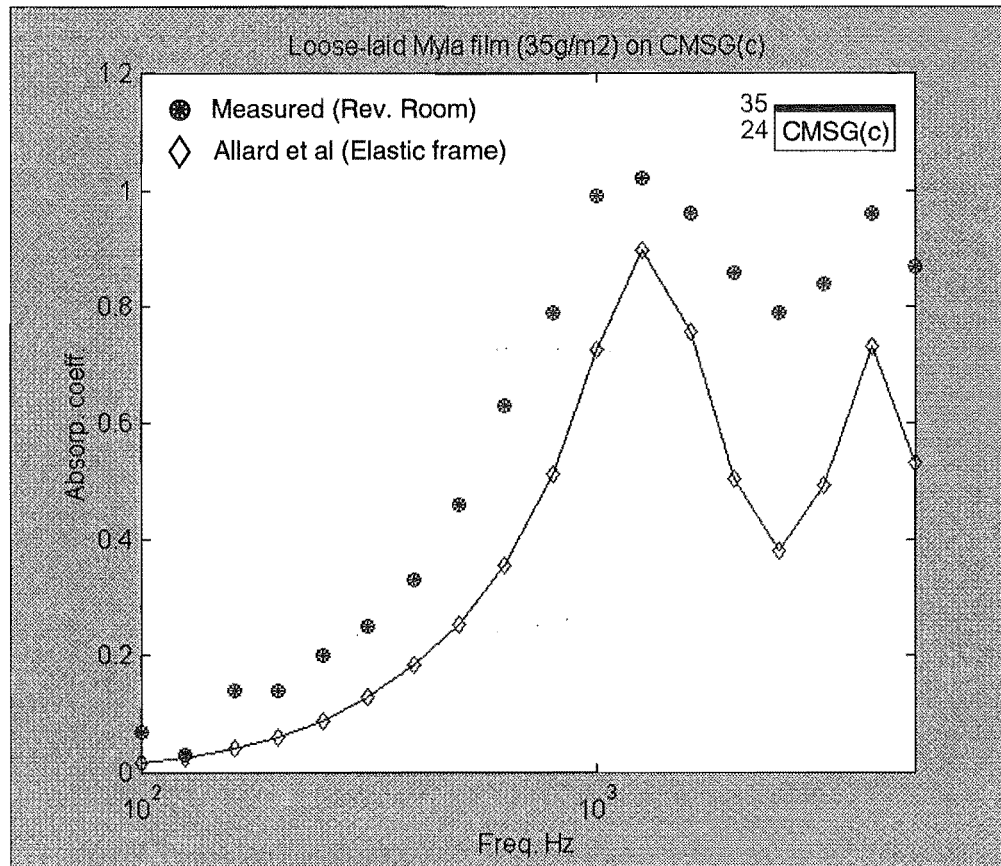


Figure 7.4 Measured and predicted absorption for crushed CMSG foam.

Table 7.5 Crushed CMSG foam material parameters for Allard et al, elastic frame model in Figure 7.4.

Material	Tortuosity, $k_s$	Frame density, $\rho_1$ ( $\text{kg/m}^3$ )	Porosity, h	Shear modulus, N ( $\text{N/m}^2$ )	Poisson coefficient, $\nu$	Form factor, c
CMSG(c)	4*	43	0.96	$8 \times 10^5(1+0.1j)^*$	0.3*	1.4*

The measured and predicted absorption coefficients of crushed CMSG foam covered with a loose-laid Mylar™ film are shown in Figure 7.5. The loose-laid film was modelled by incorporating a thin layer of air between the foam and film. The modelled results gave the same trend as the measured results but with lower absorption values. The predicted results also appear to be underdamped.



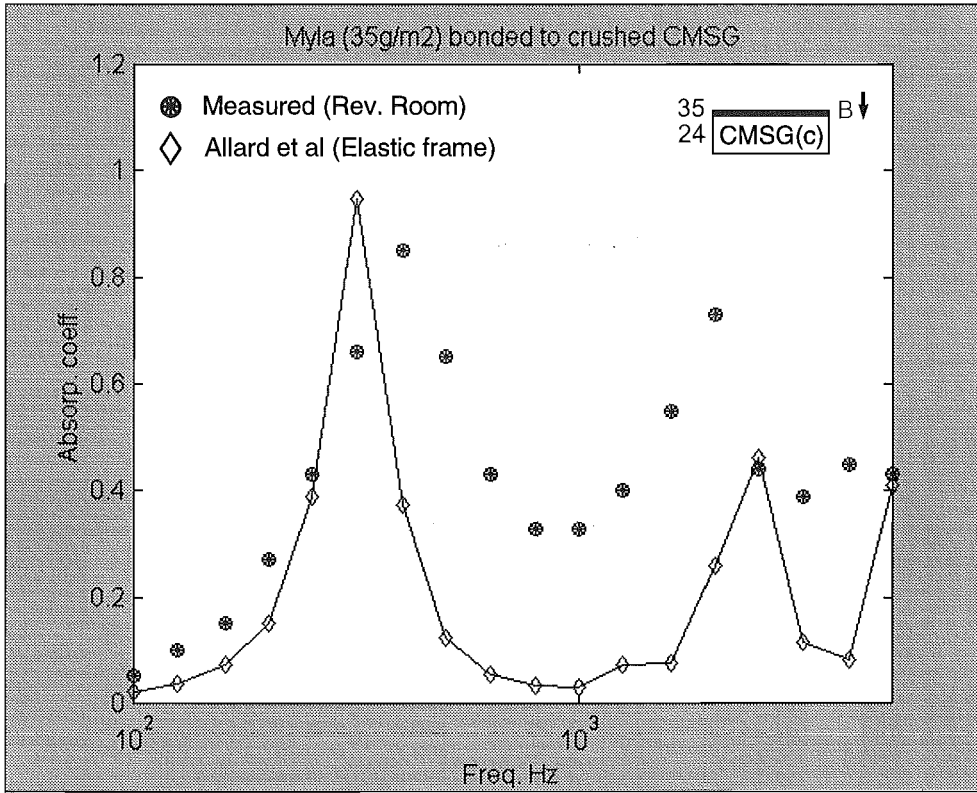
**Figure 7.5** Measured and predicted absorption for loose-laid Mylar™ (35g/m<sup>2</sup>).

The crushed CMSG foam parameters of Table 7.5 were used in Figure 7.5.

**Table 7.6** Mylar™ film parameters for use in Allard et al, elastic frame model in Figure 7.5.

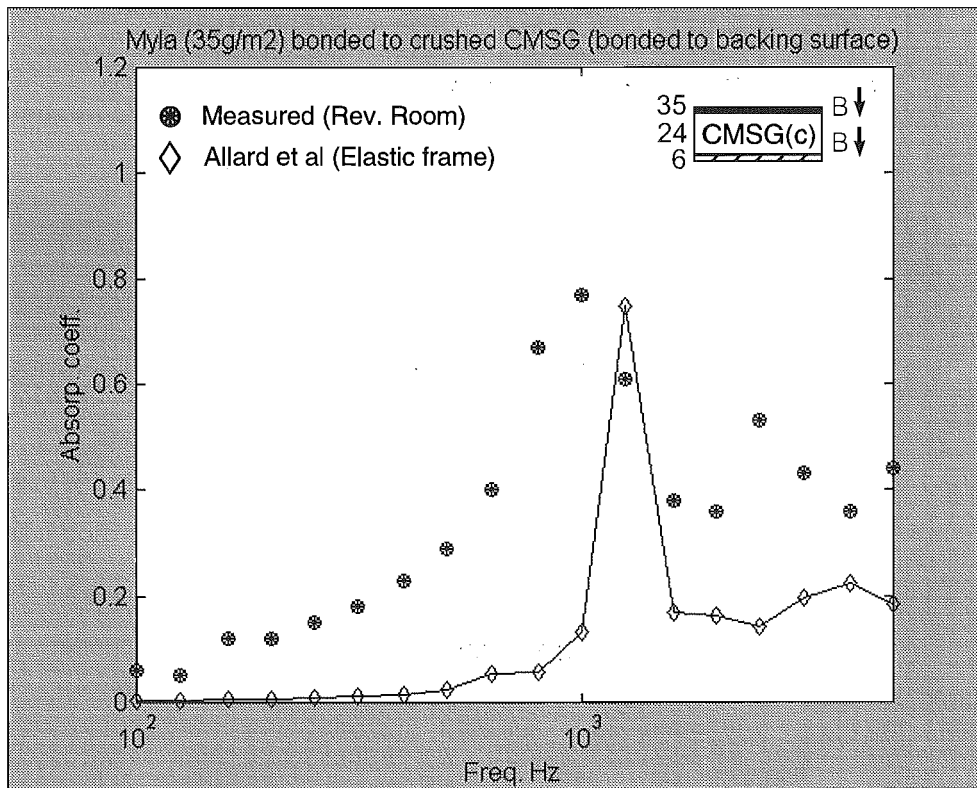
Material	Surface density, $\rho$ (kg/m <sup>2</sup> )	Stiffness, S	Tension, t
Mylar™ film	0.035	0	0

Figure 7.6 shows the absorption of CMSG with a bonded Mylar™ film. To model this system it was important to decouple the foam layer from the backing surface. This was done by incorporating a thin air layer between the foam and backing surface in the model. If this was not accounted for then the predictions in Figure 7.7 were produced. The two measured absorption peaks in Figure 7.6 were predicted by the model while the absorption coefficients between the peaks were considerably less than the measured results.



**Figure 7.6 Measured and predicted absorption for film faced crushed CMSG.**

The crushed CMSG foam parameters of Table 7.5 and the Mylar™ film parameters of Table 7.6 were used in Figure 7.6.



**Figure 7.7 Measured and predicted absorption for film faced crushed CMSG which is bonded to the backing surface.**

The crushed CMSG foam parameters of Table 7.5 and the Mylar™ film parameters of Table 7.6 were used in Figure 7.7.

A comparison between measured and predicted results is shown in Figure 7.7 for a film faced CMSG foam that was bonded to its backing surface. The model predicted an absorption peak close to the measured absorption peak. The difference in peak location was probably due to the Gib board thickness, which was not accounted for in the model. The rest of the predicted results were less than those measured.

The effect of a fabric covering on polyester board is shown, experimentally and theoretically, in Figure 7.8. It is clear that the measured and predicted results do not match directly but do however, show similar trends. The increase in absorption due to a fabric covering was shown in the measured data and was predicted by the model.

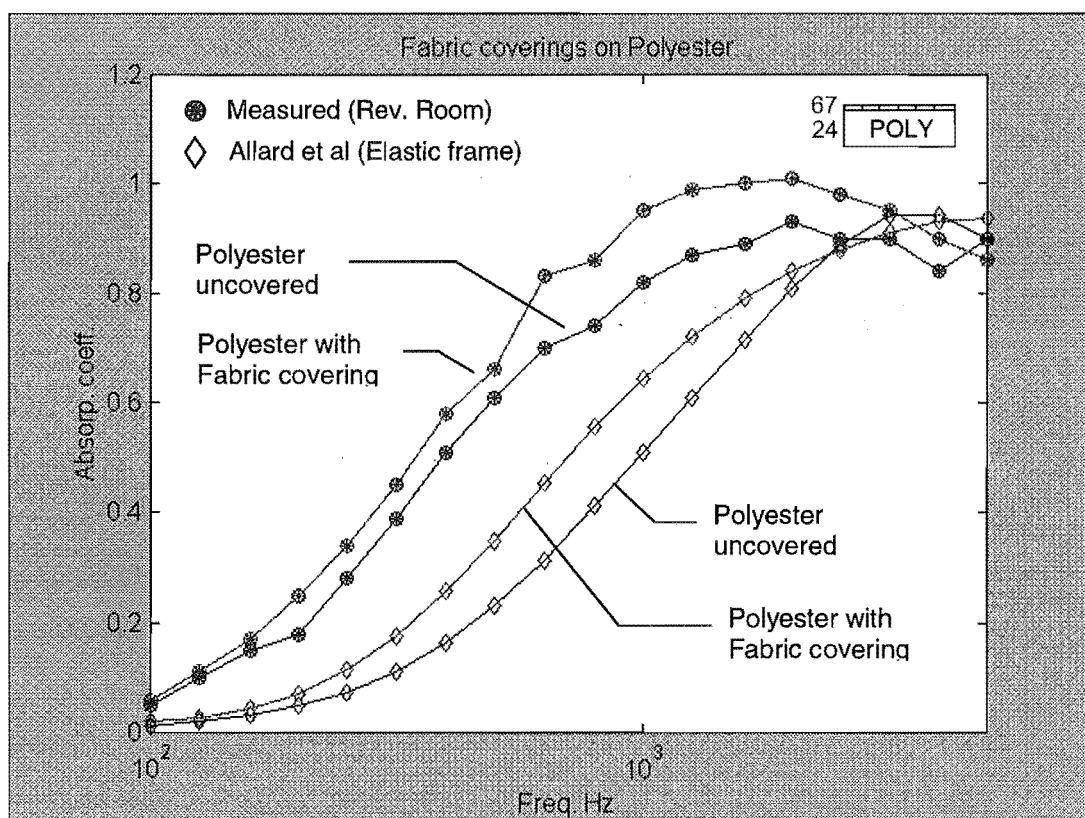


Figure 7.8 Measured and predicted absorption of fabric coverings on polyester.

**Table 7.7 Material parameters for Allard et al, elastic frame models in Figure 7.8.**

Material	Tortuosity, $k_s$	Frame density, $\rho_1$ ( $\text{kg/m}^3$ )	Porosity, $h$	Shear modulus, $N$ ( $\text{N/m}^2$ )	Poisson coefficient, $\nu$	Form factor, $c$
Polyester	1*	80	0.94	$10^6(1+0.1j)^*$	0.3*	1.4*
Fabric covering	1*	330	0.75	$10^6(1+0.1j)^*$	0.3*	1.4*

The fabric covering had a flow resistivity of 838000 mks rays/m and thickness of 0.8 mm.

In general it would seem that the models predicted similar absorption trends to the measured results. Their predictions were for the most part, less than the measured absorption and were usually under-damped. Many of the material parameters required for the model of Allard et al were estimated. This would account for some of the differences between the measured and predicted results. The measured results were made in a reverberant field while the predicted results were the statistical average of all angles of incidence in a diffuse field. This difference will also account for some of the discrepancies.

The modelled results gave similar trends to the measured results but with lower absorption coefficients. This indicates that optimal modelled results correspond to optimal measured results. The models can therefore be used to predict absorption trends and to optimise for various material or system parameters. However, optimal modelled systems should be tested experimentally to give the correct absolute values of absorption coefficient.

It is worth noting that the more complicated elastic frame model of Allard et al was necessary to predict the absorption of film faced foams. Motion was induced in the foam by the film and was critical to the absorption trend. The general method of section 6 was very useful for producing models of complicated systems comprised of many layers. This method was especially useful when incorporating loose-laid materials which were decoupled in the model by including a thin air layer between the material and its adjacent surface.

## 8. Conclusion

The absorption characteristics of many tested materials have been modelled. The models of Delany and Bazley, Allard and Champoux and Allard et al gave similar results for the fibrous materials tested. It was clear that the more complicated model of Allard et al was required to predict the absorption of partially reticulated foams and layered systems. While the model did not predict the actual values of the measured absorption coefficients, it was clear that the modelled results did follow the measured absorption trends. Absorbers can now be optimised for different material parameters and combinations of materials in the model instead of using material intensive and time consuming reverberation room tests. Optimal modelled absorbers can then be verified experimentally.

## References

Allard, J.F., Champoux, Y. (1991), "New empirical equations for sound propagation in rigid frame fibrous materials", *J. Acoust. Soc. Am.*, v91, 1992:3346-3353.

Allard, J.F., Brouard, B., Lafarge, D., (1993), "A general method of modelling sound propagation in layered media", *Journal of Sound and Vibration*, v183, no. 1, 1995:129-142.

Allard, J.F., Depollier, C., Rebillard, P., Cops, A., Lauriks, W., (1989a), "Inhomogeneous Biot waves in layered media", *Journal of Applied Physics*, v66, no. 6, 1989:2278-2284.

Allard, J.F., Depollier, C., Rebillard, P., Cops, A., Lauriks, W., (1989b), "Modelization at oblique incidence of layered porous materials with impervious screens", *J. Acoust. Soc. Am.*, v87, no. 3, 1990:1200-1206.

Biot, M.A., (1955), "Theory of propagation of elastic waves in a fluid-saturated porous solid", *J. Acoust. Soc. Am.*, v28, no. 2, 1956:168-191.

Delany, M., Bazley, E., (1969), "Acoustical properties of fibrous absorbent materials", *Applied Acoustics*, v3, 1970:105-116.

Qunli, W., (1988), "Empirical relations between acoustical properties and flow resistivity of porous plastic open-cell foam", *Applied Acoustics*, v25, 1988:141-148.



## Bibliography

- TA            Allard, J.F., "Propagation of sound in porous media: modelling sound  
418.9        absorbing materials", Elsevier, New York, 1993.  
.P6  
.A419
- QC            Ingard, U., "Notes on sound absorption technology", Noise Control  
233        Foundation, 1994.  
.I44
- TA            Lauriks, W., Chapter 10, "Acoustic characteristics of low density foams"  
455        in "Low density cellular plastics – Physical basis of behaviour", Chapman  
.P5        and Hall, London, 1994.  
.L912

---

# 6

## Project Findings

---

### Summary

This chapter provides guidelines for the use of acoustic absorbers. The measured results of Chapter 4 were assessed according to their potential as tuned or wideband absorbers. They were also analysed in terms of cost and ability to withstand fire. Foams in combination with impervious films can easily be tuned to absorb sound in specific frequencies. The impervious films sandwiched between foam layers and the contoured foam had the best wideband absorption with an NRC of 0.85 at 48 mm thickness. Foam by itself also had good wideband absorption; NRC of 0.80 at 50 mm. Fabric coverings on polyester gave the highest absorption at 24 mm thickness with an NRC of 0.75. Foam costs can be reduced by lowering the density of the foam compared to those tested or using air cavities, with little effect on absorption.

## Table of Contents

<b>Table of Contents.....</b>	<b>xvi</b>
<b>List of Tables.....</b>	<b>xvi</b>
<b>1. Introduction.....</b>	<b>97</b>
<b>2. Aims .....</b>	<b>97</b>
<b>3. Results.....</b>	<b>97</b>
3.1 <i>Tuned absorbers</i> .....	97
3.2 <i>Wideband absorbers</i> .....	98
3.3 <i>Costs</i> .....	99
3.4 <i>Fire resistance</i> .....	100
<b>4. Conclusions.....</b>	<b>100</b>

## List of Tables

<u>Table No.</u>	<u>Page</u>
Table 3.1 Approximate material costs at 24 mm thickness. ....	99
Table 3.2 Material fire resistance. ....	100

## 1. Introduction

An aim of this project was to use the measured results to design optimal tuned and wideband absorbers. Tuned absorbers have large absorption coefficients in specific frequency bands. These are useful to absorb noise when it consists of one or two tones. Wideband absorbers have high absorption across most of the frequency range. These are used for more common noise problems.

NRC stands for the Noise Reduction Coefficient. This is a single figure indication of absorber performance. NRC is the arithmetic average of the absorption coefficients in the 250, 500, 1000 and 2000 Hz frequency bands. It is not as indicative of an absorber's performance as one third octave frequency band absorption plots but has been used extensively in the past.

## 2. Aims

To develop guidelines for the use of the tested materials as tuned or wideband absorbers.

## 3. Results

The important parameters or material systems are discussed below with reference to their ability to produce a significant tuned or wideband absorber.

### 3.1 *Tuned absorbers*

CMSG foam thickness and flow resistance were found to be critical to the material's performance as a tuned absorber. It was clear that the absorption peak moved to lower frequencies with thicker foams. Crushing the foam lowered its flow resistance and moved the absorption peak to higher frequencies.

The use of impervious films with CMSG foam gave perhaps the most potential for tuned absorbers. The absorption peak of loose-laid and strip adhered films on crushed CMSG foam, moved considerably with different film weights. Heavier films moved this absorption peak to lower frequencies.

It was clear that small changes in film bonding type produced very different absorption characteristics. Bonded films on crushed CMSG produced a large absorption peak at low

frequencies. An absorber of only 24 mm thickness gave absorption coefficients near unity at 314 and 400 Hz. This peak was relatively insensitive to film weight but was moved to lower frequencies with thicker foam. However, this low frequency peak was only apparent when the foam's rear surface was decoupled (unbonded) from the backing wall. In practice, this absorber could be adhered to the backing wall around its perimeter, leaving for the most part, a decoupled rear surface.

### **3.2 Wideband absorbers**

Fibreglass was the most absorbent of all the materials at high frequencies. It has been noted previously that the fibreglass had near optimum flow resistance at 24 mm thickness. It appears that CMSG foam and polyester board would absorb more sound at high frequencies if optimised for flow resistance.

Impervious films, that were useful for tuning absorbers, can also be used effectively to produce wideband absorbers. A film sandwiched between two layers of CMSG foam had the highest equal NRC of 0.85 at 48 mm thickness. It had slightly more absorption at low frequencies than a solid layer of foam (NRC of 0.80) of the same thickness. However, the sandwiched film system usually has less absorption than plain foam at high frequencies. Many of the commercially available absorbers presented in Chapter 1 had NRCs of 1.0 at 50 mm thickness. These products had absorption exceeding unity in some frequency bands which inflated their NRCs.

The phenomenon of excess sound absorption, produced by alternating strips of different materials on the absorber's top surface, was useful for combining the absorption characteristics of different absorbers. Alternating strips of foam and film produced an effective wideband absorber with more absorption than the arithmetic average of each material's absorption.

Fabric coverings on fibrous or foam based absorbers have much potential for producing wideband absorbers. The thin coverings dramatically increased the absorption of the fibrous or foam substrate in most frequencies. The largest NRC at 24 mm thickness (0.75) was produced with a fabric covered polyester board. The largest NRC at 24 mm thickness, of the commercially available absorbers in Chapter 1, was 0.85 for an acoustic textile faced, polyester absorber. This product also had absorption exceeding unity and hence had a slightly inflated NRC. The fabrics tested had flow resistances that were significantly less than the

theoretical optimum. Making use of optimised fabrics would greatly increase the absorption of the substrate, producing an excellent wideband absorber.

Contoured foams also appear to be effective as wideband absorbers. The contoured SPF foam had relatively high absorption in all frequency bands, giving an NRC of 0.85.

Fabric covered substrates and contoured foams were the only absorbers that performed significantly better than a fibrous or foam material by itself. It would seem that the extra work and cost of bonding impervious films and foam layers is unnecessary when a plain foam has quite high broadband absorption. This would be especially true for foams with optimised flow resistance.

### 3.3 Costs

**Table 3.1 Approximate material costs at 24 mm thickness.**

Material	Cost (\$/m <sup>2</sup> )
CMSG foam	18.20
Polyester	18.70
Fibreglass	19.30

Table 3.1 shows that the costs of each material are roughly the same. The “worth” of each material is more clearly seen from their fire resistance and acoustic characteristics.

The effect of impervious films on the absorption of foams has been determined. The absorption of bonded film faced foams was insensitive to film weight. Therefore, light weight films with low cost should be used instead of heavier films.

Air cavities behind porous absorbing materials have significant potential for reducing the cost of absorbers. The tests showed that an air cavity produced almost the same amount of absorption as a solid layer of foam. Hence, for example, a 50 mm absorber could be made from a 25 mm layer of porous material and a 25 mm air cavity. This would halve the amount of material required and so reduce the cost. However, this cost saving would need to be offset against the cost of providing and installing the air cavity.

The use of low density foams with optimised flow resistance has potential to reduce material costs. Preliminary modelling results have shown that halving the foam density has an

insignificant effect on the absorption, providing that the flow resistance is kept constant. A low density foam would reduce the material costs as foams are typically costed according to weight.

### 3.4 Fire resistance

This is an important parameter with regard to acoustic absorbers but is strictly outside the scope of the project. Some data and discussion is however, presented below for completeness.

**Table 3.2 Material fire resistance.**

Material	Smoke Developed Index (0-10) <sup>1</sup>
CMSG foam	5
Polyester	2
Fibreglass	0

The Early Fire Hazard Indices for places of assembly in New Zealand require a maximum smoke developed of 5. The three materials meet this requirement, Table 3.2. However, most absorbers are installed with fabric coverings to meet ascetic requirements. It is understood that CMSG foam and polyester perform quite poorly when covered with fabric while fibreglass still performs well. Buildings with sprinklers do not require absorber materials to be fire resistant. Fibreglass is the only material able to be used in places of assembly without sprinklers. CMSG foam, polyester or fibreglass absorbers can be used in buildings with sprinklers or rooms not classified as places of assembly.

## 4. Conclusions

In conclusion, the most promising tuned absorbers at this time would use a low density polyurethane foam optimised for flow resistance, making use of various films and film bonding conditions to tune for specific frequencies. The most effective wideband absorbers would make use of a low density foam, polyester board or fibreglass in combination with a fabric covering; each material would be optimised for flow resistance. Contoured foams would be competitive as wideband absorbers if the material cutting costs are low. Both tuned and wideband absorbers could incorporate air cavities to reduce material costs.

<sup>1</sup> AS 1530 part 3, 1989, "Simultaneous determination of ignitability, flame propagation, heat release and smoke release".

---

# Project Conclusion

---

The Acoustic Absorber Design project was successful. The literature search on absorbers highlighted the relevant absorption theory and revealed a large range of commercially available absorbers. The Reverberation Room was successfully calibrated to produce repeatable and reliable measurements. Equipment was built to measure the flow resistance of porous materials that were used as absorbers. Many different materials were tested in the Reverberation Room to determine their absorption coefficients. Absorption predictions were then made with a variety of theoretical and empirical models. These gave similar trends to the measured results. The performance of CMSG foam could be easily tuned with impervious films to give high absorption in selected frequencies. Low cost but effective wideband absorbers can be made from low density foam, polyester or fibreglass with fabric coverings, each optimised for flow resistance. Contoured foams were also very effective as wideband absorbers.

## Further Work

### ***Reverberation Room Calibration***

The performance of the Reverberation Room could be investigated further by participating in a series of round robin absorption tests. A standard material is tested according to a standard test method in several laboratories to determine the variation of results between laboratories. This would give further confidence to the measured results in the Reverberation Room.

### ***Material Parameters***

Equipment could be developed to measure bulk porous material parameters such as tortuosity and shear modulus. This would be useful for the theoretical modelling of absorbers and would provide a more thorough understanding of the materials tested.



### ***Testing***

Equipment could be developed to measure absorption making use of alternative methods. The normal incidence absorption coefficient of absorbers can be determined with the aid of an intensity analyser or two microphones and a noise source. This method, detailed by Allard (1994) requires only 1 m<sup>2</sup> of absorber. Material costs and time used in absorber development could be reduced with this method.

The concept of an absorption limit at each thickness could be investigated. The different absorbers studied seemed to have similar amounts of absorption but in different frequency bands. The area under the absorption curve for each absorber could be compared and perhaps optimised at each thickness.

The effect of perforating an impervious film which is subsequently bonded to foam could be investigated. This may improve the high frequency absorption of film faced foams.

### ***Optimised Absorbers***

The models developed could be used to optimise for different material parameters or layered systems. Non-dimensional parameters could also be developed and used in this analysis.

Absorption tests could be carried out on low density foams with optimised flow resistance. Similarly, fabric coverings with optimal flow resistance could be identified and tested. Contoured foams could be tested and optimised with different shapes and sizes. Hanging absorbers could also be developed and tested for absorption.

### ***Fire Resistance***

Fire resistance was an important absorber parameter outside the scope of this acoustic project. Tests could be carried out to determine the effect of various fabric coverings and impervious films on the fire resistance of CMSG foam, polyester and fibreglass.

# Appendices

## Appendix A Reverberation Room Calibration

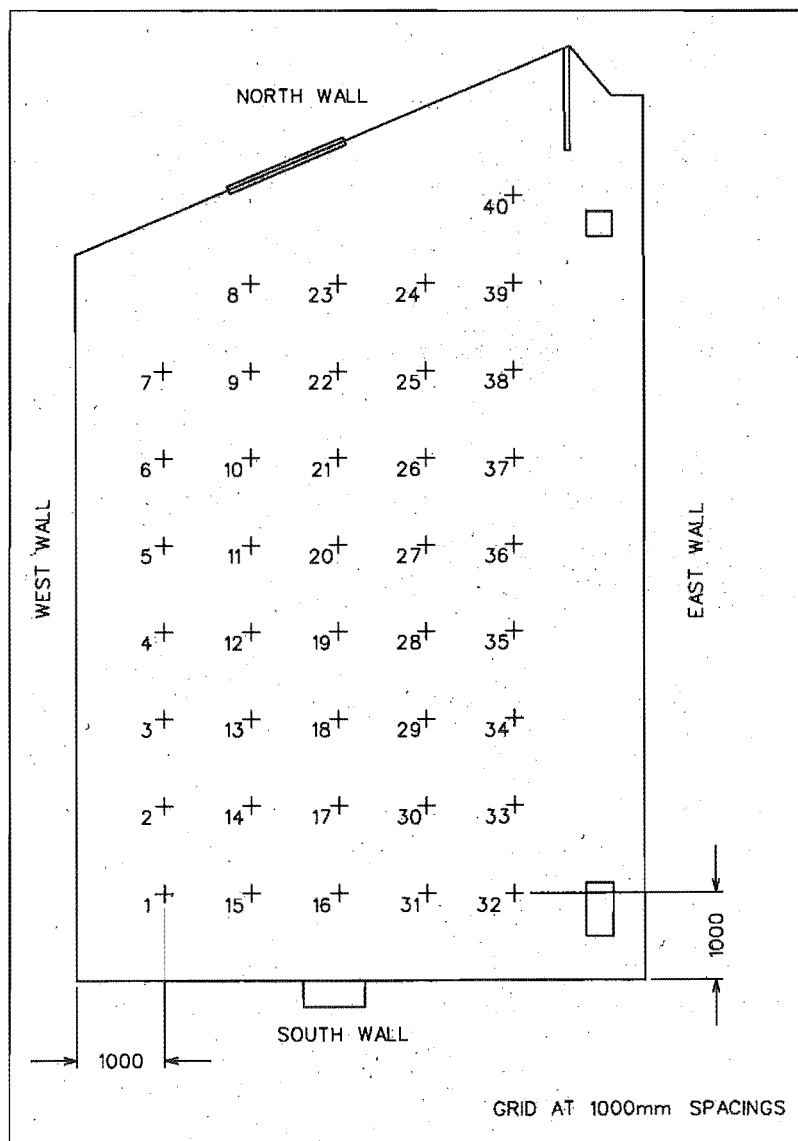


Figure A.1 Speaker and microphone positions in the Reverberation Room.

**Table Appendix A .1 Intensity speaker and microphone locations.**

Original Room		Refurbished Room	
Speaker	Mic.	Speaker	Mic.
Pt 14 Northwest	Pt 20	Pt 17 North	Pt 6
		Pt 38 South	Pt 30

**Table Appendix A .2 Reverberation time speaker and microphone locations.**

Original Room		Original Room + four diffusers		Refurbished		Refurbished + six diffusers	
Speaker	Mic	Speaker	Mic	Speaker	Mic	Speaker	Mic
Pt 6 East	Pt 19	Pt 6 East	Pt 19	Pt 6 East	Pts 2, 17, 33	Pt 6 East	Pts 2, 17, 33
Pt 9 Northwest	Pt 14	Pt 9 Northwest	Pt 14	Pt 9 Northwest	Pts 35, 19, 4	Pt 9 Northwest	Pts 19, 4
Pt 19 North	Pt 14	Pt 19 North	Pt 14	Pt 29 South	Pts 6, 21, 37	Pt 29 South	Pts 6, 21, 37
Pt 38 South	Pt 12	Pt 38 South	Pt 12	Pt 11 North	Pts 39, 24	Pt 11 North	Pts 39, 24
		Pt 13 West	Pt 22				
		Pt 16 South	Pt 36				
		Pt 6 East	Pt 19				

**Table Appendix A .3 Benchmark speaker and microphone positions**

Speaker	Microphone
Pt 4 South	Pt 23
Pt 17 East	Pt 6
Pt 38 Northwest	Pt 30

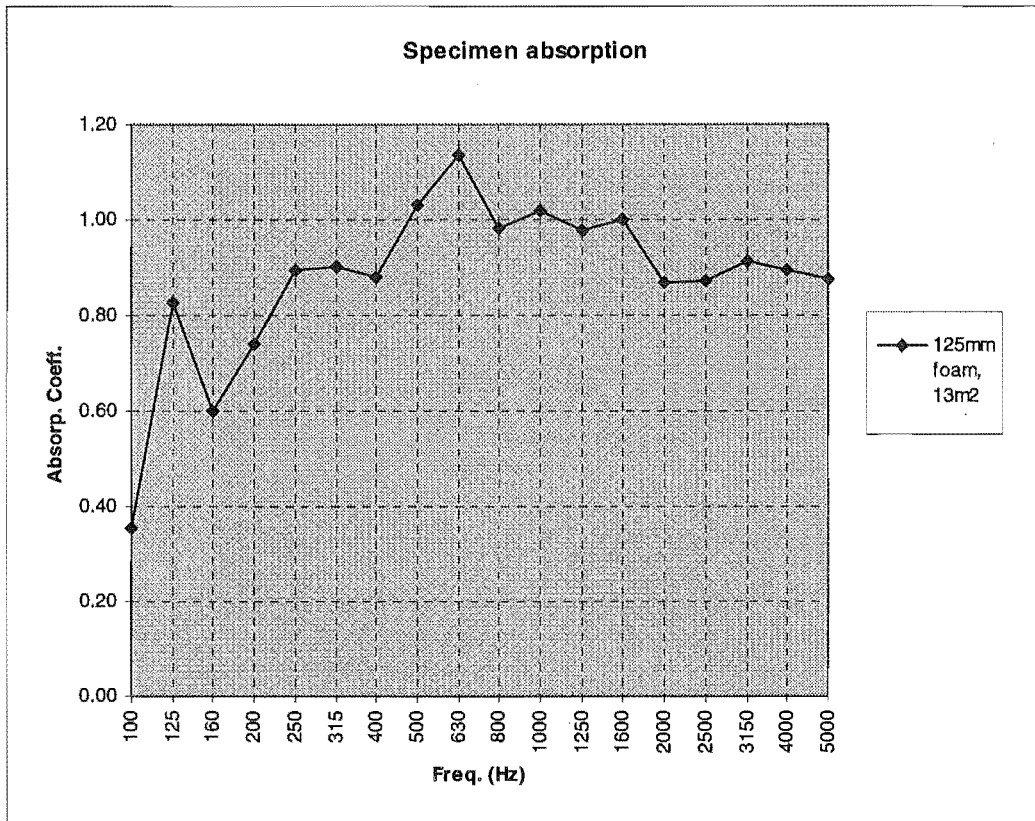
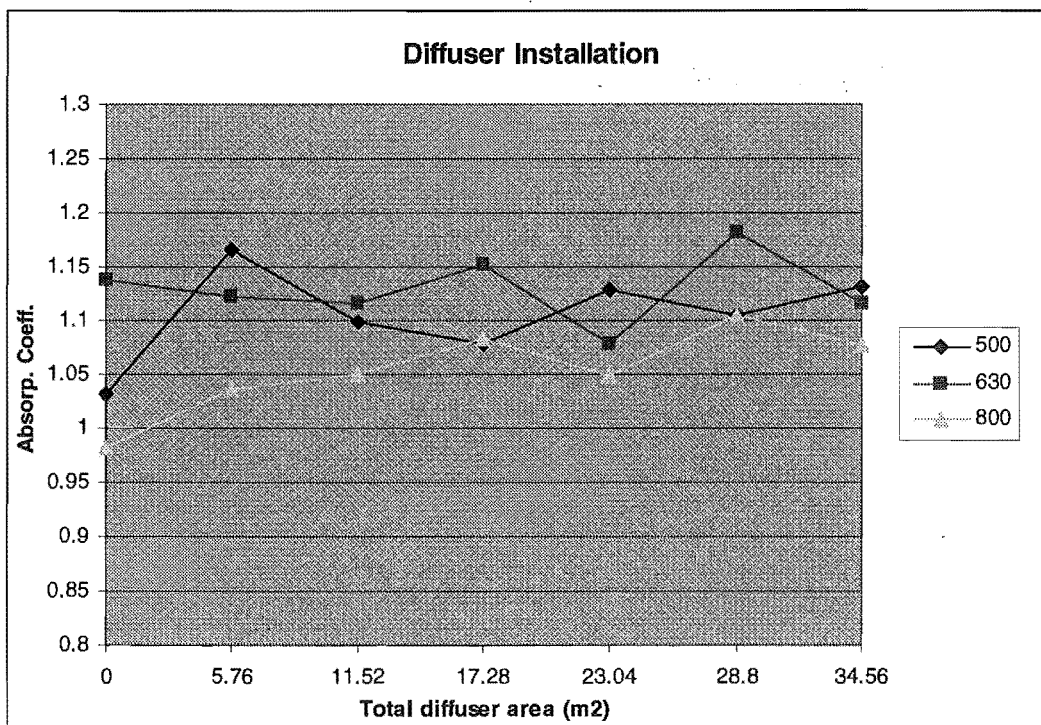
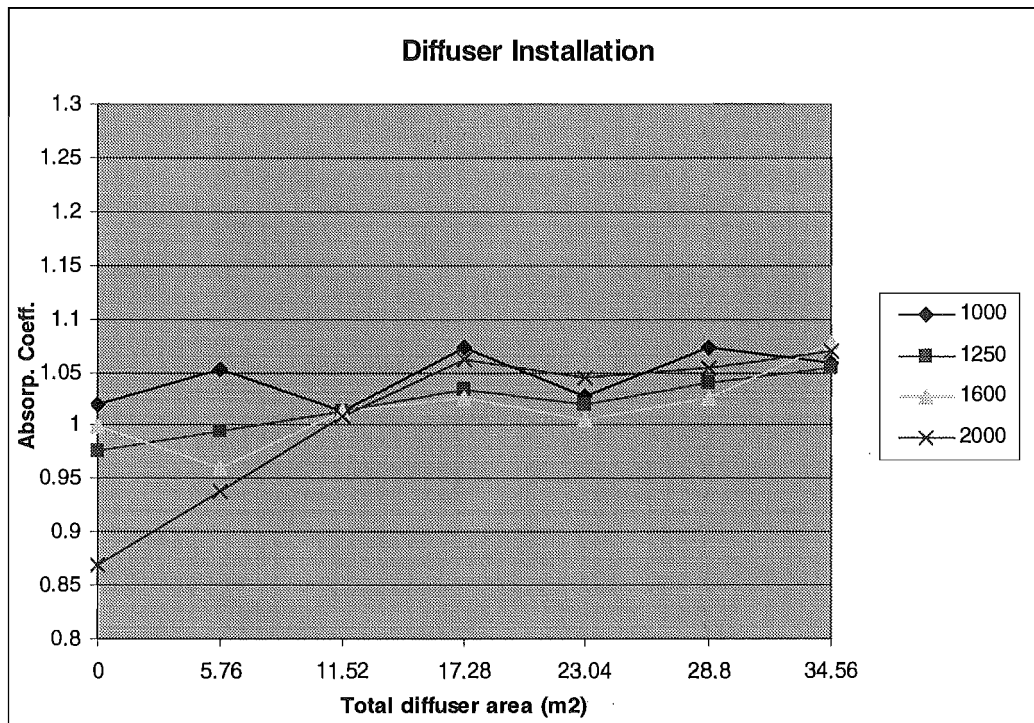


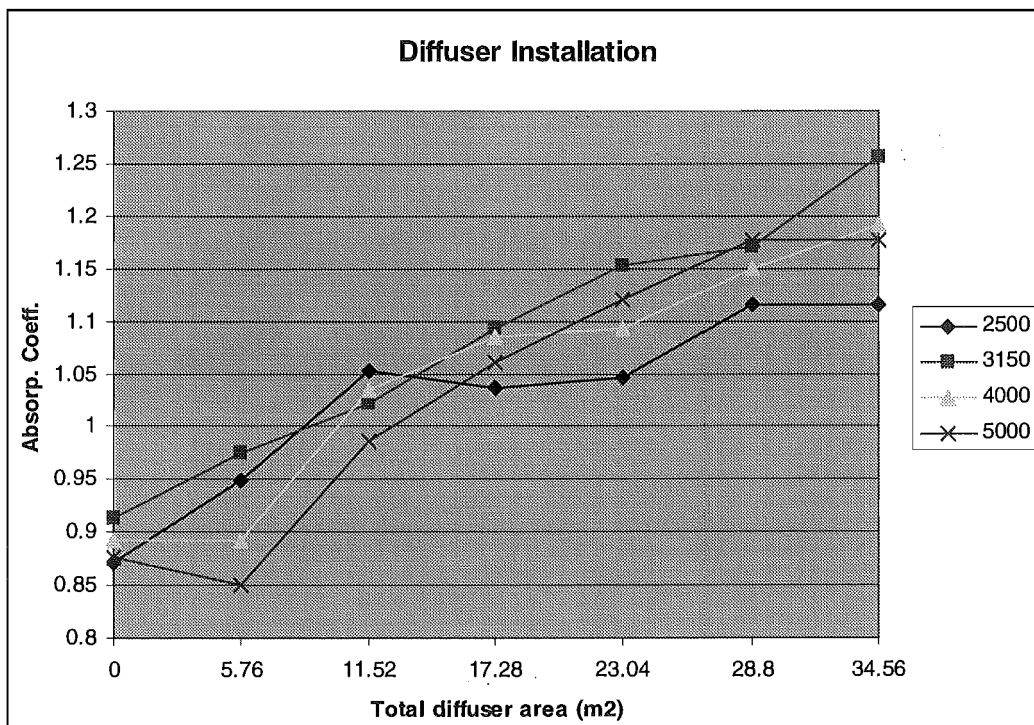
Figure A.2 Test specimen absorption for the diffuser installation procedure.



(a)



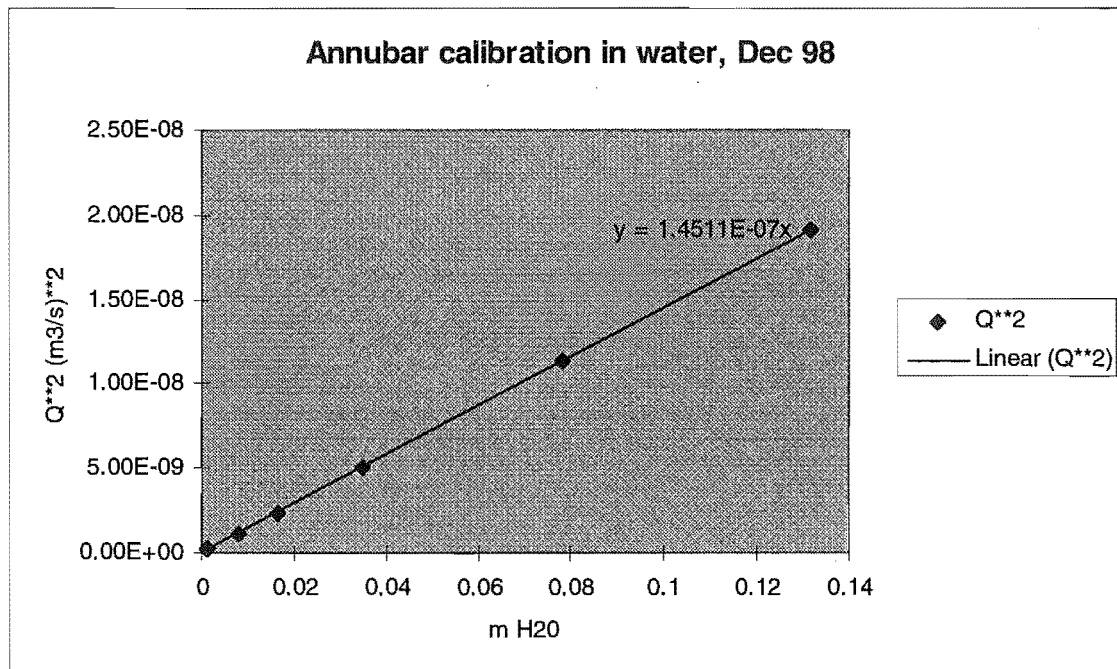
(b)



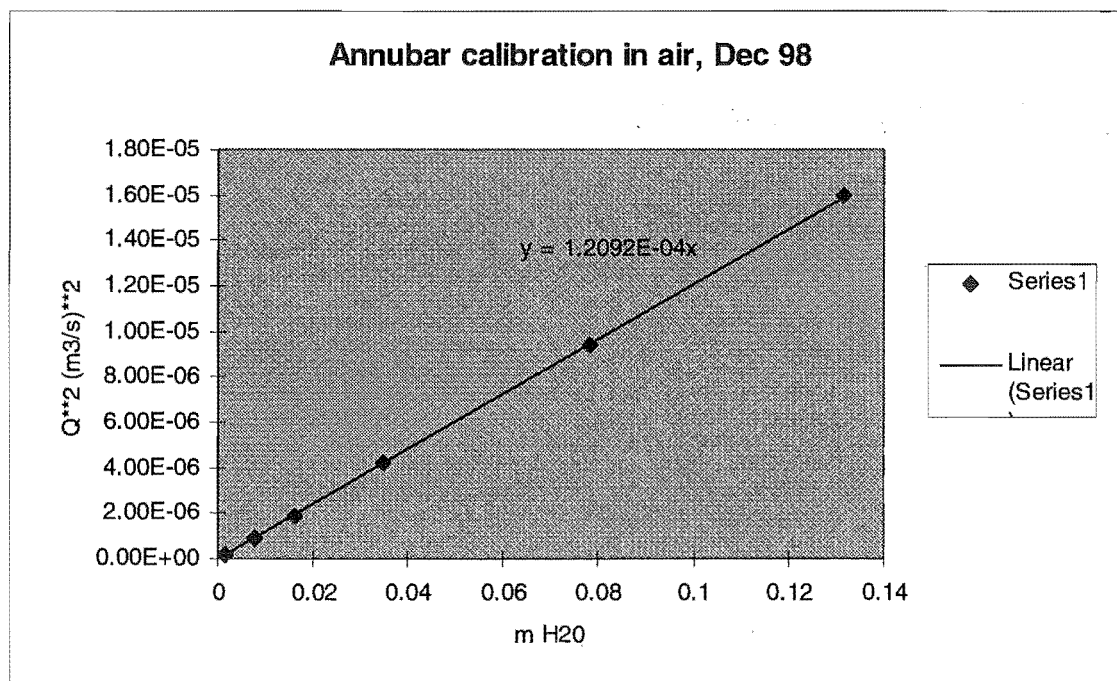
(c)

Figure A.3 Diffuser installation - absorption versus diffuser area in each 1/3 octave band.

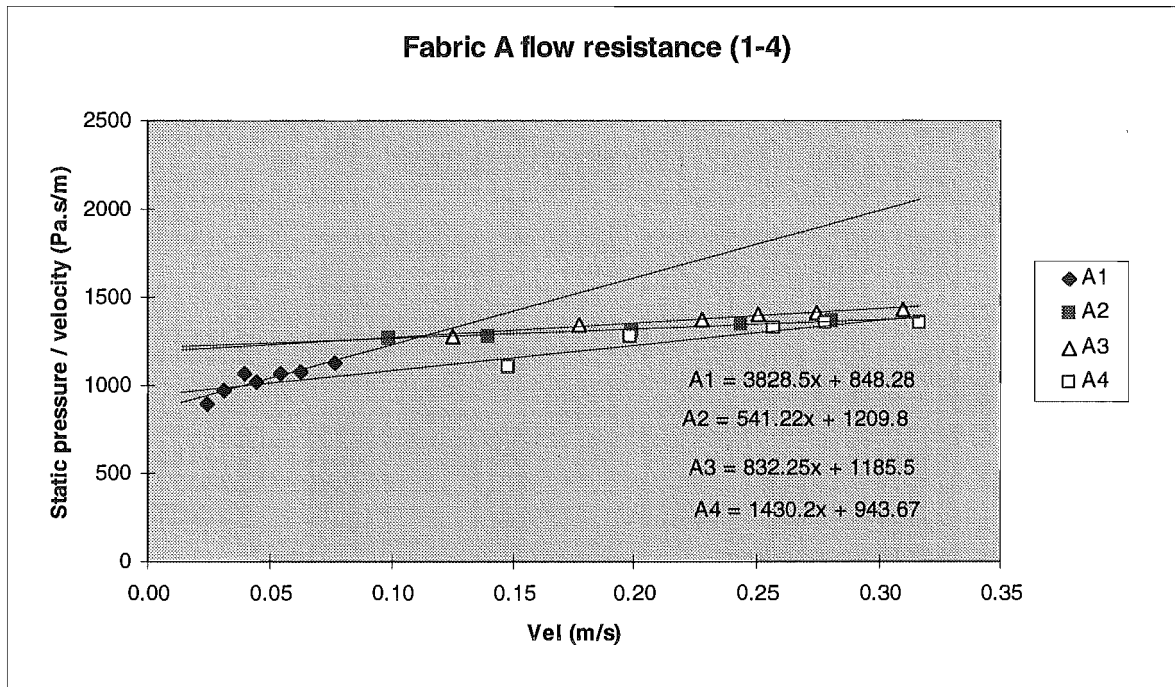
## Appendix B Absorber Materials



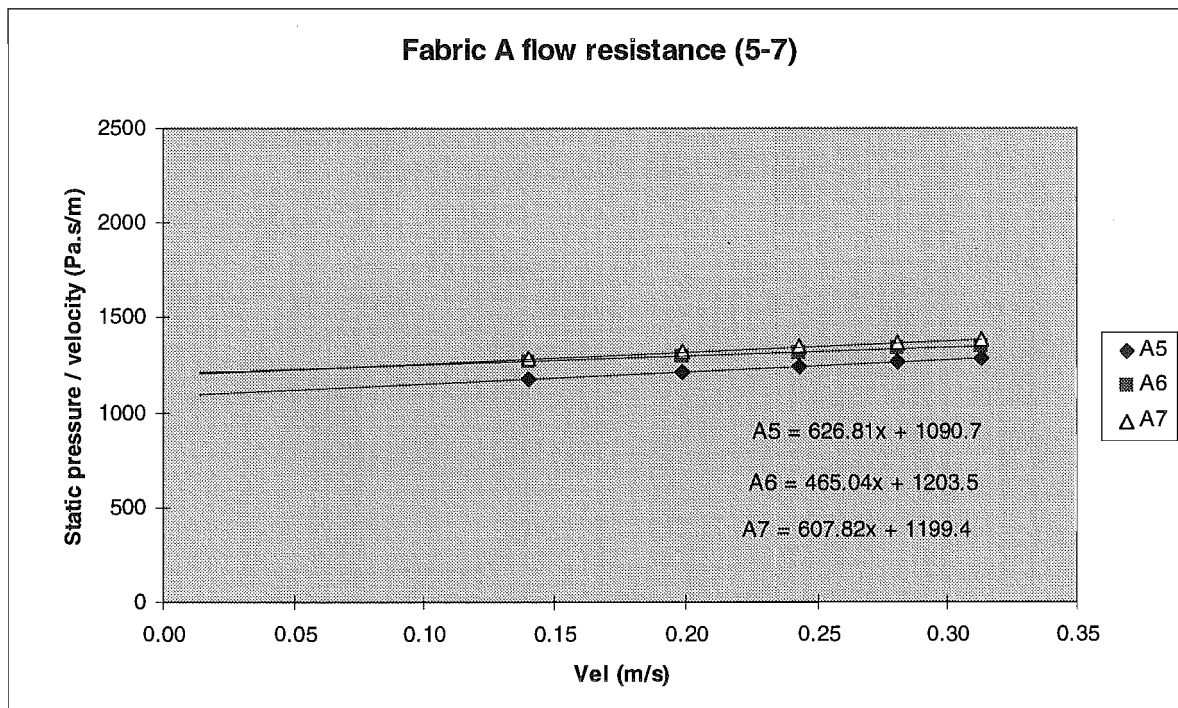
**Figure B.1** Calibration of 1/2" Annubar in water.



**Figure B.2** Calibration of 1/2" Annubar in air (calculated from water calibration).



(a)



(b)

Figure B.3 Fabric A flow resistance, (a) samples 1 to 4, (b) samples 5 to 7.

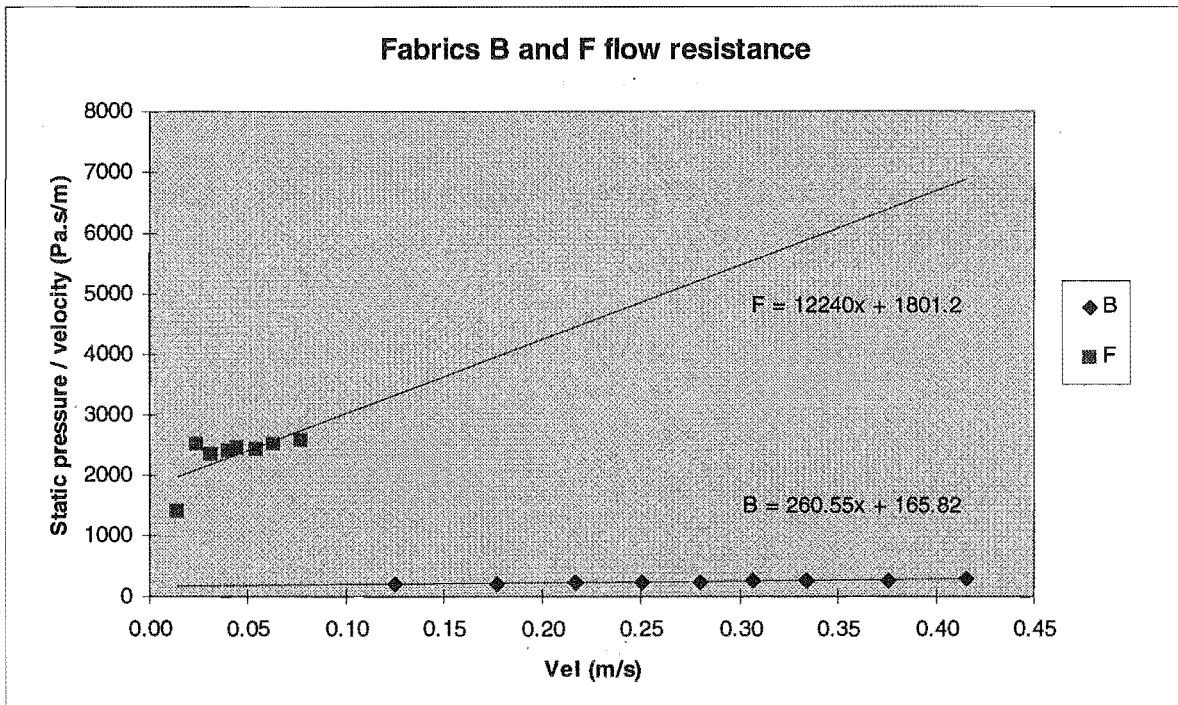
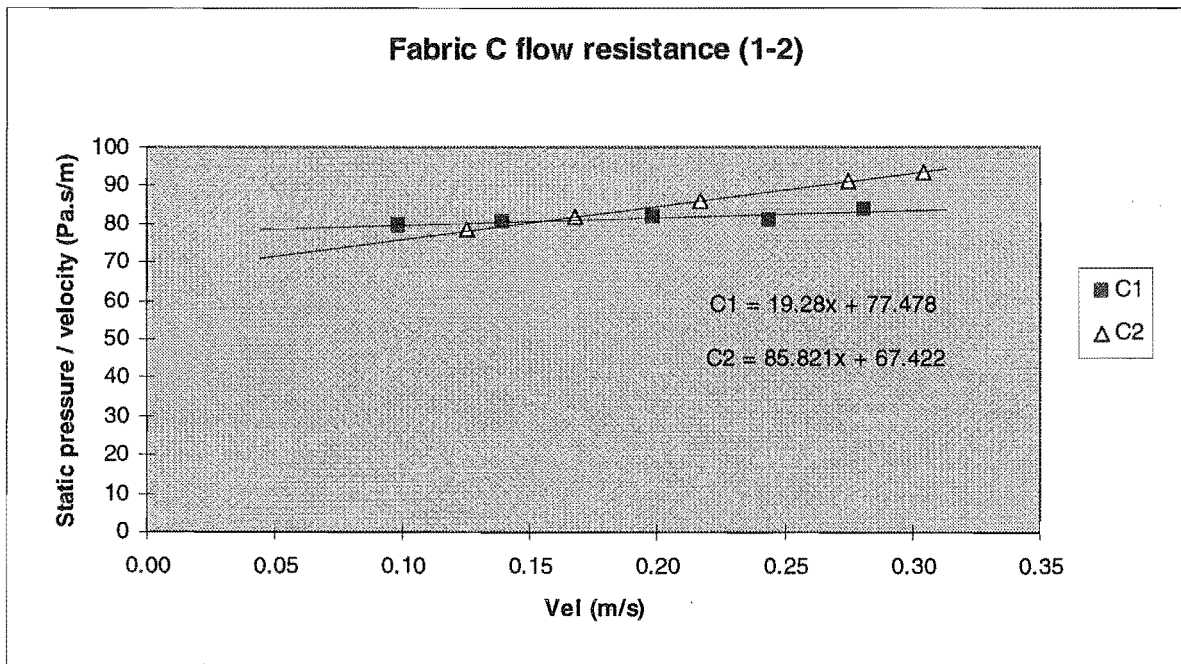
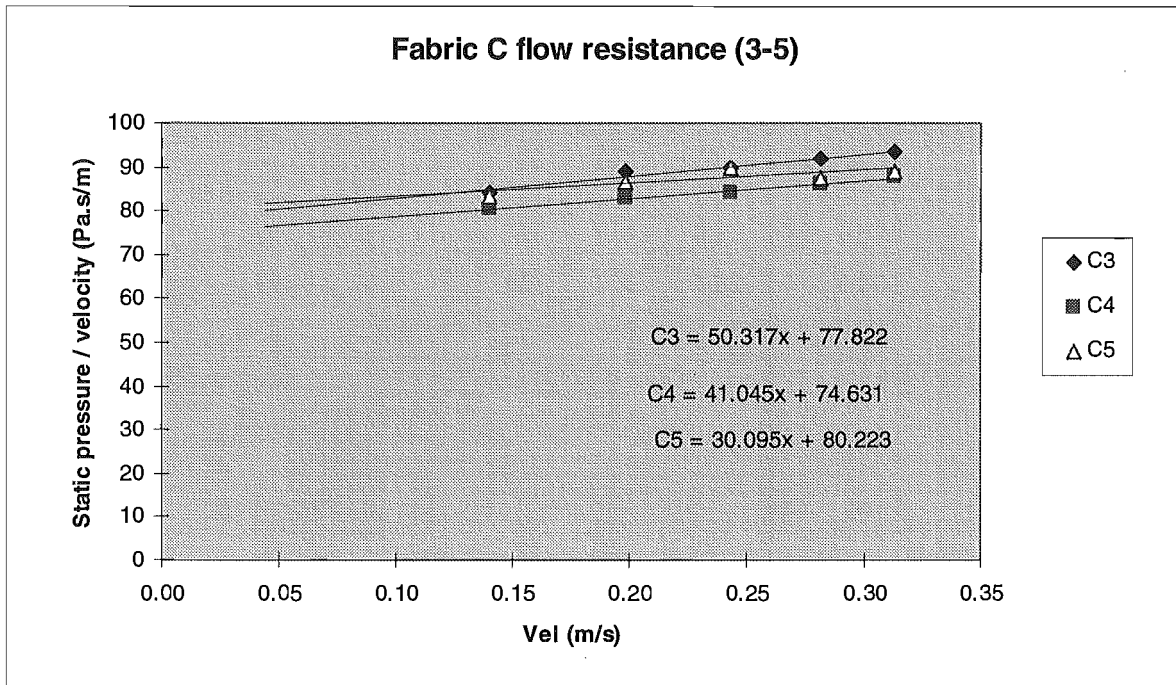


Figure B.4 Fabric B and F flow resistance.



(a)





(b)

Figure B.5 Fabric C flow resistance, (a) samples 1 to 2, (b) samples 3 to 5.

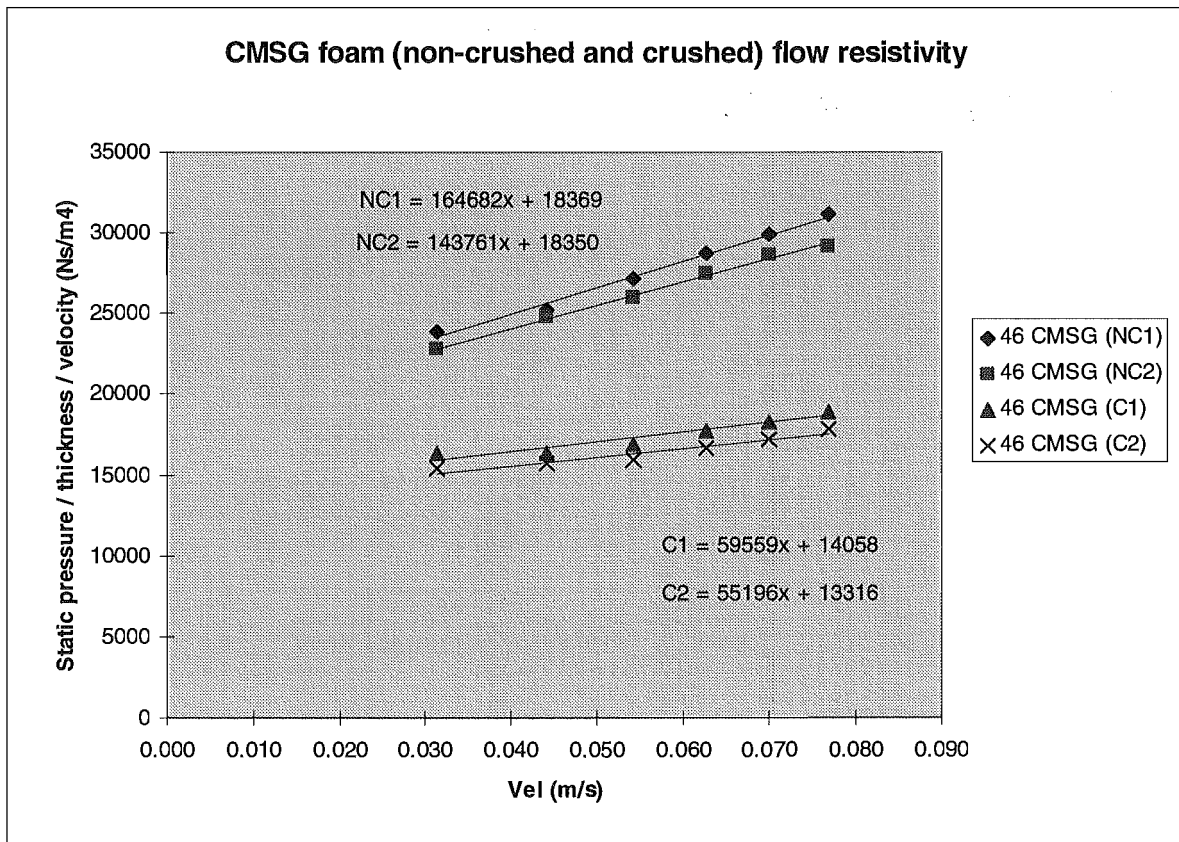


Figure B.6 CMSG foam flow resistivity at 46 mm thickness.

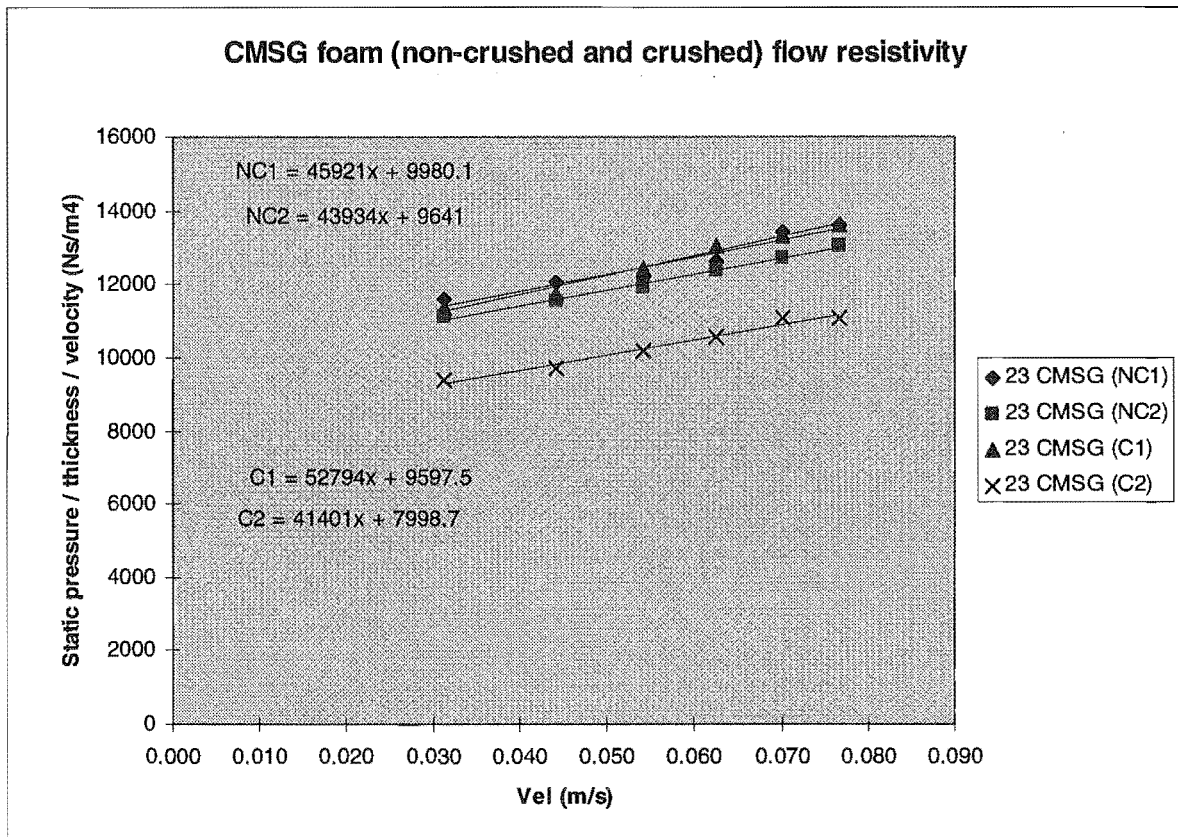


Figure B.7 MSG foam flow resistivity at 23 mm thickness.

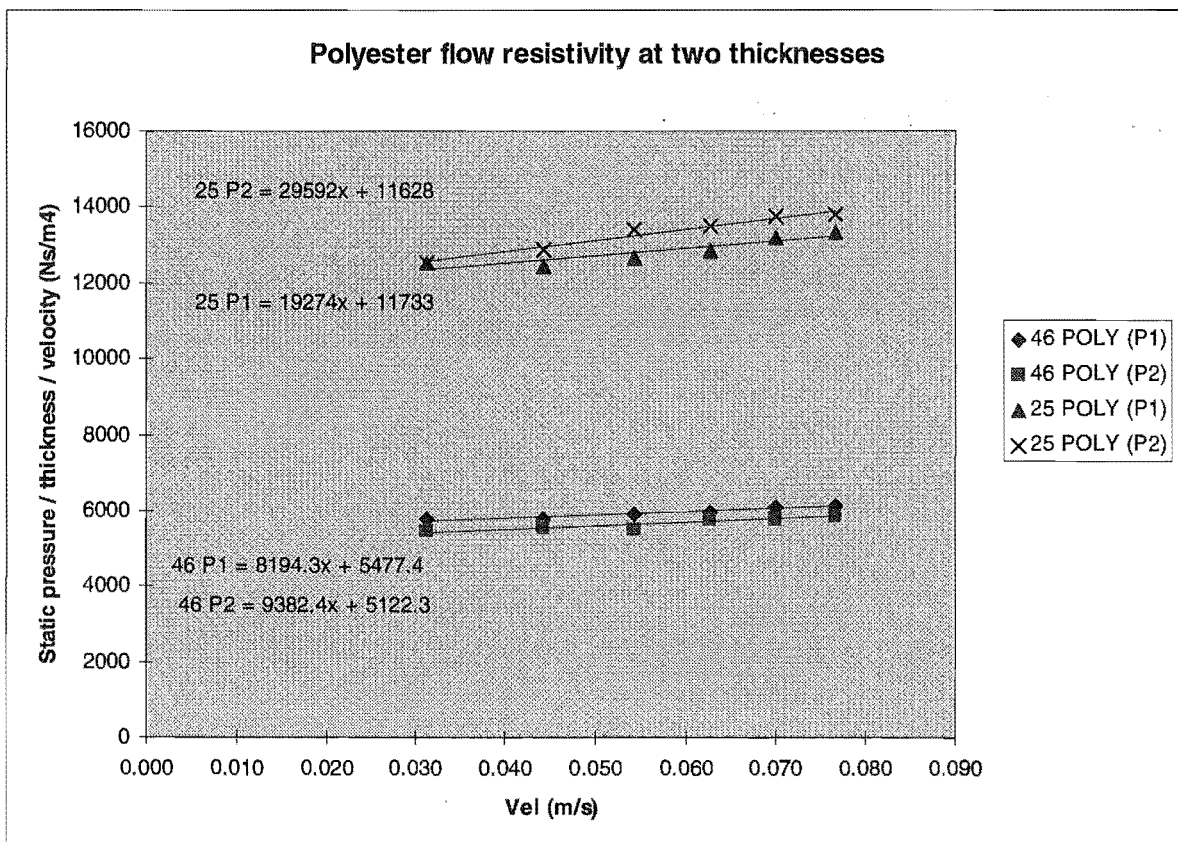


Figure B.8 Polyester flow resistivity.

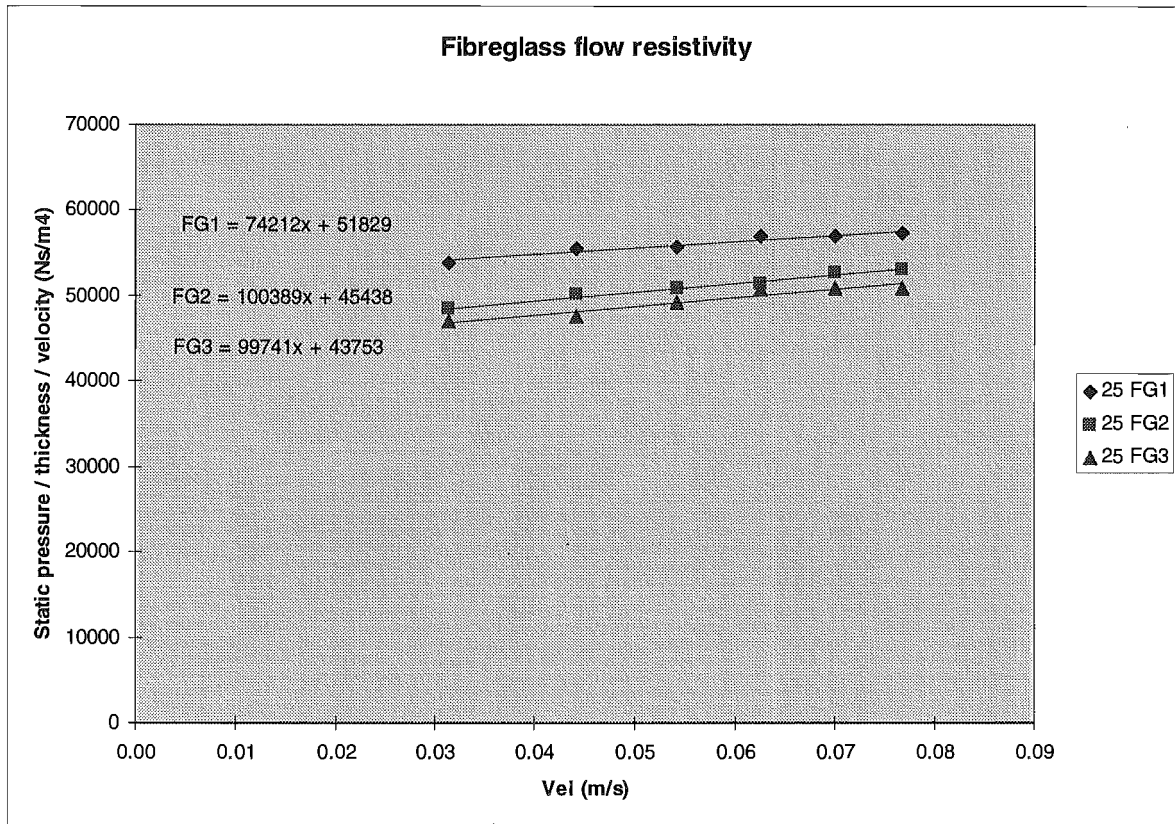


Figure B.9 Fibreglass flow resistivity.

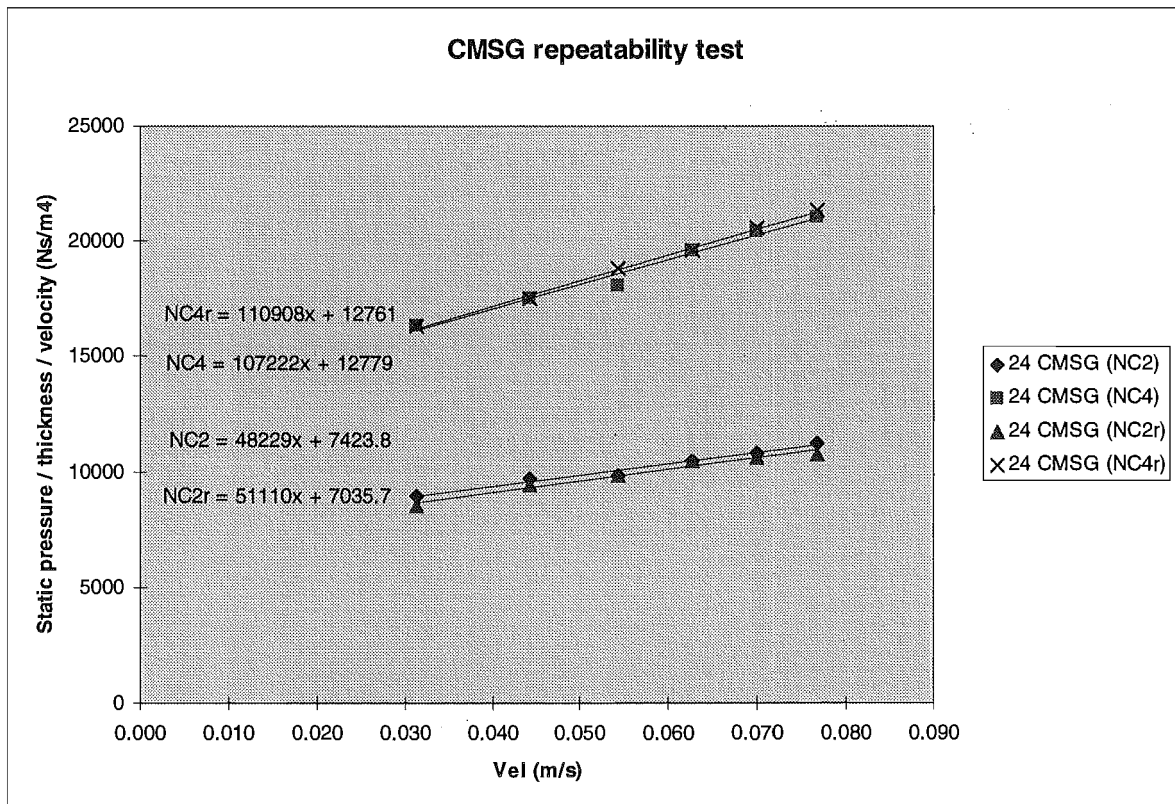


Figure B.10 Repeatability test with CMSG foam.

Figure C.1 Absorber test frame design.

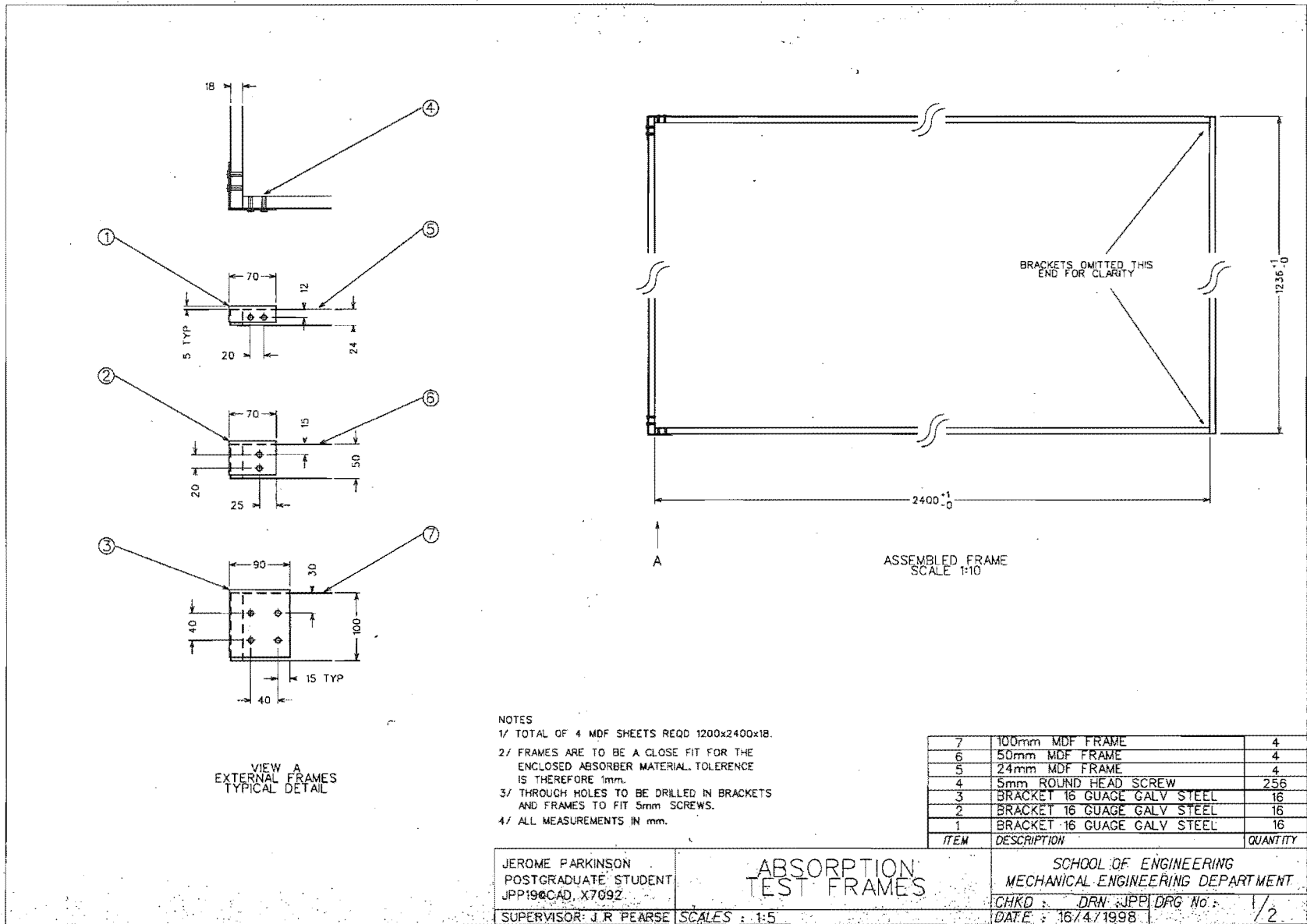
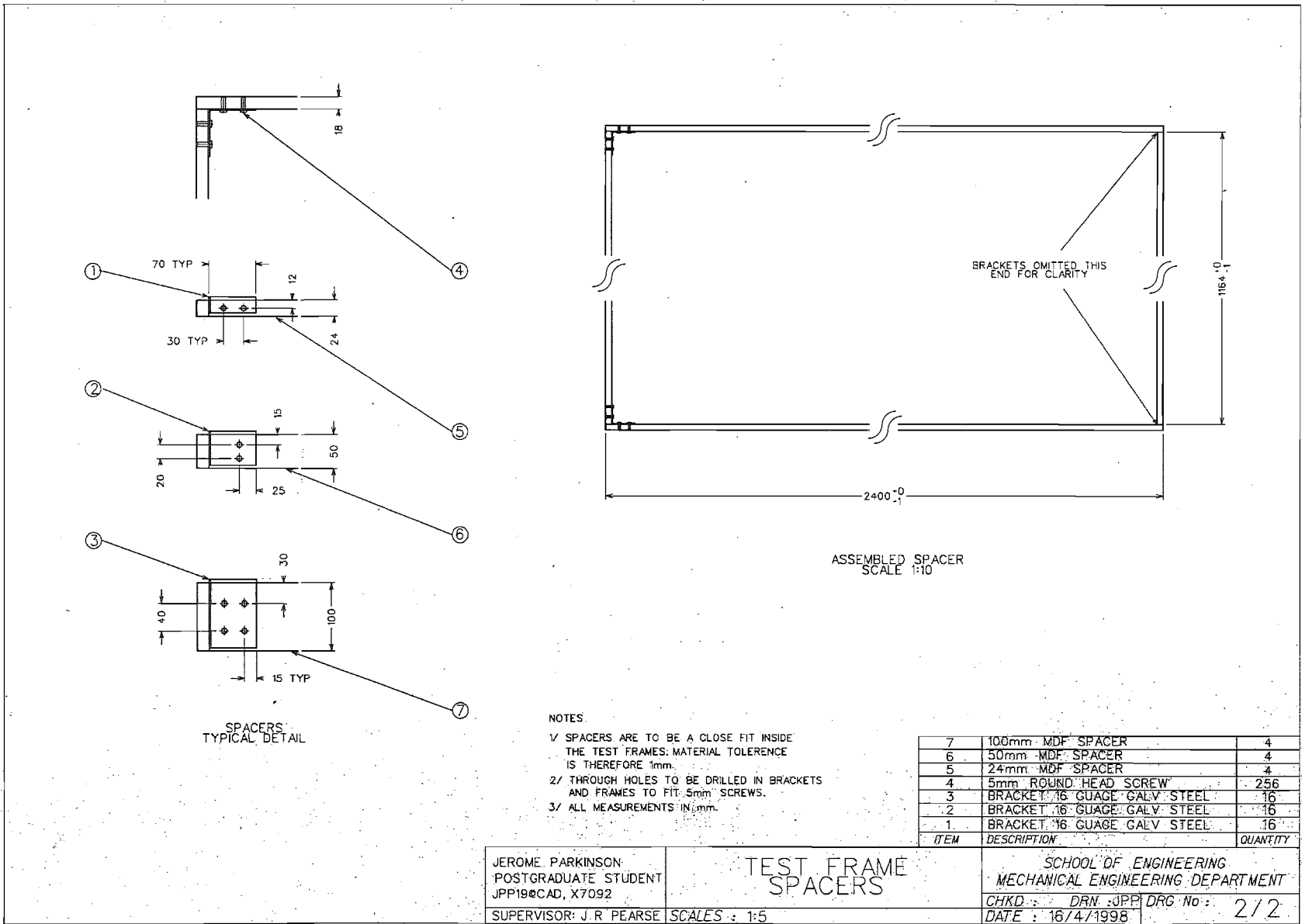


Figure C.2 Absorber frame spacers.



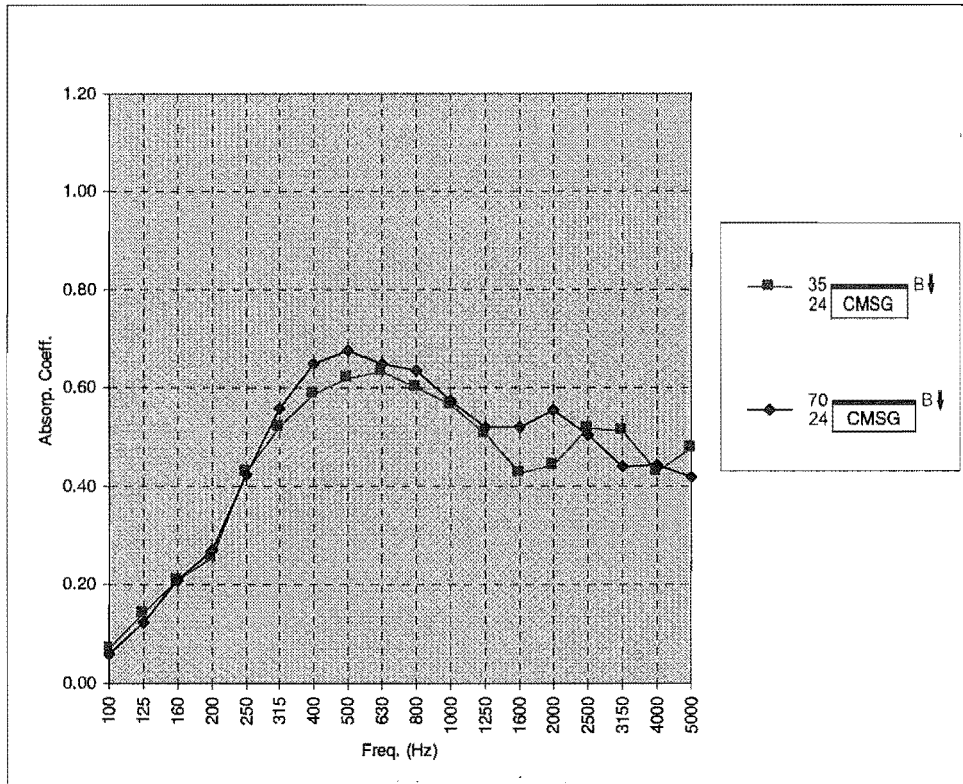


Figure C.3 Different films bonded to CMSG.

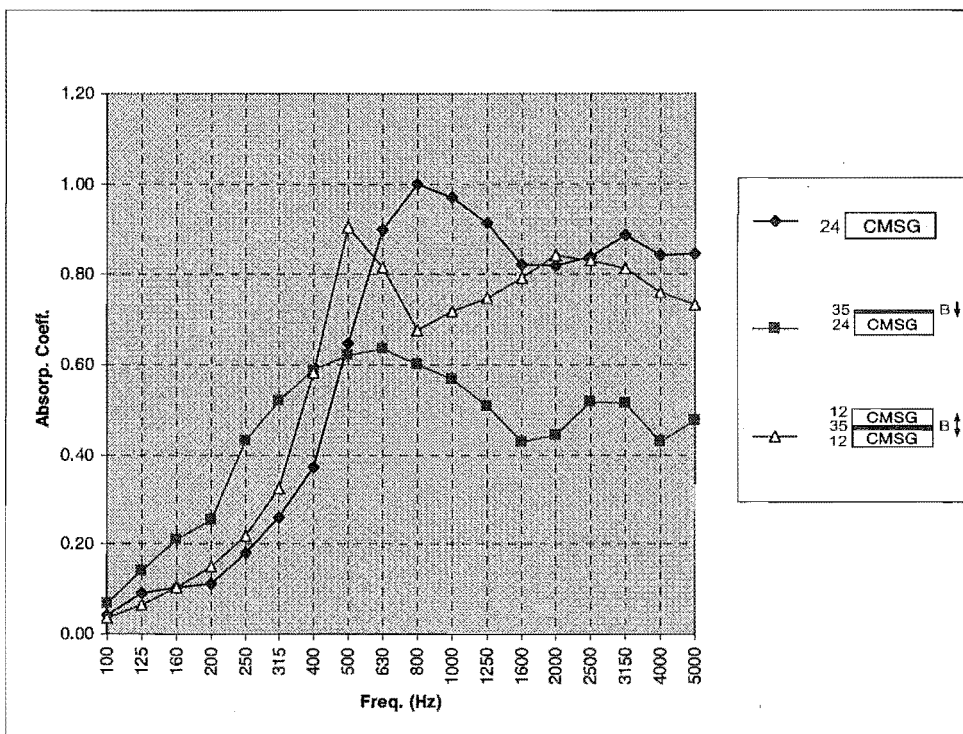


Figure C.4 Film position at 24 mm thickness.

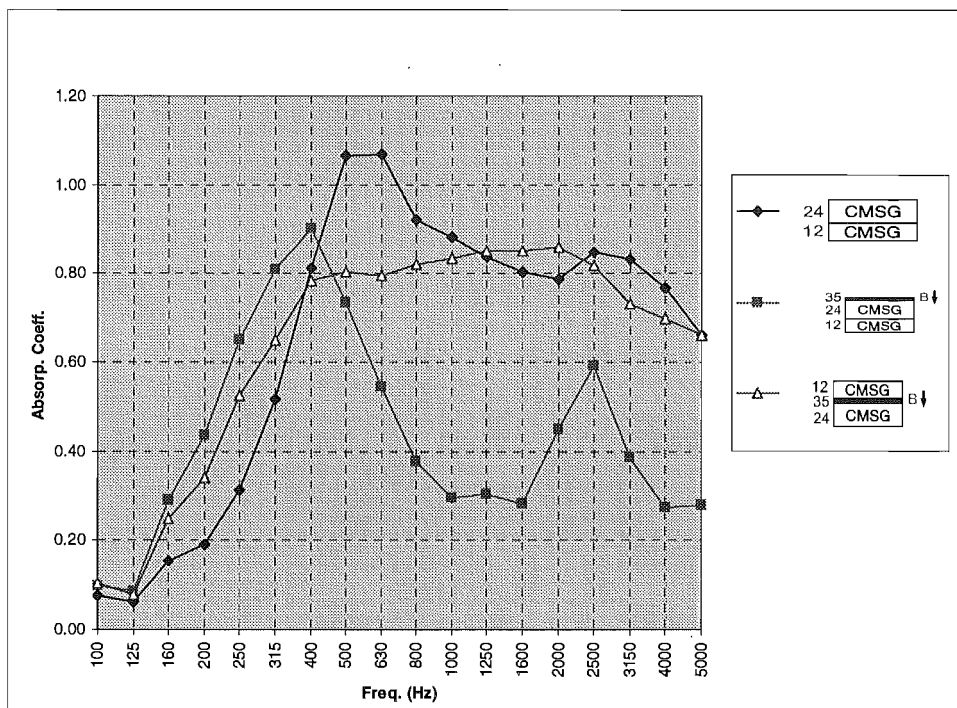


Figure C.5 Film position at 36 mm thickness.

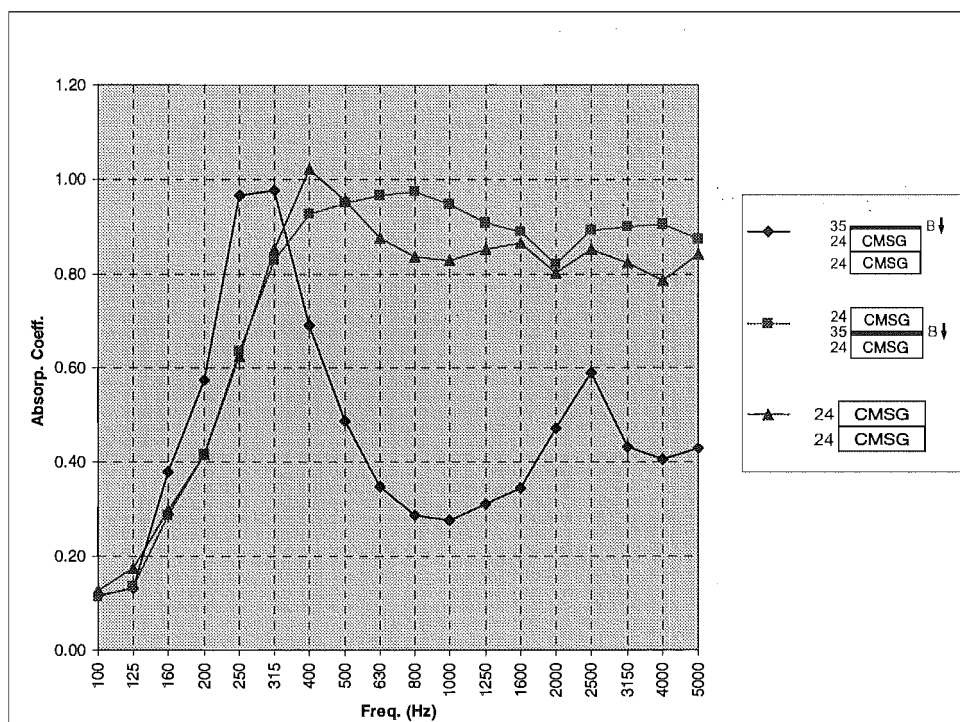


Figure C.6 Film position at 48 mm thickness.

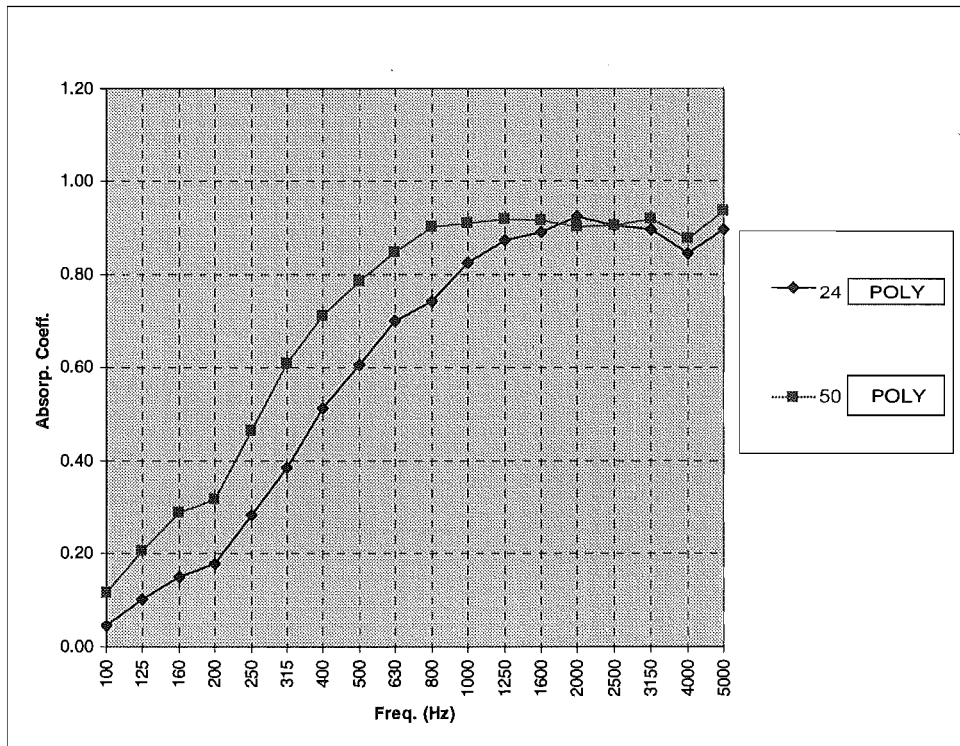


Figure C.7 Absorption for two polyester thicknesses.

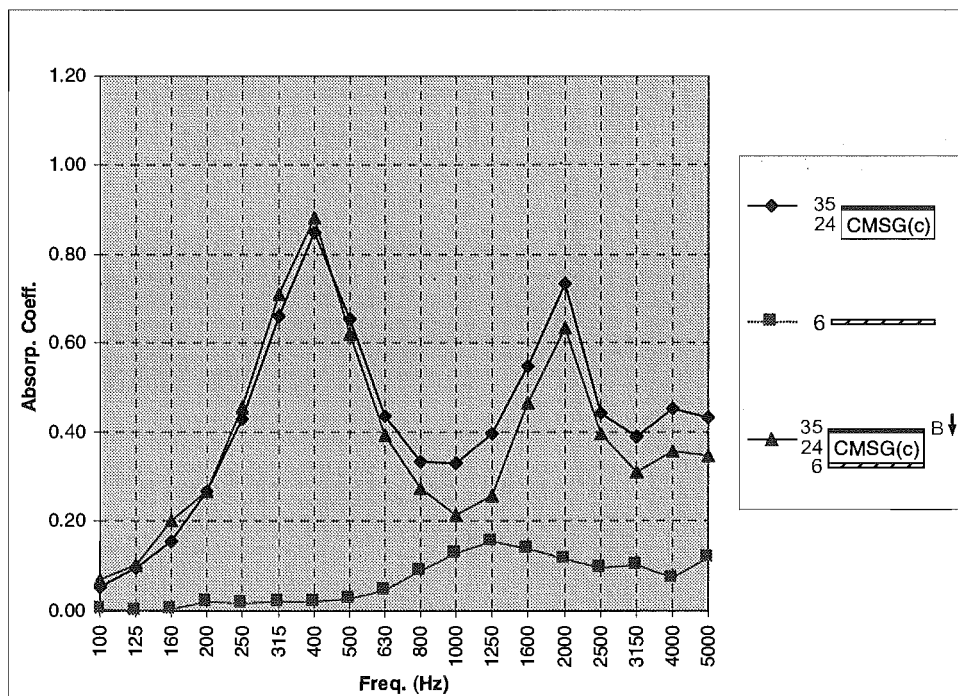


Figure C.8 Comparison of film faced CMSG on Gib board and on the Reverberation Room floor.



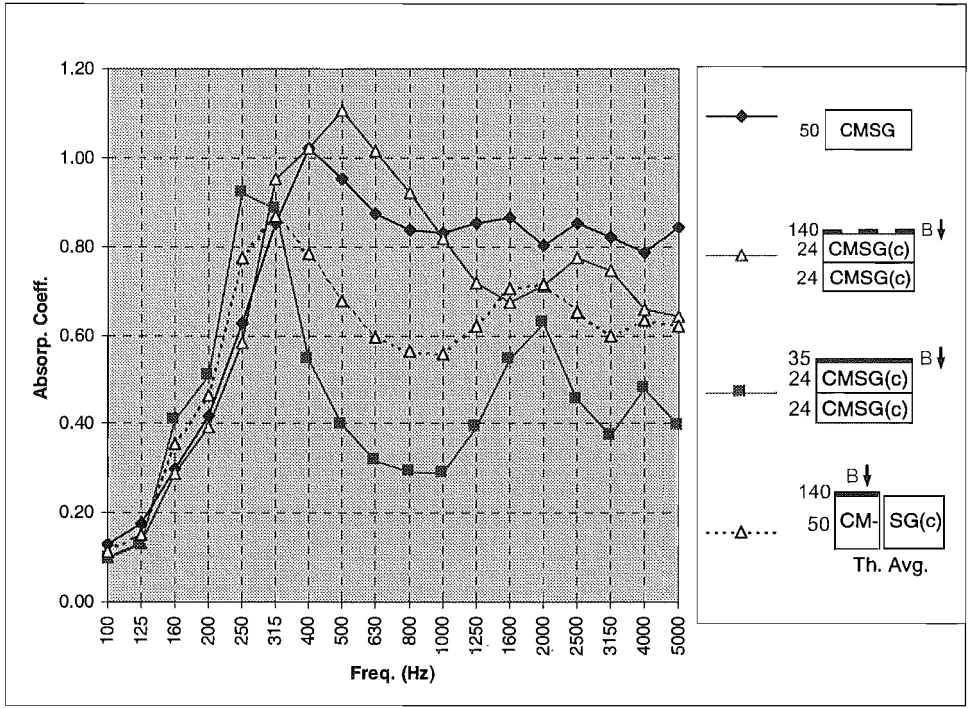


Figure C.9 Alternating strips of film and foam compared to foam by itself, film faced foam and the average of the two at 50 mm thickness.

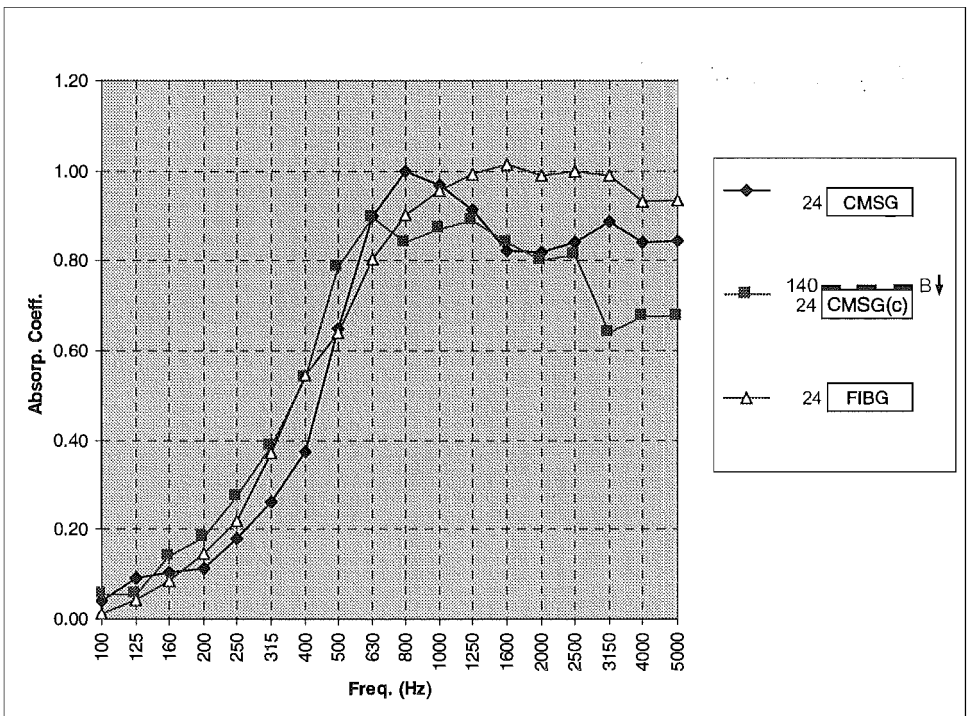


Figure C.10 Foam and film strips compared to CMSG and fibreglass at 24 mm thickness.

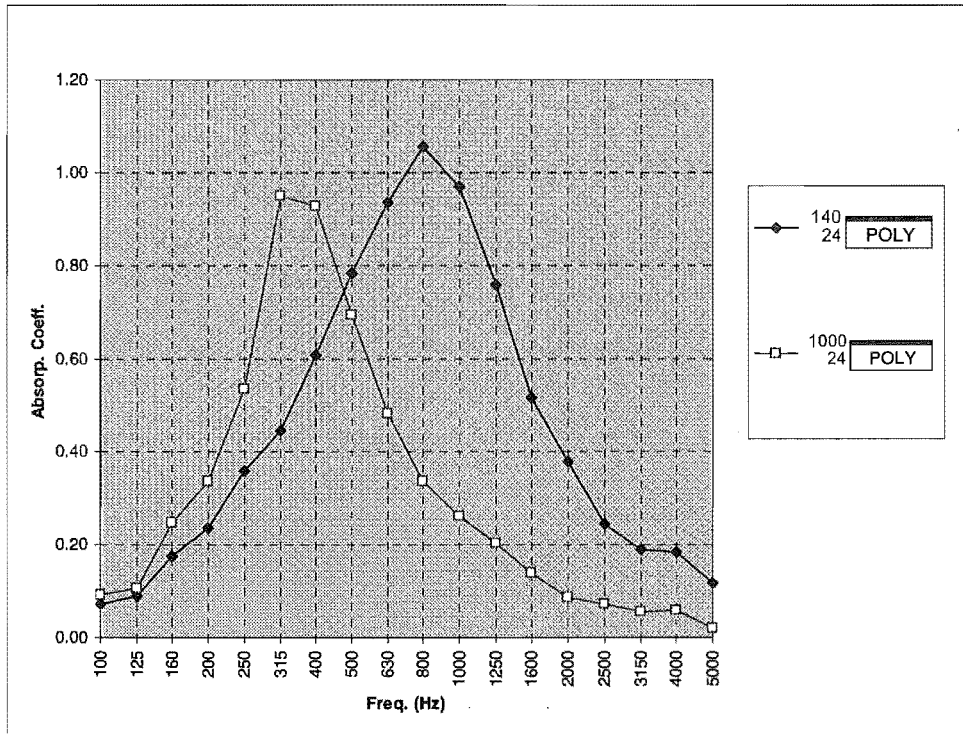


Figure C.11 Loose-laid films on polyester at 24 mm thickness.

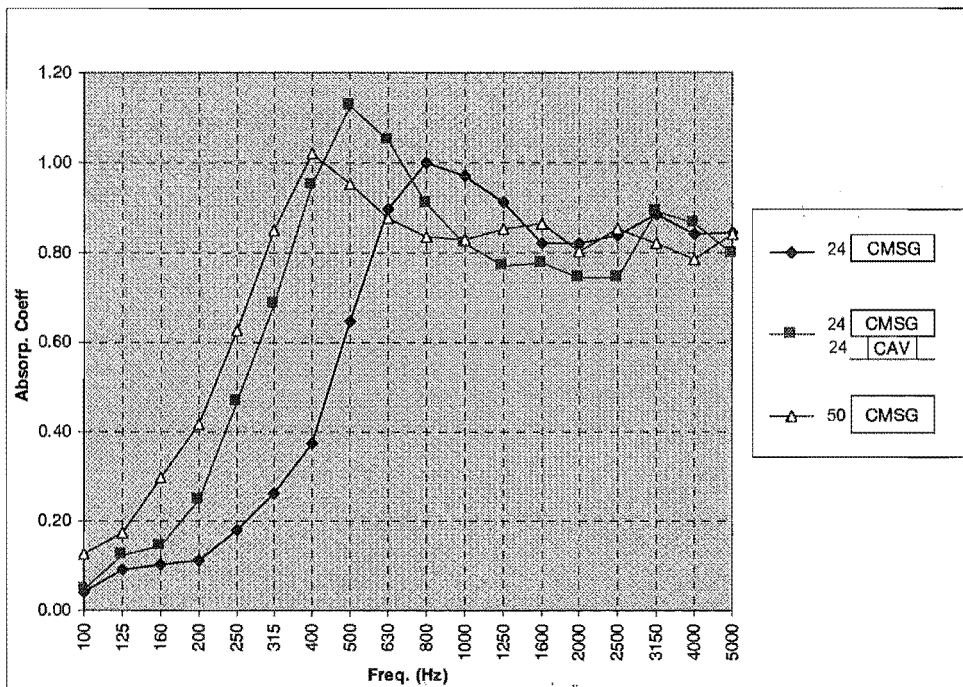


Figure C.12 The effect of air cavities on CMSG.

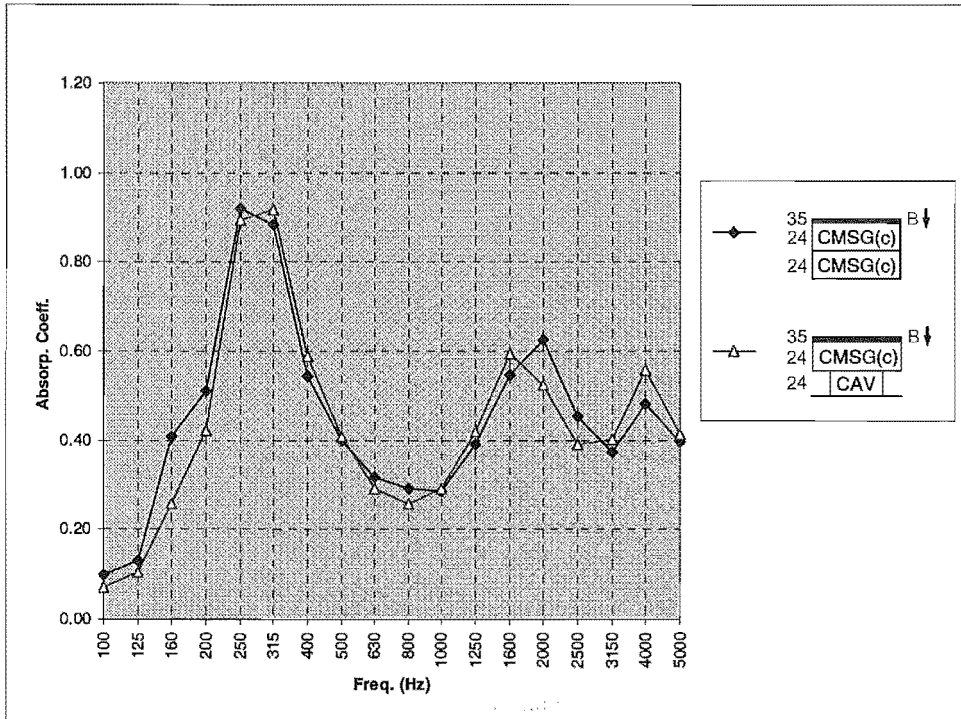


Figure C.13 The effect of air cavities on film faced foam.

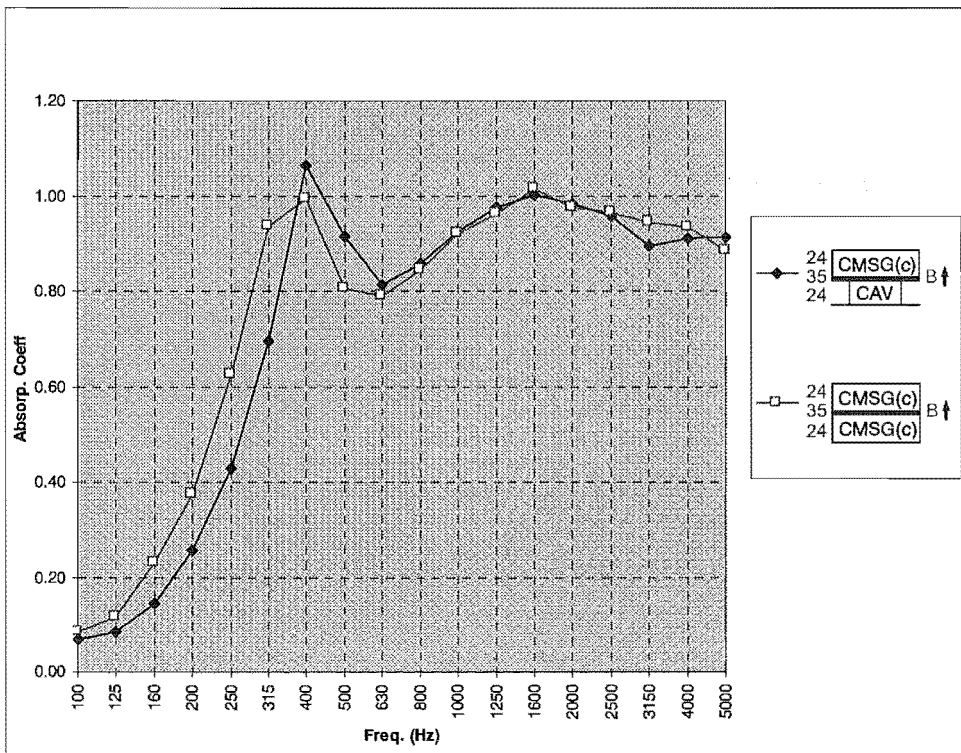


Figure C.14 The effect of air cavities on film faced foam.

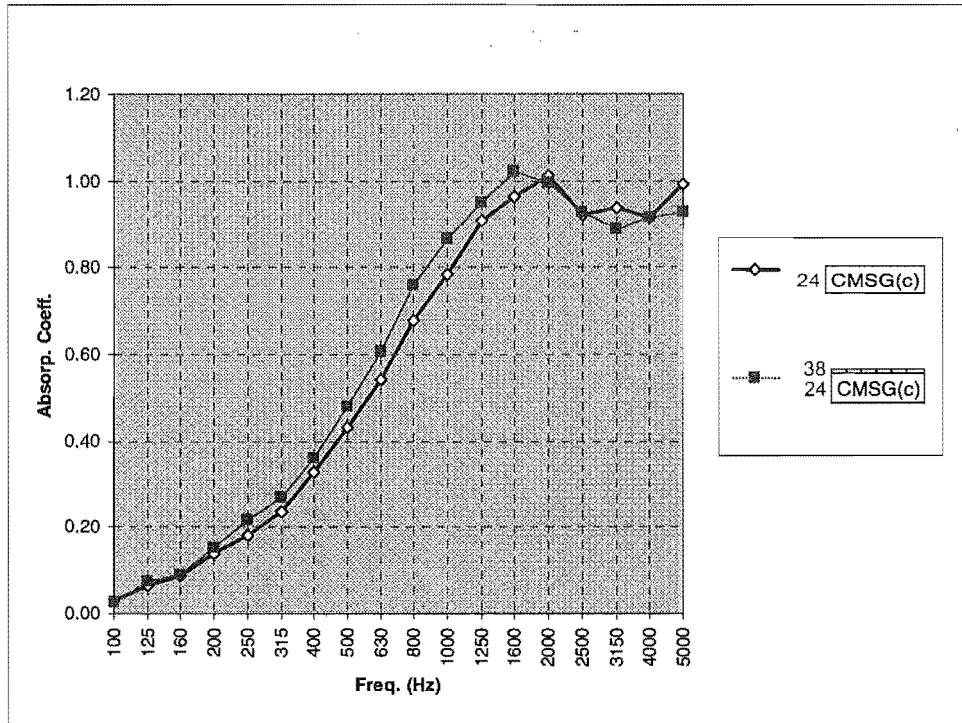


Figure C.15 Loose-laid fabric on crushed CMSG.

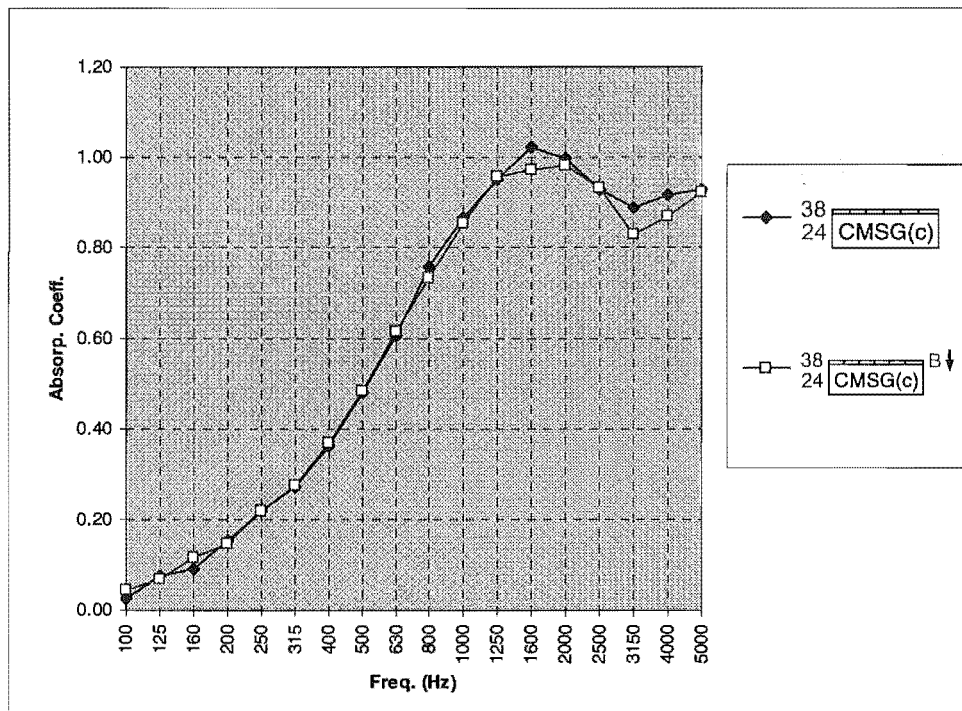


Figure C.16 Comparison of loose-laid and bonded fabrics on crushed CMSG.

ABSORPTION COEFFICIENTS  
Figure 6.3

T30 Freq.	6.3				6.4				6.5			
	24 CMSG	24 CMSG 6 CMSG	24 CMSG 12 CMSG	24 CMSG 24 CMSG	35 CMSG 24 CMSG B↓	35 CMSG 24 CMSG 6 CMSG B↓	35 CMSG 24 CMSG 12 CMSG B↓	35 CMSG 24 CMSG 24 CMSG B↓	6 CMSG 35 CMSG B↓	12 CMSG 35 CMSG B↓	24 CMSG 35 CMSG 24 CMSG B↓	
100	0.04	0.06	0.08	0.13	0.07	0.10	0.10	0.12	0.08	0.10	0.11	
125	0.09	0.08	0.06	0.17	0.14	0.12	0.09	0.13	0.10	0.08	0.13	
160	0.10	0.13	0.15	0.30	0.21	0.25	0.29	0.38	0.23	0.25	0.29	
200	0.11	0.14	0.19	0.42	0.25	0.35	0.43	0.58	0.30	0.34	0.42	
250	0.18	0.24	0.31	0.63	0.43	0.53	0.65	0.97	0.46	0.52	0.64	
315	0.26	0.38	0.52	0.85	0.52	0.67	0.81	0.98	0.54	0.65	0.83	
400	0.37	0.60	0.81	1.02	0.59	0.78	0.90	0.69	0.63	0.78	0.93	
500	0.65	0.92	1.07	0.95	0.62	0.78	0.73	0.49	0.68	0.80	0.95	
630	0.90	1.06	1.07	0.88	0.63	0.69	0.55	0.35	0.73	0.80	0.96	
800	1.00	1.04	0.92	0.84	0.60	0.52	0.36	0.29	0.73	0.82	0.97	
1000	0.97	0.94	0.88	0.83	0.57	0.41	0.30	0.28	0.70	0.83	0.95	
1250	0.91	0.83	0.84	0.85	0.51	0.34	0.30	0.31	0.63	0.85	0.91	
1600	0.82	0.78	0.80	0.87	0.43	0.29	0.28	0.34	0.60	0.85	0.89	
2000	0.82	0.72	0.79	0.80	0.44	0.41	0.45	0.47	0.68	0.86	0.82	
2500	0.84	0.82	0.85	0.85	0.52	0.58	0.59	0.59	0.74	0.82	0.89	
3150	0.89	0.81	0.83	0.82	0.51	0.40	0.38	0.43	0.67	0.73	0.90	
4000	0.84	0.77	0.77	0.79	0.43	0.25	0.27	0.41	0.71	0.70	0.91	
5000	0.84	0.73	0.66	0.84	0.48	0.31	0.28	0.43	0.68	0.68	0.87	
NRC	0.65	0.70	0.76	0.80	0.52	0.53	0.53	0.55	0.63	0.76	0.84	

ABSORPTION COEFFICIENTS  
Figure

	6.6		6.7		6.8		6.9		6.10		
T30 Freq.	$\frac{6}{35} \frac{\text{CMMSG}}{24} B \downarrow$	$\frac{35}{24} \frac{\text{CMMSG}}{6} B \downarrow$	$\frac{24}{6} \frac{\text{CMMSG}}{\text{CMMSG}}$	24 CMMSG	24 CMMSG(c)	24 POLY	24 FIBG	$\frac{140}{24} \frac{\text{CMMSG}(c)}{\text{CMMSG}(c)}$	$\frac{140}{24} \frac{\text{CMMSG}(c)}{\text{CMMSG}(c)} B \downarrow$	$\frac{140}{24} \frac{\text{POLY}}{\text{POLY}} B \downarrow$	$\frac{140}{24} \frac{\text{POLY}}{\text{POLY}} B \downarrow$
100	0.08	0.10	0.06	0.04	0.03	0.05	0.01	0.04	0.07	0.07	0.09
125	0.10	0.12	0.08	0.09	0.09	0.10	0.04	0.09	0.12	0.09	0.13
160	0.23	0.25	0.13	0.10	0.08	0.15	0.09	0.11	0.18	0.18	0.42
200	0.30	0.35	0.14	0.11	0.12	0.18	0.14	0.16	0.30	0.24	0.33
250	0.46	0.53	0.24	0.18	0.18	0.28	0.22	0.24	0.47	0.36	0.27
315	0.54	0.67	0.38	0.26	0.23	0.39	0.37	0.31	0.71	0.45	0.33
400	0.63	0.78	0.60	0.37	0.31	0.51	0.54	0.46	0.82	0.61	0.56
500	0.68	0.78	0.92	0.65	0.43	0.61	0.64	0.67	0.67	0.78	0.69
630	0.73	0.69	1.06	0.90	0.58	0.70	0.80	0.94	0.48	0.94	0.91
800	0.73	0.52	1.04	1.00	0.76	0.74	0.90	1.06	0.29	1.06	0.99
1000	0.70	0.41	0.94	0.97	0.91	0.82	0.96	1.01	0.26	0.97	1.01
1250	0.63	0.34	0.83	0.91	1.01	0.87	0.99	0.80	0.25	0.76	0.82
1600	0.60	0.29	0.78	0.82	1.01	0.89	1.01	0.55	0.30	0.51	0.65
2000	0.68	0.41	0.72	0.82	0.98	0.93	0.99	0.44	0.47	0.38	0.48
2500	0.74	0.58	0.82	0.84	0.90	0.90	1.00	0.40	0.56	0.25	0.37
3150	0.67	0.40	0.81	0.89	0.83	0.90	0.99	0.36	0.29	0.19	0.24
4000	0.71	0.25	0.77	0.84	0.92	0.84	0.93	0.22	0.17	0.18	0.23
5000	0.68	0.31	0.73	0.84	0.90	0.90	0.93	0.12	0.29	0.12	0.16
NRC	0.63	0.53	0.70	0.65	0.62	0.66	0.70	0.59	0.47	0.62	0.66

ABSORPTION COEFFICIENTS  
Figure 6.11

T30 Freq.	6.11		6.12			6.13				
	$\begin{matrix} 35 \\ 24 \\ 6 \end{matrix} \text{CM} \text{SG}(c) \text{ B} \downarrow$	$\begin{matrix} 35 \\ 24 \\ 6 \end{matrix} \text{CM} \text{SG}(c) \text{ B} \downarrow$	$\begin{matrix} 140 \\ 24 \end{matrix} \text{CM} \text{SG}(c)$	$\begin{matrix} 140 \\ 24 \end{matrix} \text{CM} \text{SG}(c) \text{ B} \downarrow$	$\begin{matrix} 140 \\ 24 \end{matrix} \text{L L} \text{CM} \text{SG}(c) \text{ B} \downarrow$	$\begin{matrix} 140 \\ 24 \end{matrix} \text{B} \downarrow \text{CM} \text{L} \text{SG}(c) \text{ Th. Avg.}$	$\begin{matrix} 24 \end{matrix} \text{CM} \text{SG}(c)$	$\begin{matrix} 140 \\ 24 \end{matrix} \text{CM} \text{SG}(c) \text{ B} \downarrow$	$\begin{matrix} 140 \\ 24 \end{matrix} \text{CM} \text{SG}(c) \text{ B} \downarrow$	$\begin{matrix} 140 \\ 24 \end{matrix} \text{B} \downarrow \text{CM} \text{L} \text{SG}(c) \text{ Th. Avg.}$
100	0.07	0.06	0.04	0.07	0.06	0.05	0.03	0.07	0.06	0.05
125	0.10	0.05	0.09	0.12	0.06	0.11	0.09	0.12	0.05	0.10
160	0.20	0.12	0.11	0.18	0.16	0.15	0.08	0.18	0.14	0.13
200	0.27	0.12	0.16	0.30	0.20	0.23	0.12	0.30	0.18	0.21
250	0.46	0.15	0.24	0.47	0.30	0.36	0.18	0.47	0.27	0.33
315	0.71	0.18	0.31	0.71	0.41	0.51	0.23	0.71	0.39	0.47
400	0.88	0.23	0.46	0.82	0.67	0.64	0.31	0.82	0.54	0.57
500	0.62	0.29	0.67	0.67	0.90	0.67	0.43	0.67	0.79	0.55
630	0.39	0.40	0.94	0.48	1.00	0.71	0.58	0.48	0.90	0.53
800	0.27	0.67	1.06	0.29	0.94	0.68	0.76	0.29	0.84	0.52
1000	0.22	0.77	1.01	0.26	0.82	0.64	0.91	0.26	0.87	0.59
1250	0.26	0.61	0.80	0.25	0.69	0.52	1.01	0.25	0.89	0.63
1600	0.47	0.38	0.55	0.30	0.54	0.43	1.01	0.30	0.84	0.66
2000	0.63	0.36	0.44	0.47	0.48	0.46	0.98	0.47	0.80	0.72
2500	0.40	0.53	0.40	0.56	0.49	0.48	0.90	0.56	0.81	0.73
3150	0.31	0.43	0.36	0.29	0.36	0.32	0.83	0.29	0.64	0.56
4000	0.36	0.36	0.22	0.17	0.38	0.19	0.92	0.17	0.68	0.54
5000	0.35	0.44	0.12	0.29	0.26	0.20	0.90	0.29	0.68	0.59
NRC	0.48	0.39	0.59	0.47	0.63	0.53	0.62	0.47	0.68	0.55

ABSORPTION COEFFICIENTS  
Figure

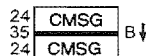
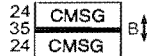
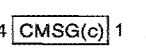
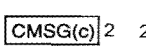
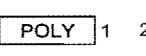
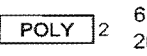

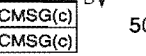
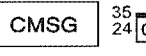
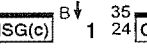
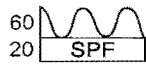
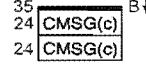
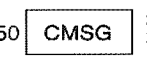
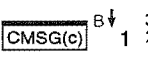
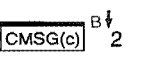
T30 Freq.	6.14			6.15			6.16			6.17		
	$\frac{35}{24}$ CMSG(c)	$\frac{140}{24}$ CMSG(c)	$\frac{1000}{24}$ CMSG(c)	$\frac{35}{24}$ CMSG(c) B↓	$\frac{140}{24}$ CMSG(c) B↓	$\frac{1000}{24}$ CMSG(c) B↓	$\frac{35}{24}$ CMSG(c) B↓	$\frac{35}{24}$ CMSG(c) B↓	50 POLY	$\frac{24}{24}$ POLY CAV	$\frac{24}{24}$ POLY	
100	0.07	0.04	0.06	0.05	0.07	0.06	0.05	0.10	0.12	0.05	0.04	
125	0.09	0.09	0.06	0.10	0.12	0.08	0.10	0.13	0.21	0.10	0.09	
160	0.14	0.11	0.15	0.15	0.18	0.19	0.15	0.41	0.29	0.18	0.12	
200	0.14	0.16	0.22	0.27	0.30	0.29	0.27	0.51	0.32	0.28	0.20	
250	0.20	0.24	0.40	0.43	0.47	0.44	0.43	0.92	0.47	0.44	0.27	
315	0.25	0.31	0.65	0.66	0.71	0.69	0.66	0.88	0.61	0.56	0.37	
400	0.33	0.46	0.95	0.85	0.82	0.76	0.85	0.54	0.71	0.69	0.48	
500	0.46	0.67	0.81	0.65	0.67	0.53	0.65	0.40	0.79	0.79	0.60	
630	0.63	0.94	0.54	0.43	0.48	0.32	0.43	0.32	0.85	0.84	0.68	
800	0.79	1.06	0.32	0.33	0.29	0.21	0.33	0.29	0.90	0.87	0.74	
1000	0.99	1.01	0.20	0.33	0.26	0.17	0.33	0.29	0.91	0.94	0.81	
1250	1.02	0.80	0.15	0.40	0.25	0.17	0.40	0.39	0.92	0.94	0.88	
1600	0.96	0.55	0.09	0.55	0.30	0.21	0.55	0.54	0.92	0.91	0.88	
2000	0.86	0.44	0.06	0.73	0.47	0.24	0.73	0.63	0.90	0.89	0.91	
2500	0.79	0.40	0.06	0.44	0.56	0.11	0.44	0.45	0.91	0.81	0.89	
3150	0.84	0.36	0.04	0.39	0.29	0.02	0.39	0.37	0.92	0.85	0.92	
4000	0.96	0.22	0.05	0.45	0.17	0.02	0.45	0.48	0.88	0.93	0.94	
5000	0.87	0.12	0.01	0.43	0.29	0.00	0.43	0.40	0.94	0.93	0.99	
NRC	0.63	0.59	0.37	0.54	0.47	0.34	0.54	0.56	0.77	0.76	0.65	



ABSORPTION COEFFICIENTS  
Figure 6.18

T30 Freq.	6.18		6.19		6.20		6.21				
	24 POLY	5 24 POLY	38 24 POLY	67 24 POLY	67 24 POLY	67 24 POLY	70 24 CMSG	70 24 CMSG(c)	70 24 SPF	12 35 12 CMSG	12 35 12 CMSG
100	0.04	0.04	0.05	0.06	0.06	0.06	0.06	0.06	0.07	0.04	0.04
125	0.09	0.10	0.09	0.09	0.09	0.11	0.12	0.14	0.11	0.07	0.06
160	0.12	0.13	0.12	0.14	0.14	0.17	0.21	0.15	0.18	0.10	0.09
200	0.20	0.21	0.20	0.23	0.23	0.25	0.27	0.24	0.22	0.15	0.13
250	0.27	0.28	0.29	0.33	0.33	0.34	0.42	0.43	0.45	0.22	0.21
315	0.37	0.39	0.43	0.43	0.43	0.45	0.56	0.67	0.75	0.32	0.30
400	0.48	0.51	0.55	0.55	0.55	0.58	0.65	0.85	0.92	0.58	0.50
500	0.60	0.62	0.68	0.69	0.69	0.66	0.68	0.67	0.58	0.90	0.88
630	0.68	0.74	0.77	0.80	0.80	0.83	0.65	0.49	0.37	0.82	0.79
800	0.74	0.80	0.84	0.88	0.88	0.86	0.64	0.41	0.27	0.68	0.57
1000	0.81	0.83	0.88	0.95	0.95	0.95	0.57	0.41	0.25	0.72	0.53
1250	0.88	0.89	0.94	1.00	1.00	0.99	0.52	0.50	0.29	0.75	0.56
1600	0.88	0.92	0.96	1.02	1.02	1.00	0.52	0.68	0.35	0.79	0.63
2000	0.91	0.94	0.97	1.01	1.01	1.01	0.56	0.71	0.61	0.84	0.73
2500	0.89	0.91	0.97	0.99	0.99	0.98	0.50	0.46	0.64	0.83	0.77
3150	0.92	0.92	0.92	0.98	0.98	0.95	0.44	0.46	0.30	0.81	0.86
4000	0.94	0.90	0.98	0.98	0.98	0.90	0.44	0.54	0.30	0.76	0.92
5000	0.99	0.94	0.98	0.96	0.96	0.86	0.42	0.64	0.42	0.73	0.94
NRC	0.65	0.67	0.71	0.74	0.74	0.74	0.56	0.55	0.47	0.67	0.59

ABSORPTION COEFFICIENTS  
Figure

	6.22	6.23	6.24	6.25	6.26
T30 Freq.					
					
					
100	0.10	0.08	0.03	0.03	0.05
125	0.12	0.12	0.09	0.07	0.10
160	0.26	0.23	0.08	0.09	0.15
200	0.41	0.37	0.12	0.14	0.18
250	0.64	0.63	0.18	0.18	0.28
315	0.81	0.94	0.23	0.24	0.39
400	0.97	0.99	0.31	0.33	0.51
500	0.96	0.81	0.43	0.43	0.61
630	0.81	0.79	0.58	0.54	0.70
800	0.78	0.84	0.76	0.68	0.74
1000	0.91	0.92	0.91	0.78	0.82
1250	0.98	0.96	1.01	0.91	0.87
1600	1.00	1.02	1.01	0.96	0.89
2000	0.98	0.98	0.98	1.01	0.93
2500	0.96	0.97	0.90	0.92	0.90
3150	0.90	0.94	0.83	0.94	0.90
4000	0.93	0.93	0.92	0.92	0.84
5000	0.91	0.88	0.90	0.99	0.90
NRC	0.85	0.83	0.62	0.60	0.66

ABSORPTION COEFFICIENTS  
Figure

T30 Freq.	C.3			C.4			C.5			C.6		
	$\frac{35}{24}$ CMSG(c) B↓	$\frac{70}{24}$ CMSG B↓	24 CMSG	$\frac{70}{24}$ CMSG B↓	$\frac{35}{12}$ CMSG B↓	24 CMSG	$\frac{35}{24}$ CMSG B↓	$\frac{12}{35}$ CMSG B↓	$\frac{35}{24}$ CMSG B↓	$\frac{35}{24}$ CMSG B↓	$\frac{24}{35}$ CMSG B↓	24 CMSG
100	0.07	0.06	0.04	0.07	0.04	0.08	0.10	0.10	0.12	0.11	0.13	
125	0.14	0.12	0.09	0.14	0.07	0.06	0.09	0.08	0.13	0.13	0.17	
160	0.21	0.21	0.10	0.21	0.10	0.15	0.29	0.25	0.38	0.29	0.30	
200	0.25	0.27	0.11	0.25	0.15	0.19	0.49	0.34	0.58	0.42	0.42	
250	0.43	0.42	0.18	0.43	0.22	0.31	0.65	0.52	0.97	0.64	0.63	
315	0.52	0.56	0.26	0.52	0.32	0.52	0.81	0.65	0.98	0.83	0.85	
400	0.59	0.65	0.37	0.59	0.58	0.81	0.90	0.78	0.69	0.93	1.02	
500	0.62	0.68	0.65	0.62	0.90	1.07	0.73	0.80	0.49	0.95	0.95	
630	0.63	0.65	0.90	0.63	0.82	1.07	0.55	0.80	0.35	0.96	0.88	
800	0.60	0.64	1.00	0.60	0.68	0.92	0.38	0.82	0.29	0.97	0.84	
1000	0.57	0.57	0.97	0.57	0.72	0.88	0.30	0.83	0.28	0.95	0.83	
1250	0.51	0.52	0.91	0.51	0.75	0.84	0.30	0.85	0.31	0.91	0.85	
1600	0.43	0.52	0.82	0.43	0.79	0.80	0.28	0.85	0.34	0.89	0.87	
2000	0.44	0.56	0.82	0.44	0.84	0.79	0.45	0.86	0.47	0.82	0.80	
2500	0.52	0.50	0.84	0.52	0.83	0.85	0.59	0.82	0.59	0.89	0.85	
3150	0.51	0.44	0.89	0.51	0.91	0.83	0.38	0.73	0.43	0.90	0.82	
4000	0.43	0.44	0.84	0.43	0.76	0.77	0.27	0.70	0.41	0.91	0.79	
5000	0.48	0.42	0.84	0.48	0.73	0.66	0.28	0.66	0.43	0.87	0.84	
NRC	0.52	0.56	0.65	0.52	0.67	0.76	0.53	0.76	0.55	0.84	0.80	

ABSORPTION COEFFICIENTS

Figure

T30 Freq.	C.7		C.8			C.9		C.9		Th. Avg.
	24 POLY	50 POLY	35 24 CMSG(c)	6	35 24 6 CMSG(c) B↓	50 CMSG	140 24 24 CMSG(c) B↓	35 24 24 CMSG B↓	140 50 CM-SG(c) B↓	
100	0.04	0.12	0.07	0.00	0.05	0.13	0.10	0.12	0.11	
125	0.09	0.21	0.10	0.00	0.10	0.17	0.13	0.13	0.15	
160	0.12	0.29	0.20	0.00	0.15	0.30	0.29	0.38	0.35	
200	0.20	0.32	0.27	0.02	0.27	0.42	0.39	0.58	0.46	
250	0.27	0.47	0.46	0.02	0.43	0.63	0.58	0.97	0.77	
315	0.37	0.61	0.71	0.02	0.66	0.85	0.95	0.98	0.87	
400	0.48	0.71	0.88	0.02	0.85	1.02	1.02	0.69	0.78	
500	0.60	0.79	0.62	0.03	0.65	0.95	1.11	0.49	0.68	
630	0.68	0.85	0.39	0.05	0.43	0.88	1.02	0.35	0.60	
800	0.74	0.90	0.27	0.09	0.33	0.84	0.92	0.29	0.56	
1000	0.81	0.91	0.22	0.13	0.33	0.83	0.82	0.28	0.56	
1250	0.88	0.92	0.26	0.16	0.40	0.85	0.72	0.31	0.62	
1600	0.88	0.92	0.47	0.14	0.55	0.87	0.68	0.34	0.71	
2000	0.91	0.90	0.63	0.11	0.73	0.80	0.71	0.47	0.71	
2500	0.89	0.91	0.40	0.10	0.44	0.85	0.78	0.59	0.65	
3150	0.92	0.92	0.31	0.10	0.39	0.82	0.75	0.43	0.60	
4000	0.94	0.88	0.36	0.07	0.45	0.79	0.66	0.41	0.63	
5000	0.99	0.94	0.35	0.12	0.43	0.84	0.64	0.43	0.62	
NRC	0.65	0.77	0.48	0.07	0.54	0.80	0.80	0.55	0.68	

ABSORPTION COEFFICIENTS  
Figure C.10

	C.11		C.12		C.13					
T30 Freq.	24 CMSG	140 CMSG(c) B↓	24 FIBG	140 POLY	1000 POLY	24 CMSG	24 CMSG / 24 CAV	50 CMSG	35 CMSG / 24 CMSG B↓	35 CMSG(c) / 24 CAV B↓
100	0.04	0.06	0.01	0.07	0.09	0.04	0.05	0.13	0.10	0.07
125	0.09	0.05	0.04	0.09	0.11	0.09	0.12	0.17	0.13	0.11
160	0.10	0.14	0.09	0.18	0.25	0.10	0.14	0.30	0.41	0.26
200	0.11	0.18	0.14	0.24	0.34	0.11	0.25	0.42	0.51	0.42
250	0.18	0.27	0.22	0.36	0.54	0.18	0.47	0.63	0.92	0.89
315	0.26	0.39	0.37	0.45	0.95	0.26	0.68	0.85	0.88	0.92
400	0.37	0.54	0.54	0.61	0.93	0.37	0.95	1.02	0.54	0.59
500	0.65	0.79	0.64	0.78	0.69	0.65	1.13	0.95	0.40	0.41
630	0.90	0.90	0.80	0.94	0.48	0.90	1.05	0.88	0.32	0.29
800	1.00	0.84	0.90	1.06	0.34	1.00	0.91	0.84	0.29	0.26
1000	0.97	0.87	0.96	0.97	0.26	0.97	0.82	0.83	0.29	0.29
1250	0.91	0.89	0.99	0.76	0.20	0.91	0.77	0.85	0.39	0.42
1600	0.82	0.84	1.01	0.51	0.14	0.82	0.78	0.87	0.54	0.59
2000	0.82	0.80	0.99	0.38	0.09	0.82	0.74	0.80	0.63	0.52
2500	0.84	0.81	1.00	0.25	0.07	0.84	0.74	0.85	0.45	0.39
3150	0.89	0.64	0.99	0.19	0.06	0.89	0.89	0.82	0.37	0.40
4000	0.84	0.68	0.93	0.18	0.06	0.84	0.86	0.79	0.48	0.56
5000	0.84	0.68	0.93	0.12	0.02	0.84	0.80	0.84	0.40	0.41
NRC	0.65	0.68	0.70	0.62	0.39	0.65	0.79	0.80	0.56	0.53

ABSORPTION COEFFICIENTS

Figure	C.14	C.15	C.16	C.16	C.16	
T30 Freq.	$\frac{24}{35} \frac{\text{CMSSG}(c)}{\text{CAV}} \uparrow$	$\frac{24}{35} \frac{\text{CMSSG}(c)}{\text{CMSSG}(c)} \uparrow$	$\frac{24}{24} \text{CMSSG}(c)$	$\frac{38}{24} \frac{\text{CMSSG}(c)}{\text{CMSSG}(c)}$	$\frac{38}{24} \frac{\text{CMSSG}(c)}{\text{CMSSG}(c)}$	$\frac{38}{24} \frac{\text{CMSSG}(c)}{\text{CMSSG}(c)} \downarrow$
100	0.07	0.08	0.03	0.03	0.03	0.04
125	0.08	0.12	0.07	0.08	0.08	0.07
160	0.14	0.23	0.09	0.09	0.09	0.12
200	0.26	0.37	0.14	0.15	0.15	0.15
250	0.43	0.63	0.18	0.22	0.22	0.22
315	0.70	0.94	0.24	0.27	0.27	0.28
400	1.06	0.99	0.33	0.36	0.36	0.37
500	0.91	0.81	0.43	0.48	0.48	0.48
630	0.81	0.79	0.54	0.61	0.61	0.61
800	0.86	0.84	0.68	0.76	0.76	0.73
1000	0.93	0.92	0.78	0.87	0.87	0.85
1250	0.97	0.96	0.91	0.95	0.95	0.96
1600	1.00	1.02	0.96	1.02	1.02	0.97
2000	0.98	0.98	1.01	1.00	1.00	0.98
2500	0.96	0.97	0.92	0.93	0.93	0.93
3150	0.89	0.94	0.94	0.89	0.89	0.83
4000	0.91	0.93	0.92	0.92	0.92	0.87
5000	0.91	0.88	0.99	0.93	0.93	0.92
NRC	0.81	0.83	0.60	0.64	0.64	0.63

## Appendix D Modelling

$$\begin{aligned}
G(z)_{11} &= i\zeta \cos(\alpha_1 z), \\
G(z)_{12} &= +\zeta \sin(\alpha_1 z), \\
G(z)_{13} &= i\zeta \cos(\alpha_2 z), \\
G(z)_{14} &= +\zeta \sin(\alpha_2 z), \\
G(z)_{15} &= \alpha_3 \sin(\alpha_3 z), \\
G(z)_{16} &= +i\alpha_3 \cos(\alpha_3 z), \\
G(z)_{21} &= -\alpha_1 \sin(\alpha_1 z), \\
G(z)_{22} &= -i\alpha_1 \cos(\alpha_1 z), \\
G(z)_{23} &= -\alpha_2 \sin(\alpha_2 z), \\
G(z)_{24} &= -i\alpha_2 \cos(\alpha_2 z), \\
G(z)_{25} &= i\zeta \cos(\alpha_3 z), \\
G(z)_{26} &= +\zeta \sin(\alpha_3 z), \\
G(z)_{31} &= -\mu_1 \alpha_1 \sin(\alpha_1 z), \\
G(z)_{32} &= -i\mu_1 \alpha_1 \cos(\alpha_1 z), \\
G(z)_{33} &= -\mu_2 \alpha_2 \sin(\alpha_2 z), \\
G(z)_{34} &= -i\mu_2 \alpha_2 \cos(\alpha_2 z), \\
G(z)_{35} &= i\mu_3 \zeta \cos(\alpha_3 z), \\
G(z)_{36} &= +\mu_3 \zeta \sin(\alpha_3 z), \\
G(z)_{41} &= -(P - 2N + \mu_1 Q)k_1^2 \cos(\alpha_1 z) - 2N\alpha_1^2 \cos(\alpha_1 z), \\
G(z)_{42} &= -i(P - 2N + \mu_1 Q)k_1^2 \sin(\alpha_1 z) - i2N\alpha_1^2 \sin(\alpha_1 z), \\
G(z)_{43} &= -(P - 2N + \mu_2 Q)k_2^2 \cos(\alpha_2 z) - 2N\alpha_2^2 \cos(\alpha_2 z), \\
G(z)_{44} &= -i(P - 2N + \mu_2 Q)k_2^2 \sin(\alpha_2 z) - i2N\alpha_2^2 \sin(\alpha_2 z), \\
G(z)_{45} &= -i2N\alpha_3 \zeta \sin(\alpha_3 z), \\
G(z)_{46} &= +2N\alpha_3 \zeta \cos(\alpha_3 z), \\
G(z)_{51} &= -i2N\zeta \alpha_1 \sin(\alpha_1 z), \\
G(z)_{52} &= +2N\zeta \cos(\alpha_1 z), \\
G(z)_{53} &= -2N\zeta \alpha_2 \sin(\alpha_2 z), \\
G(z)_{54} &= +2N\zeta \cos(\alpha_2 z), \\
G(z)_{55} &= N(\alpha_3^2 - \zeta^2) \cos(\alpha_3 z), \\
G(z)_{56} &= -iN(\alpha_3^2 - \zeta^2) \sin(\alpha_3 z), \\
G(z)_{61} &= -(Q + R\mu_1)k_1^2 \cos(\alpha_1 z), \\
G(z)_{62} &= +i(Q + R\mu_1)k_1^2 \sin(\alpha_1 z), \\
G(z)_{63} &= -(Q + R\mu_2)k_2^2 \cos(\alpha_2 z), \\
G(z)_{64} &= +i(Q + R\mu_2)k_2^2 \sin(\alpha_2 z), \\
G(z)_{65} &= 0 \\
G(z)_{66} &= 0
\end{aligned}$$